

Physical aspects explaining cyanobacteria scum formation in natural systems

Citation for published version (APA):

Aparicio Medrano, E. (2014). *Physical aspects explaining cyanobacteria scum formation in natural systems*. [Phd Thesis 1 (Research TU/e / Graduation TU/e), Applied Physics and Science Education]. Technische Universiteit Eindhoven. <https://doi.org/10.6100/IR772793>

DOI:

[10.6100/IR772793](https://doi.org/10.6100/IR772793)

Document status and date:

Published: 01/01/2014

Document Version:

Publisher's PDF, also known as Version of Record (includes final page, issue and volume numbers)

Please check the document version of this publication:

- A submitted manuscript is the version of the article upon submission and before peer-review. There can be important differences between the submitted version and the official published version of record. People interested in the research are advised to contact the author for the final version of the publication, or visit the DOI to the publisher's website.
- The final author version and the galley proof are versions of the publication after peer review.
- The final published version features the final layout of the paper including the volume, issue and page numbers.

[Link to publication](#)

General rights

Copyright and moral rights for the publications made accessible in the public portal are retained by the authors and/or other copyright owners and it is a condition of accessing publications that users recognise and abide by the legal requirements associated with these rights.

- Users may download and print one copy of any publication from the public portal for the purpose of private study or research.
- You may not further distribute the material or use it for any profit-making activity or commercial gain
- You may freely distribute the URL identifying the publication in the public portal.

If the publication is distributed under the terms of Article 25fa of the Dutch Copyright Act, indicated by the "Taverne" license above, please follow below link for the End User Agreement:

www.tue.nl/taverne

Take down policy

If you believe that this document breaches copyright please contact us at:

openaccess@tue.nl

providing details and we will investigate your claim.



Physical Aspects Explaining Cyanobacteria Scum Formation in Natural Systems

Evelyn Aparicio Medrano

Physical Aspects Explaining Cyanobacteria Scum Formation in Natural Systems

Evelyn Aparicio Medrano



Physical Aspects Explaining Cyanobacteria Scum Formation in Natural Systems

Evelyn Aparicio Medrano

Eindhoven 2014

Department of Turbulence and Vortex Dynamics
Faculty of Applied Physics

This work was financially supported by the Deltares Strategic Research funding in the Theme of Ecosystems and Environmental Quality.



A catalogue record is available from the Eindhoven University of Technology Library

ISBN: 978-90-386-3606-1

Copyright © Evelyn Aparicio Medrano, 2014

Cover design: El Taburete, Bolivia

Printed in the Netherlands by CPI-KONINKLIJKE WÖHRMANN

Physical Aspects Explaining Cyanobacteria Scum Formation in Natural Systems

PROEFSCHRIFT

ter verkrijging van de graad van doctor aan de Technische Universiteit Eindhoven, op gezag van de rector magnificus prof.dr.ir. C.J. van Duijn, voor een commissie aangewezen door het College voor Promoties, in het openbaar te verdedigen op dinsdag 6 mei 2014 om 16:00 uur

door

Evelyn Aparicio Medrano

geboren te Cochabamba, Bolivia

Dit proefschrift is goedgekeurd door de promotoren en de samenstelling van de promotiecommissie is als volgt:

voorzitter:	prof.dr.ir. G.M.W. Kroesen
1 ^e promotor:	prof.dr. H.J.H. Clercx
copromotor(en):	dr.ir. R.E. Uittenbogaard (Deltares) dr.ir. B.J.H. van de Wiel
leden:	prof.dr.ir. A.A. van Steenhoven prof.dr.ir. W.S.J. Uijttewaal (TUD) prof.dr. W.M. Mooij (WUR)
adviseur(s):	dr. L.M. Dionisio Pires (Deltares)

Contents

Contents	vii
1. Introduction	1
1.1 Background	1
1.2 Cyanobacteria Bloom, Scum and Hyperscum	2
1.3 Potential mechanism of scum formation	4
1.3.1 <i>Microcystis aeruginosa</i> colony composition	5
1.3.2 Vertical migration of <i>Microcystis aeruginosa</i>	6
1.3.3 The role of Hydrodynamics	9
1.4 Research objective	12
1.5 Thesis Outline	12
1.6 References	15
2. Coupling hydrodynamics and buoyancy regulation in <i>Microcystis aeruginosa</i> for its vertical distribution in lakes	19
2.1 Introduction	21
2.2 Methods	25
2.2.1 Hydrodynamic model	25
2.2.2 Model for cell-tissue density changes	28
2.2.3 The rising/sinking velocity in stagnant water	30
2.2.4 The Langevin-Fokker-Planck approach	32
2.3 Study sites	34
2.3.1 Lake Vlietland	34
2.3.2 Lakes IJsselmeer and Vinkeveen	37
2.4 Entrainment coefficient	38
2.5 Results	39
2.5.1 Lake Vlietland	39
2.5.2 Lake IJsselmeer	44

2.5.3	Lake Vinkeveen	46
2.6	Discussion and Conclusions	50
2.7	References	55
3.	Simulations of the diurnal migration of	
	<i>Microcystis aeruginosa</i> based on a scaling model	
	for physical-biological interactions	59
3.1	Introduction	61
3.2	Modelling approach	65
3.2.1	Direct Numerical Simulations (DNS)	66
3.2.2	Lagrangian Particle Tracking	67
3.2.3	Buoyancy regulation system	70
3.2.4	Lambert Beer's law – light attenuation	73
3.3	Scaling Procedure	73
3.3.1	Definition of the system scale parameters and Nondimensionalization of the equations	74
3.3.2	Characterization of the non-dimensional numbers τ_1 to τ_9	75
3.3.3	Definition of external variables for a realistic, natural case	76
3.3.4	Choice of the numerical values for the non-dimensional numbers τ_1 to τ_9	77
3.4	Application of the scaling procedure	79
3.4.1	Overview	79
3.4.2	Reference case C1: low turbulence	81
3.4.3	Effect of turbulence intensity	83
3.4.4	Effect of colony size	85
3.4.5	Light attenuation effect and day-night cycle	86

3.4.6	Domain without water surface	88
3.5	The buoyancy Stokes number	89
3.6	Discussion and Conclusions	94
3.7	References	98
4.	Scum Formation by Oxygenic Photosynthesis of Cyanobacteria	103
4.1	Introduction	105
4.2	Literature review of scum formation mechanisms	108
4.3	Hypothesis for the formation of cyanobacteria scum	113
4.3.1	Sequence resulting in scum formation	113
4.3.2	Photosynthetic oxygen supersaturation	117
4.3.3	Conditions for bubble growth	118
4.3.4	Stability of gas bubbles	122
4.4	Experimental evidence of scum formation	124
4.4.1	Sites description	125
4.4.2	Collection of samples	128
4.4.3	Experimental procedure	128
4.5	Results	130
4.6	Discussion and Conclusions	135
4.7	References	138
5.	Conclusions	143
5.1	Recommendations	148
5.2	References	150
	Annex A	151
	Thesis Summary	177
	Acknowledgements	181
	Curriculum Vitae	183

Chapter 1

General Introduction

1.1 Background

This thesis discusses several physical aspects related to cyanobacteria scum formation. These aquatic species obtain their energy through photosynthesis (phototropic organisms). Photosynthesis of cyanobacteria is divided into two reactions. The first one is light-dependent. At this stage, among others, water (H₂O) is broken down to release hydrogen and oxygen gas. The second stage is light-independent and is known as the Calvin cycle (Calvin and Benson, 1961), the source is ambient carbon dioxide (CO₂) and the output of this complicated process are carbohydrates such as sugars, expressed in its simplest form as CH₂O. Commonly both reactions involved in photosynthesis are simplified with $H_2O + CO_2 \rightarrow CH_2O + O_2$. The former equation conveys that organic matter (*e.g.* sugars) CH₂O and oxygen (O₂) are produced out of water (H₂O) and carbon dioxide (CO₂). Cyanobacteria are related to bacteria and often referred to as blue-green algae and/or cyanophyta (Huisman *et al.*, 2005). Cyanobacteria can be found in all climatic zones in water bodies ranging in size from ponds to oceans (fresh to salty water) (Güven and Howard, 2006). Cyanobacteria correspond to a subclass of aquatic phytoplankton; there are more than 2000 identified species of cyanobacteria. Among the more common in freshwater bodies are: *Microcystis* spp. (species), *Anabaena* spp., *Aphanizomenon* spp. *Oscillatoria* spp. and *Planktothrix* spp. (Reynolds, 1987). For aquatic ecosystems cyanobacteria play an important role because oxygen is released as a by-product of their photosynthesis (Calvin and Benson, 1961; Canfield, 2005). Therefore, cyanobacteria support ecosystems and have facilitated life on earth. Under certain conditions cyanobacteria grow excessively and form what is referred as a bloom (Section 1.2). These blooms can collect at the surface forming so-called scums (Figure 1.1). The major problem with cyanobacteria scum formation is that some species are potentially harmful to other living organisms (Figure 1.2). Many cyanobacterial species produce toxins (Codd *et al.*, 2005). In extreme cases this may locally deteriorate the recreational sector (Chorus and Bartram, 1999). In this thesis

the focus is on the species *Microcystis aeruginosa*. The reason for focusing on *Microcystis* is because it is the most ubiquitous and the most studied one (Reynolds *et al.*, 1981; Huisman *et al.*, 2005).

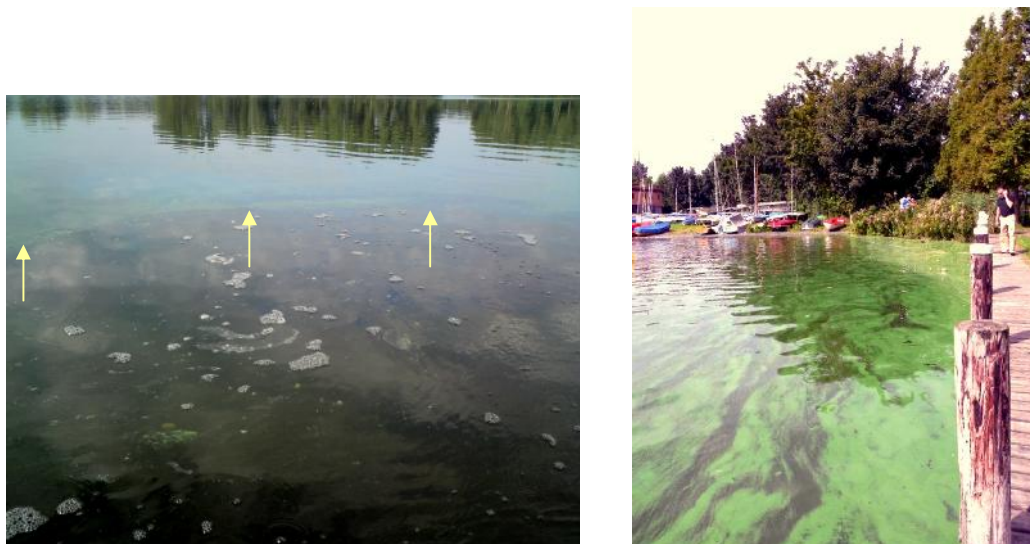


Figure 1.1: Cyanobacteria scum formation in Lake Vlietland (The Netherlands). The photograph on the left shows a scum in the middle of the lake (pointed by the arrows). The right figure shows accumulation of scum near the shore transported by wind drift from the lake.

1.2 Cyanobacteria Bloom, Scum and Hyperscum

It is important to make a clear distinction between a cyanobacteria bloom, a scum or a hyperscum (Figure 1.3). A *bloom* is defined here as the very large concentration of cyanobacteria present in the water column, not necessarily floating at the surface but dispersed mainly in the top part of the water column (epilimnion). In a eutrophic lake, chlorophyll-a concentrations may reach $300 \mu\text{g}\cdot\text{L}^{-1}$. Conditions favoring the formation of cyanobacterial blooms in lakes and reservoirs are: summer density-stratification, high water temperatures, low turbulent diffusion, high level of nutrients (eutrophication, especially nitrogen and phosphorus), low light extinction (clear waters), and their high resistance to grazing by zooplankton (Paerl and Ustach, 1982; Reynolds, 1987; Shapiro, 1997). Additionally, nutrients availability may affect photosynthetic activity by promoting or limiting growth (Huisman and Hulot, 2005; Reynolds, 2006). The common notion is that nutrients; such as nitrogen, phosphorus and carbon; show a strong decrease in concentration after the occurrence of high concentrations of cyanobacteria in a lake. In this study nutrient concentrations in Lake Vlietland (The Netherlands) were measured and studied during the summer of

2009). The results are summarized in Annex A. Lake Vlietland is considered a eutrophic lake. The lake is connected to a canal system that continuously discharges water with high concentration of phosphorus and other nutrients (from agricultural land). The measurements results in Lake Vlietland presented in Annex A do not demonstrate high consumption of nutrients after high blooms.

The reason for many cyanobacteria to outcompete other phytoplankton is because cyanobacteria are capable of regulating their buoyancy status (Walsby and Bleything, 1988; Ibelings *et al.*, 1991). Sometimes a very thin layer of cyanobacteria occurs at the water surface. This layer is called a *scum* which may persist for several hours to days. Visually the scum appears as “green paint” covering parts or the whole surface of a lake (Figure 1.1). Note that a bloom does not necessarily produce a scum (Zohary and Breen, 1990). The conditions for the change of a bloom into a scum are the principal subjects of this PhD study. Sometimes the scum is transported by wind to the shores of a lake or reservoir where they accumulate (right Figure 1.1) to form thick scums defined as *hyperscums* (Zohary and Robarts, 1990).



Figure 1.2: Photograph of a dead fish caught in a scum in Lake Vlietland (Source: Victor Langeberg).

Both, the processes leading to a cyanobacteria bloom and the processes leading to the formation of hyperscums are beyond the scope of this thesis. Los (2009) presents the causes and numerical simulations of cyanobacteria biomass composition. The formation, composition and consequences of hyperscums have been studied extensively by Zohary and Robarts (1990). It is not the intention of this thesis to study the conditions under which cyanobacteria become toxic and the effects of toxicity. For that subject the reader is referred to *e.g.* Lurling and Faassen (2013). Instead, the focus of this thesis is on the stage at which the formation of a

cyanobacteria *scum* occurs. Until now this subject has not been directly addressed from an integrated physical-biological approach. Moreover, the prediction of a scum constitutes the weak link in currently existing scums forecasting tools (*e.g.* early warning against scums EWACS).

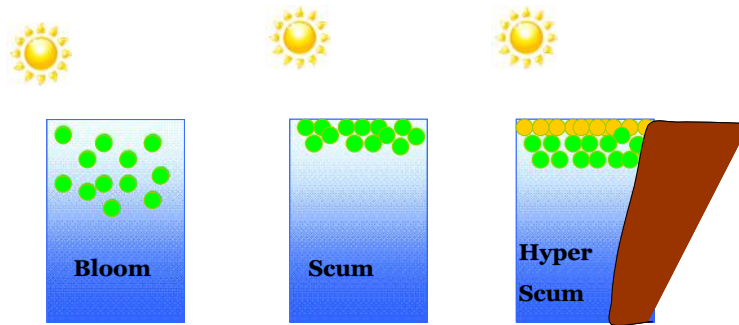


Figure 1.3: Difference between a bloom, a scum and a hyperscum. a) Bloom is defined as high concentrations of cyanobacteria in the water column, b) scum is defined as the very high concentration of cyanobacteria at the surface and c) hyperscum is defined as the even higher concentration of cyanobacteria collected on the shores or wall embankments in reservoirs. In a hyperscum there is a crust of dry material, represented in the figure with yellow colonies.

1.3 Potential mechanisms of scum formation

For the formation of a scum a state of irreversible buoyancy of cyanobacterial colonies is needed. This state appears to arise from a complex interaction between biological, physical and chemical processes. Statistical analysis on the correlation between physical, chemical and biotic factors do not show a clear predictability of scum formation (Soranno, 1997). This thesis mainly focuses on biological and physical processes involved in explaining scum formation. Biologically two major aspects are studied. The first aspect is the composition of a *Microcystis aeruginosa* colony in itself. The second aspect is the property of vertical migration by cyanobacterial cells or colonies due to carbohydrate synthesis and respiration. Physically two aspects are considered: the hydrodynamics of the containing water body and the possibility of oxygen bubble growth, including the diffusion of gasses.

The coupled effect of biological and physical aspects on the vertical migration of *Microcystis* and its role in scum formation is presented in Chapters 2 and 3 of this thesis. Next, in this thesis the hypothesis is presented that bubble growth under

oxygen super-saturation conditions may be the decisive phenomenon responsible for cyanobacteria scum formation (Chapter 4). Notably, evidence will be presented that support the latter hypothesis.

Microcystis aeruginosa is capable to perform daily vertical migration due to the presence of gas vesicles in their cells and by regulating its carbohydrates content. These two fascinating features enable *Microcystis* to move vertically through the water column and profit from photosynthesis in the epilimnion and nutrients in the dark and deeper layers (Ibelings *et al.*, 1991). Consequently, an important feature in the daily vertical migration cycle is the presence of gas vacuoles inside the cells of *Microcystis aeruginosa* (Section 1.3.1). A gas vacuole contains a group of gas vesicles which are single cylindrical voids to which gas diffuses (Figure 1.4). The surface of the gas vesicles are not as bubbles but are permeable, rigid structures of proteins. Due to their rigidity the vesicles decrease negligibly in volume after compression (when the colonies sink to deeper water depths). Gas vacuoles bring the density of a colony to a nearly neutrally buoyant state (Reynolds *et al.*, 1981; Visser *et al.*, 2005). Initially it was thought that the gas vacuoles where (by themselves) responsible for the formation of a scum (Reynolds and Walsby, 1975). However, detailed laboratory experiments showed that the main mechanisms responsible for this vertical migration are the colony composition (cells and mucilage) and the accumulation and utilization of carbohydrates (Visser *et al.*, 1997) (Section 1.3.2), rather than diurnal changes in volume of gas vacuoles.

The general overview presented in the previous paragraph is complicated by the existence of turbulence which influences the vertical mobility of cyanobacteria colonies (Section 1.3.3).

1.3.1 *Microcystis aeruginosa* colony composition

A *Microcystis* colony consists of several thousands of cells embedded in mucilage. The mucilage (Dutch: slijm) is mainly composed of polysaccharides. The mucilage has a mass-density similar to water density (Reynolds, 2006). Each cell contains a large number of gas vacuoles (group of gas vesicles). In general, a colony of *Microcystis* has a sphere-like structure (Reynolds, 1987) and for modeling purposes it is therefore approximated as a sphere (Figure 1.4). The gas-vacuoles inside the cells

reduce the specific density of the entire colony and as such contribute to its nearly neutrally buoyant status. A comprehensive study on the gas vacuoles is presented in Walsby (1994). The volumetric composition of a colony is described in Chapter 2 of this thesis.

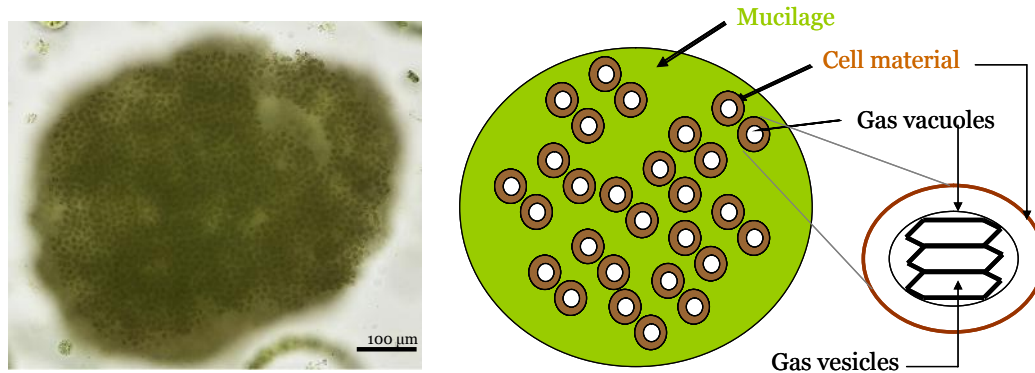


Figure 1.4: Structure of *Microcystis* colonies and gas vesicles. Left: Microscopic image of a colony (Courtesy: Marta Demarteau). Middle: schematic drawing of the composition of a colony. Right: sketch of gas vesicles forming a gas vacuole.

1.3.2 Vertical migration of *Microcystis aeruginosa* due to buoyancy regulation

Through the production of carbohydrates during photosynthesis and release of carbon during respiration the cell density of *M. aeruginosa* changes diurnally. This process has been quantified by Visser *et al.* (1997) and is shown in Figure 1.5. When exposed to sufficient light ($>6 \text{ W m}^{-2}$) the cell density of *M. aeruginosa* increases by the synthesis of carbohydrates (Figure 1.5). Cell density decreases under dark conditions when carbohydrates are used up for fuel (respiration). The measured light intensity at which the maximum increase in cell mass-density occurs was 140 Wm^{-2} . It is important to notice that the curve presented in Figure 1.5 provides an overview of the carbohydrates production process. There are three intervals in irradiation that can be identified. In the first interval the production of carbohydrates increases positively with solar irradiance until a maximum of carbohydrates accumulation is reached (interval I in Figure 1.5). The second interval is characterized by

photoinhibition (interval II in Figure 1.5). Finally, the third interval where there is no production of carbohydrates, but a reduction of carbohydrates (Visser *et al.* 1997) (interval III in Figure 1.5). When carbohydrates are produced during photosynthesis, oxygen is produced as a by-product and released as molecular oxygen which dissolves in water. During respiration, oxygen is consumed by the cyanobacteria, for breaking down the carbohydrates to supply energy. CO₂ and H₂O are then produced as by-products.

The lake volume that provides enough light for assimilation is called here the illuminated depth ($I(z) > 6 \text{ Wm}^{-2}$). Note that the euphotic depth is defined as the depth at which 1% of the surface irradiance is reached. Figure 1.6 shows the diurnal cycle of a *Microcystis* colony. During the light-time, the water column is divided in a region where the light is sufficient for synthesis of carbohydrates (photic zone) and a deeper region with relatively dark conditions (rest of the epilimnion and the hypolimnion). Figure 1.6 also shows an horizontal axis where the colony mass-density (ρ_{col}) varies from a minimum to a maximum (from left to right). If a colony starts the day in the illuminated region with a colony density lower than water (indicated by the number 1 in Figure 1.6), its terminal vertical velocity is in the rising mode ($w_s < 0$). Note that the axis in the vertical direction (z) is defined positive downwards. As the day continues, the density of the cell (ρ_{cell}), and thus that of the colony, increases. The colony mass-density becomes larger than the water density and the colony begins to sink ($w_s > 0$) (2). The colony sinks and because it enters darker regions, its mass-density starts to reduce due to respiration (3). When the colony density becomes smaller than the water density, the colony begins to rise again (4). This buoyancy regulated mechanism has been quantified prior to Visser *et al.*, 1997 in other cyanobacteria species such as *Oscillatoria agardhii* (Kromkamp and Walsby, 1990).

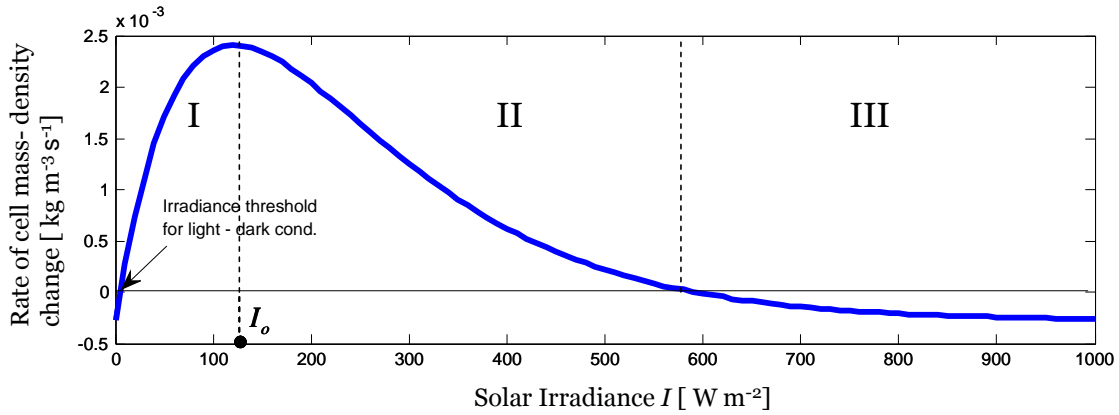


Figure 1.5: Rates of change in *Microcystis* cell-tissue density as a function of solar irradiation (light intensity). Interval I represents the positive increment of density with irradiance, interval II is characterized by photoinhibition and interval III where there is no production of carbohydrates. Redrawn from Visser *et al.* (1997). Note that in the Netherlands the irradiance during summer is around 800 W m^{-2} .

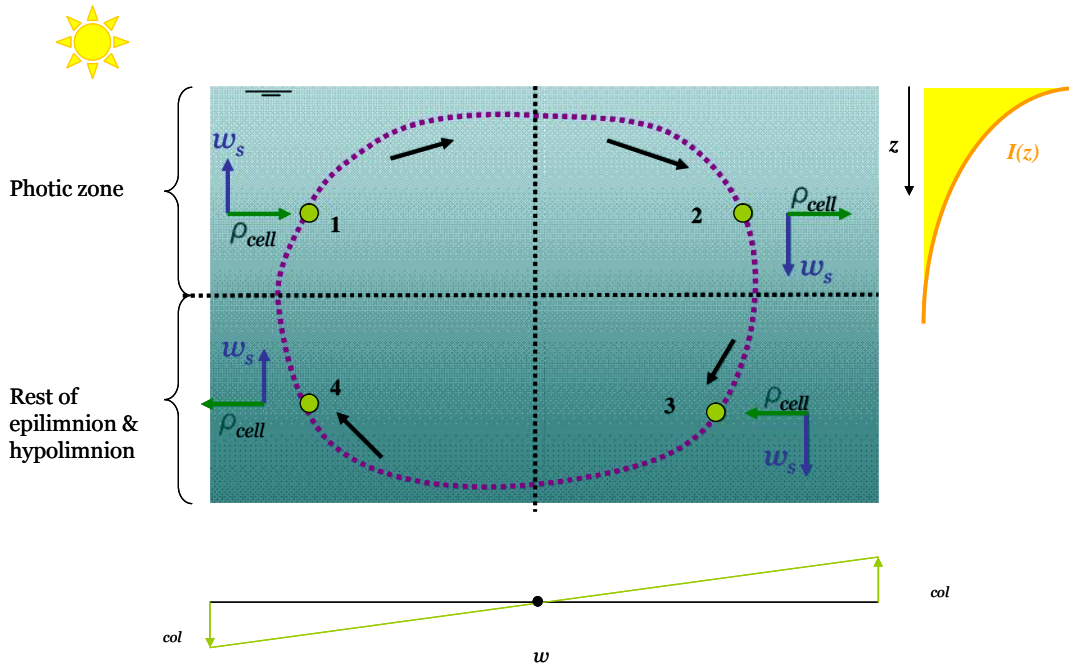


Figure 1.6: Vertical migration of *M. aeruginosa* during the light time. The numbers 1,2,3 and 4 refer to different migration stages of *Microcystis* through the light-time and are described in the text. The terminal velocity in the vertical direction is represented by w_s . The density of water, colony and cell are represented by ρ_w , ρ_{col} and ρ_{cell} , respectively. The water depth is represented by z and $I(z)$ represents the light attenuated at water depth z .

1.3.3 The role of hydrodynamics

The “deterministic” mechanism of vertical migration described in the previous section applies for the simplified case in which turbulence is absent. In reality, however, the turbulence and the hydrodynamic characteristics of a lake in general will influence the vertical migration of *Microcystis*. For example, diffusion, temperature gradients, local water velocities (small-scale turbulent velocity fluctuations) and flow direction amongst others play a major role in the population dynamics and spatial migration of cyanobacteria. The effect of turbulence on vertical migration and population growth is mainly because the hydrodynamic characteristics influence the availability of nutrients and the light environment (Ghosal *et al.*, 2000). Additionally, the mobility of the cells or colonies themselves influences their spatial distribution.

Figure 1.7 shows in a cartoon the complex relation between meteorology, hydrodynamics and cyanobacteria. There are three domains depicted in Figure 1.7, the atmosphere, the water column and the benthic layer. At both boundaries (air-water and soil-water interfaces) there is exchange of gasses and heat. In the atmosphere solar radiation and wind are the two main drivers for heat fluxes, surface waves, and the interior hydrodynamic characteristics of the lake. The heat flux is the sum of solar radiation, atmospheric radiation, latent heat flux and sensible heat flux. In the water column turbulence mixing and Langmuir circulation create vertical mobility. Other processes like internal waves are not shown in the figure. All of the previous processes influence among others the temperature T of the water column which changes along the depth (z). The light intensity diminishes along the depth depending on the extinction of water in itself and by suspended material and reflection (Kirk, 1975). The figure shows an approximation of the horizontal velocity profile $u(z)$ induced by wind. In the water column there are nutrients in solution, and detritus (dead organic material) in suspension. The growth and spatial distribution of cyanobacteria is a result of the complex inter-relation between all of the factors mentioned above. Please note that the list presented is not exhaustive. For instance chemical deposition from the atmosphere to the water column is not shown. The latter might provide nutrients to influence the biology of cyanobacteria.

Although flow patterns (*e.g.* Langmuir circulations creating converging zones) influence not only the vertical but also the horizontal concentrations of cyanobacteria, the main focus of this investigation is on the vertical transport of cyanobacteria by turbulence. It is assumed in this thesis that the phenomenon of *scum formation* is independent of complicated horizontal flow patterns. This subject will play a role in the horizontal transport of a formed scum, which is outside the scope of this thesis.

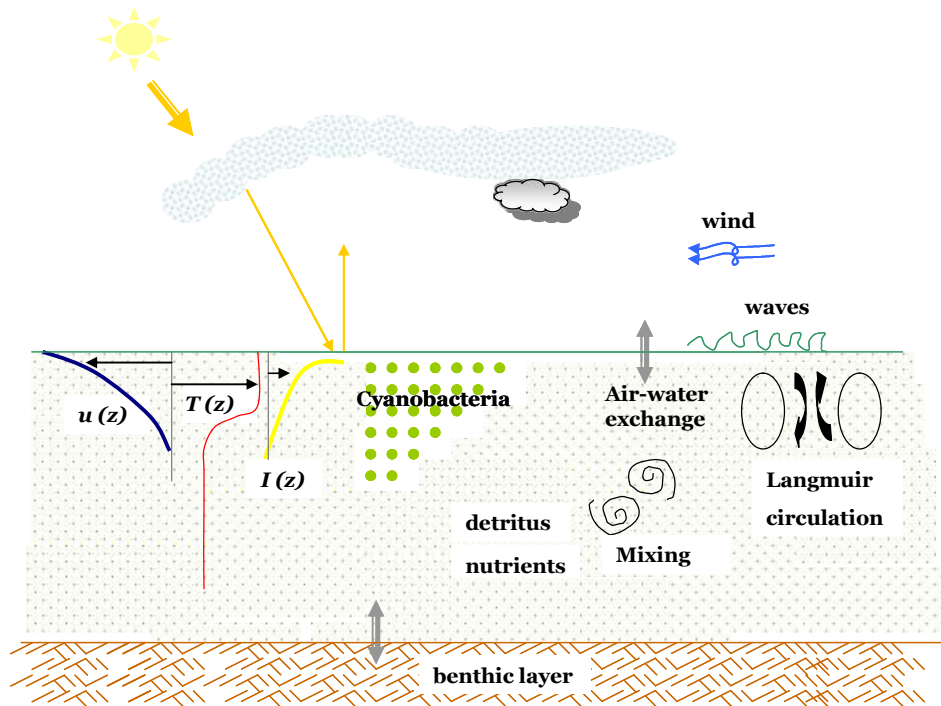


Figure 1.7: Schematic overview of physical processes involved in the interaction between hydrodynamics and a cyanobacteria population. $T(z)$ represents the temperature of the water column. $I(z)$ represents the light attenuated at water depth z . $u(z)$ represents the horizontal flow velocity as a function of depth resulting from wind stresses.

Figure 1.8 shows a schematic profile of the turbulence kinetic energy in a lake. The upper part, called the surface layer, is usually turbulent and is mainly created by the shear that suppresses the stress caused by wind. The interior layer is usually stably stratified. The bottom boundary layer may be turbulent and influenced by the bottom shear stresses (Wüest *et al.*, 2000). In terms of turbulence characteristics there are two requirements that allow cyanobacteria to bloom (Huisman and Sommeijer, 2002). Firstly, the level of turbulence must be low enough to permit the

formation of blooms *i.e.* high concentrations near the surface (eddy diffusivities between 10^{-1} to 10^1 $\text{cm}^2 \text{s}^{-1}$). Secondly, the upward vertical velocities of the colonies (induced by buoyancy) must be larger than the turbulence velocities inducing mixing. The smallest scales of turbulence are characterized by the Kolmogorov scales (length, time and velocity). The latter scales are related to the turbulence kinetic energy dissipation and the viscosity. The shearing at Kolmogorov millimetric scales will tear up the biological tissues of some cyanobacteria colonies leading to an overall reduction in colony size (O'brian *et al.*, 2004). A smaller colony size will have a reduced vertical mobility (Stokes velocity) compared to larger sizes (quadratic relation $w_s = (d^2 (\rho_{col} - \rho_w) g) / (18 \nu \rho_w)$).

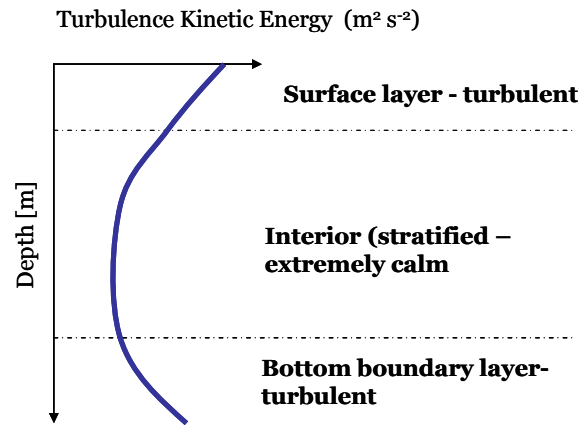


Figure 1.8: Schematic overview of the level of turbulence in a medium sized lake (mean depth 22 m) induced mainly by wind. Modified from Figure 4 in Wüest *et al.* (2000). Three regions are identified in a lake, the surface layer (epilimnion), the interior stratified layer (hypolimnion) and the bottom boundary layer.

Turbulence influences primary production in several ways. Firstly, mineral nutrients are transported from deeper layers to the euphotic zone through turbulence. Secondly, the light required for photosynthesis and perceived by cyanobacteria depends on the transport due to mixing. Thirdly, the uptake of nutrients depends on the intensity of turbulence. Finally, turbulence maintains sinking species immersed in the upper mixed layers (Ghosal *et al.*, 2000; Hondzo and Warnars, 2008), thereby reducing the advantage of the buoyant *Microcystis*. Changes in the turbulence environment of lakes (different dissipations and eddy diffusivities) also contribute to changes in species composition of phytoplankton

from a dominating presence of *Microcystis* species at low turbulence levels (low diffusivities) to diatoms or green algae at high turbulence levels (Huisman *et al.*, 2004).

The role of turbulence coupled to the vertical migration of *M. aeruginosa* and its possible role in scum formation is studied and discussed in detail in Chapters 2 and 3 of this thesis.

1.4 Research objective

The aim of this PhD study is to explain the formation of cyanobacterial scums in natural lakes or reservoirs and to identify the key responsible physical and biological processes involved.

The main question is: *Why do scums form and remain at the surface of lakes?*

This main question is split up into the following sub questions:

- 1.- How does wind induced turbulence affect the vertical migration of *Microcystis aeruginosa* in deep lakes? (Chapter 2)
- 2.- Can scum formation by *M. aeruginosa* be explained by its vertical migration alone? (Chapter 2)
- 3.- How does (small scale) turbulence influence vertical migration of *Microcystis*? (Chapter 3)
- 4.- What is the role of the interaction between light, colony size and daylight length on the vertical distribution of *Microcystis*? (Chapter 3)
- 5.- Can oxygen gas bubbles be contained on or inside the mucilage of cyanobacteria cells? (Chapter 4)
- 6.- Can the growth of oxygen bubbles be the mechanism responsible for scum formation? (Chapter 4)

1.5 Thesis Outline

For answering the main research question this thesis applies an integrated approach of essential physics and biology. By using different tools, the interdisciplinary topic of scum formation is studied. More specifically, this thesis considers the role of lake hydrodynamics, in particular (stratified) turbulence, the physiological response of

cyanobacteria to light, and the buoyancy created by the growth of oxygen (gas) bubbles in cyanobacteria vertical migration yielding scum formation (Figure 1.9).

Chapter 1	Introduction		
Chapter 2	Colony composition Vertical Migration Hydrodynamics	Applied Model Fokker – Planck $k - \epsilon$ Turbulence model	1D Vertical Model
Chapter 3	Colony composition Vertical Migration Small scale Turbulence	Fundamental model Particle Tracking Full Navier - Stokes	3D Model
Chapter 4	Oxygen Production O₂ Bubble growth Irreversible buoyancy	Physical Experiments	
Chapter 5	Conclusion Outlook		
Annex A	Lake Vlietland Meteorology Temperature and Oxygen, Nutrients	Field Measurements	

Figure 1.9: Thesis content overview. The second column describes the processes covered by the chapter. The third column mentions the tools employed in each chapter. The fourth column indicates the spatial dimension of the applied model.

Firstly, the role of vertical migration coupled to the hydrodynamics of a lake is investigated. Due to the dominance of vertical mixing, heat transfer and vertical mobility a model is applied with one dimension along the vertical (1DV). The 1DV model includes explicitly the buoyancy regulation under the influence of light intensity in the cells of *M. aeruginosa*. The combined effects of turbulence mixing and buoyancy regulation on the vertical migration of cyanobacteria under natural conditions are applied through the Langevin-Fokker-Planck (LFP) approach. This approach simulates the total colony number concentration along the water column. Turbulence mixing is simulated by the $k-\epsilon$ turbulence model including thermal buoyancy effects. This approach is presented in Chapter 2 of this thesis.

Secondly, this thesis presents a coupled model of Direct Numerical Simulations of turbulent flow with particle tracking of *Microcystis aeruginosa* colonies. The purpose of these simulations is to support the findings presented in Chapter 2 by solving the fundamental Navier-Stokes equations instead of using a turbulence model.

This model is referred as the 3D model, given that the DNS simulates the three dimensional flow field in space and time and therefore it is considering the transport of colonies in all directions. The *Microcystis* colonies are treated as biologically active organisms because the cell mass–density is continuously changing as explained in section 1.3.2. However, the intrinsic gap between biological and flow time scales makes such an endeavor a non-trivial exercise. In order to conceal time scales of flow and biology a normalization-scaling procedure is performed in which biological responses of *Microcystis* cells are accelerated. This reduces the bandwidth in time scales to computationally feasible conditions and is presented in Chapter 3.

Thirdly, the physical mechanism responsible for cyanobacteria scum formation and its persistence was studied using laboratory experiments (Chapter 4). The hypothesis presented in this thesis is that irreversible buoyancy of cyanobacteria occurs due to the growth of gas bubbles in the colonies, most likely oxygen due to super-saturation by strong photosynthesis during blooms. These oxygen bubbles form within or attached to the mucus.

Next, Chapter 5 presents the conclusions of the investigation and also an outlook for future research. Finally, a summary of the general effect of nutrients during spring and summer, meteorology and hydrodynamics on the formation of a scum in Lake Vlietland is given in Appendix A.

The contents of Chapter 2 have been published in *Ecological Modeling*, Chapters 3 and 4 have been submitted to the journals of *Theoretical Biology* and *Aquatic Ecology* respectively.

1.6 References

- Calvin, M. and Benson, A. A. (1948). The path of carbon in photosynthesis. Ernest Orlando Lawrence Berkeley National Laboratory, University of California Radiation Laboratory-Berkeley.
- Canfield, D.E. (2005). The early history of Atmospheric Oxygen: Homage to Robert M. Garrels. *Annual Reviews Earth Planet*, 33, 1-36.
- Chorus, I. and Bartram, J. (1999). Toxic Cyanobacteria in Water: A guide to their public health consequences, monitoring and management. E & FN Spon, London.
- Codd, G.A., Morrison, L.F., Metcalf, J.S. (2005). Cyanobacterial toxins: risk management for health protection. *Toxicology Applied Pharmacology*, 203, 264-27.
- Ghosal, S., Rogers, M. and Wray, A. (2000). The turbulent life of phytoplankton. Center for Turbulence Research. Proceedings of the Summer Program 2000. <http://www.math.ens.fr/equipes/edp/biomath/references/ghosal.pdf>
- Güven, B. and Howard, A. (2006). A review and classification of the existing models of cyanobacteria. *Progress in Physical Geography*, 30, 1-24.
- Hondzo, M. and Warnars, T. A. (2008). Coupled effects of small-scale turbulence and phytoplankton biomass in a small stratified lake. *Journal of Environmental Engineering*, 134, 954-960.
- Huisman, J. and Sommeijer, B. (2002). Population dynamics of sinking phytoplankton in light-limited environments: simulation techniques and critical parameters. *Journal of Sea Research*, 48, 83-96.
- Huisman, J., Sharples, J., Stroom, J.M., Visser, P.M., Kardinaal, W.E.A., Verspagen, J.M.H. and Sommeijer, B. (2004). Changes in turbulent mixing shift competition for light between phytoplankton species. *Ecology*, 85, 2960-2970.
- Huisman, J., Matthijs, H.C.P., Visser, P.M. (ed.) (2005). Harmful Cyanobacteria. Springer, Dordrecht, The Netherlands.
- Huisman, J. and Hulot, F.D. (2005). Population dynamics of harmful cyanobacteria, p. 143-176. In J. Huisman, H.C.P. Matthijs, and P.M. Visser (ed.), Harmful Cyanobacteria. Springer, Dordrecht, The Netherlands.
- Ibelings, B.W., Mur, L.R. and Walsby, A.E. (1991). Diurnal changes in buoyancy and vertical distribution of *Microcystis* in two shallow lakes. *Journal of Plankton Research*, 13, 419-436.
- Kirk, J.T.O. (1975). A theoretical analysis of the contribution of algal cells to the attenuation of light within natural waters. *New Phytologist*, 75, 21-36.
- Kromkamp, J. and Walsby, A. E. (1990). A computer model of buoyancy and vertical migration in cyanobacteria. *Journal of Plankton Research*, 12, 161- 183.

- Los, H. (2009). Eco-Hydrodynamic modelling of primary production in coastal waters and lakes using BLOOM. PhD thesis, University of Wageningen.
- Lurling, M. and Faassen, E. (2013). Dog poisoning associated with a *Microcystis aeruginosa* bloom in the Netherlands. *Toxins*, 5, 556-567.
- Paerl, H.W. and Ustach, J.F. (1982). Blue-green algal scums: An explanation for their occurrence during freshwater blooms. *Limnology and Oceanography*, 27, 212-217.
- Reynolds, C. S.; Walsby, A. E. (1975). Water blooms. *Biological reviews of the Cambridge Philosophical Society*, 50, 437-481.
- Reynolds, C.S., Jaworski, G.M.H., Cmiech, H.A., Leedale, G.F. (1981). On the annual cycle of the blue-green alga *Microcystis aeruginosa* Kuntz. emend. Elenkin. *Philosophical Transactions of the Royal Society London, Series B*, 293, 419-477.
- Reynolds, C.S. (1987). Cyanobacterial water blooms. *Advances in Botanical Research*, 13, 67-143.
- Reynolds, C.S., (2006). Ecology of phytoplankton. Cambridge University Press, Cambridge, UK.
- Shapiro, J. (1997). The role of carbon dioxide in the initiation and maintenance of blue-greens dominance in lakes. *Freshwater Biology*, 37, 307-323.
- Soranno, P.A. (1997). Factors affecting the timing of surface scums and epilimnetic blooms of blue-green algae in a eutrophic lake. *Canadian Journal of Fisheries and Aquatic Sciences*, 54, 1965-1975.
- Visser, P. M., Passarge, J., and Mur, L. R. (1997). Modelling the vertical migration of the cyanobacterium *Microcystis*. *Hydrobiologia*, 349, 99-109.
- Visser, P. M., Ibelings, B. W., Mur, L. R., and Walsby, A. E. (2005). The ecophysiology of the harmful cyanobacterium *Microcystis*: features explaining its success and measures for its control, p. 109-142. In J. Huisman, H.C.P. Matthijs, and P.M. Visser (ed.), Harmful cyanobacteria. Springer, Dordrecht, The Netherlands.
- Walsby, A.E. and Bleything, A. (1988). The dimensions of cyanobacterial gas vesicles in relation to their efficiency in providing buoyancy and withstanding pressure. *Journal of General Microbiology*, 134, 2635-2645.
- Walsby, A. E. (1994). Gas vesicles. *Microbiological Reviews*, 58, 94-144.
- Wüest, A., Piepke, G., and Van Senden D.C. (2000). Turbulent kinetic energy balance as a tool for estimating vertical diffusivity in wind-forced stratified water. *Limnology and Oceanography*, 45, 1388-1400.
- Zohary, T. and Breen, C.M. (1989). Environmental factors favoring the formation of *Microcystis aeruginosa* hyperscums in a hypertrophic lake. *Hydrobiologia*, 178, 179-192.

Zohary, T., and Robarts, R.D. (1990). Hyperscums and the population dynamics of *Microcystis aeruginosa*. *Journal of Plankton Research*, 12, 423–432.

Chapter 2

Coupling hydrodynamics and buoyancy regulation in *Microcystis aeruginosa* for its vertical distribution in lakes¹

¹ The contents of this chapter have been adopted from the paper by Aparicio-Medrano *et al.* (2013) with minor modifications.

Abstract

In this research we introduce a coupled column model to simulate the vertical migration of *Microcystis aeruginosa* in natural lakes. *Microcystis aeruginosa* is a unicellular cyanobacteria that form colonies. They produce toxins and therefore become a potential threat to water quality and human health. Understanding the distribution of this species in space and time is important for improving water management strategies. The model we propose includes both hydrodynamics and physiological responses including explicitly buoyancy regulation in *Microcystis* cells. Our model applies the Langevin - Fokker - Planck approach to simulate the total colony number concentration along the water column. This approach allows the description of sinking and rising velocities of colonies of different sizes and compositions subjected to turbulent mixing. The model is first applied to the 30 m deep Lake Vlietland in the Netherlands for the summer of 2009. During this summer, the lake showed high blooms of *Microcystis* which eventually led to scum formation along the shore. The simulations show the preferential distribution of *M. aeruginosa* through the water column and their strong dependency on colony size. On a daily cycle, small colonies (50-200 μm) do not remain near the surface but are highly concentrated in the middle of the epilimnion, whereas large colonies (≥ 800 μm) are able to migrate to greater depths and concentrate only temporarily near the surface. For comparing our computer model with available measurements of *Microcystis* concentration distributions we applied it to Lakes IJsselmeer and Vinkeveen. The results show a good agreement with the observations of diurnal changes in buoyancy status.

Key words

Buoyancy regulation, cyanobacteria, vertical migration, colony distribution, colony size

2.1. Introduction

The present research presents a coupled model for the vertical distribution of *Microcystis aeruginosa* in response to light-driven cell density changes and hydrodynamic turbulence mixing. To this purpose we implement a Fokker-Planck equation while simultaneously considering biological assimilation and its effect on density changes in *Microcystis* cells. At the same time we included a mechanistic model for the density of the colony as a whole by incorporating the gas vesicle to cell volume ratio and the cell volume to colony volume ratio. In the following paragraphs we define the context of our study.

General Introduction

Microcystis aeruginosa is a colony forming cyanobacterial species. A colony is composed by a pack of cells covered by mucilage and each cell contains gas vesicles (Fig. 2.1). It is a widespread species that can form blooms in freshwaters regardless of the nutrient concentrations (Zohary and Robarts, 1990; Ibelings, 1996; Visser, 1995). Many *Microcystis* strains produce a variety of toxins, of which the so-called microcystins are the best known (Codd, 1999). These microcystins are hepatotoxins that can damage the liver of humans and animals. As a result, *Microcystis* blooms are a world wide serious threat for water quality, ecosystems, fisheries, and human health (Chorus and Bartram, 1999; Codd, 1999).

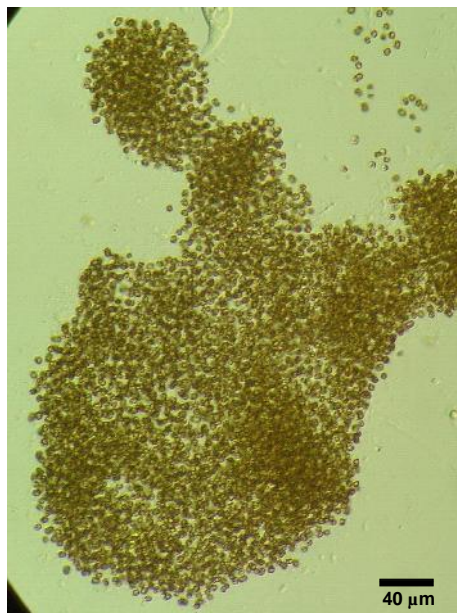


Figure 2.1: *Microcystis* colony. The microscopic picture has been taken by Frank van Oosterhout.

During summer and at higher latitudes, increasing solar radiation and weak winds create permanent and temporary thermal stratification in sufficiently deep lakes (thermocline formation). The thermocline subdivides the water column in an upper mixing zone (epilimnion) affected by wind-generated turbulence and a lower almost static layer (hypolimnion, Imberger, 1985). After the winter period, in the lake bottom, cysts of several cyanobacteria genera develop gas vesicles that allow the cells to enter the water column (Sirenko, 1972; Verspagen *et al.*, 2004). Cyanobacteria grown during spring remain mainly in the epilimnion where they take up nutrients for their further growth.

Buoyancy Regulation Mechanism

Cyanobacteria possess a buoyancy regulation mechanism to influence their vertical position along the water column (Ganf and Oliver, 1982). Buoyancy regulation is a property that allows gas vacuolated cyanobacteria to migrate along the water column, moving towards the surface to receive light for photosynthesis and growth and moving downwards to collect nutrients (Reynolds and Walsby, 1975). Cyanobacterial species with gas vacuoles usually belong to the genera *Planktothrix* and *Microcystis* (Walsby, 2005). Observations (*e.g.* Reynolds *et al.*, 1981) show that in the summer period *Microcystis* colonies mainly remain in the epilimnion (Ibelings *et al.*, 1991), where they take up nutrients, while most phytoplankton species without buoyancy regulation sink in the absence of sufficient turbulent mixing (Huisman *et al.*, 2002).

Initially, vertical migration of *Microcystis* has been explained either by changes in the cell turgor pressure (Reynolds, 1987), by synthesis of gas vesicles (Oliver and Walsby, 1984) or by changes in carbohydrate content (Van Rijn and Shilo, 1995; Ibelings *et al.*, 1991; Reynolds, 1984). The turgor pressure hypothesis is less likely to be the mechanism responsible for vertical migration of *Microcystis* due to the high turgor strength of the protein strains around gas vesicles (Walsby, 1994), which makes the cell capable to withstand the pressure existing in a lake. The synthesis of gas vesicles has a low production rate of a few days (Walsby, 1994). According to the carbohydrate hypothesis, the concentration of carbohydrates in the cell tissue depends on the temporal integration of carbon uptake in day time by photosynthesis and carbon release during the night by respiration. Based on laboratory experiments, Visser *et al.* (1997) formulated deterministic relations for the

rate of cell-tissue density changes to the amount of received light (see Section 2.2). In this study we focus on the carbohydrate mechanism and use the relations of Visser *et al.* (1997).

Coupling Biology and Hydrodynamics

Vertical migration is affected by turbulence mixing directly and also indirectly, by changing their depth level and therefore the light dose received (Humphries and Lyne, 1988). Consequently, for modeling vertical migration under natural conditions, a combination of a density regulation model (Visser *et al.*, 1997) and a model to simulate the hydrodynamics of the lake is necessary. Earlier investigations tried to couple these two factors using various approaches (Howard, 1997; Wallace and Hamilton, 2000; Chen *et al.*, 2009).

Wallace and Hamilton (2000) coupled two models (a buoyancy regulation model and a hydrodynamic model including a random walk for colonies). They successfully applied this methodology to a 1.4 m shallow water body with strong light attenuation. To simulate the actual vertical velocity of the colonies, Wallace and Hamilton (2000) took the sum of the colony vertical velocity due to gravity and the turbulent velocity component along the vertical, a similar procedure was followed by Chen *et al.* (2009). The latter researchers concluded that colonies are capable of persisting near the surface for several days provided that they are entrained in turbulence long enough for reducing their carbohydrate content and given that carbohydrate uptake is somewhat delayed.

An important aspect of the application of Visser's (1997) model for the cell-tissue density changes is the determination of the colony mass density (kg mass per m³ colony volume). Given that the carbohydrate changes were measured in the cell tissue, the volume occupied by cells in a colony and the gas volume present in a cell play a major role in the resulting colony mass density (Rabouille and Salencon, 2005). To our knowledge, this realistic aspect was not considered in the models of Wallace and Hamilton (2000) and Chen *et al.* (2009). This is the essential improvement and subject of our study.

Therefore, in this study, an explicit mathematical model description is presented for the rising/sinking velocity of *Microcystis* colonies that includes gas vesicle to cell volume ratio as well as cell volume to colony volume ratio. This approach allows a generic application of the model of Visser *et al.* (1997) for cell-tissue density changes. Another aspect is related to the fact that *Microcystis* in the field shows variations in colony size, composition and density which translate into variation in rising/sinking velocities. Rather than tracking individual colonies and afterwards estimating their vertical distribution, we apply a methodology for the ensemble of numerous colonies in which the vertical distribution of colonies is the prime variable. This methodology is based on ensemble-averaging of numerous random-walk tracks yielding the so-called Fokker-Planck equation. The latter we solve in conjunction with a model for turbulent mixing in a thermally-stratified lake.

Microcystis Aeruginosa in Natural Systems

From an observational perspective, the vertical distribution of *Microcystis* reported in the literature (Ibelings *et al.* 1991) usually shows a top heavy profile during days with low or almost no wind. This profile is characterized by maximum concentrations near the surface reducing along the vertical. During windy days, colonies distributions are nearly uniform along the epilimnion (Moreno–Ostos *et al.* 2009). Field descriptions of colony size variation along the depth of deep water bodies, however, are scarce. Wu and Knog (2009) have measured *Microcystis* colony size distribution in Lake Taihu (China), a shallow lake of 1.9 m mean depth, showing that small colonies ($< 36 \mu\text{m}$) are relatively well distributed over the mixing depth and large colonies ($> 120 \mu\text{m}$) concentrate near the surface. They suggest that large colonies show no or little density-change responses to light and therefore stay just below the surface. The dynamics of the cell-tissue density changes, reported by Visser *et al.* (1997) and applied in our model, is a continuous process, either storing carbohydrates or reducing them. With our mathematical model we can elucidate the vertical distribution for specific colony sizes dynamically changing their density under different environmental conditions. Investigation of the significance of colony size, cell to colony and gas vesicle to cell volume ratios for the vertical distribution of *Microcystis* is important for a more simplified concept applicable in three-dimensional computational models for management and forecasting.

Our goal was to investigate whether our new model can reproduce the observed concentration behavior qualitatively. For that, we applied our model to three Lakes in the Netherlands. Firstly, we consider the south basin of Lake Vlietland. During the summer of 2009, we monitored the temperature changes over its depth and used these measurements to validate our hydrodynamic model. In the past years, Lake Vlietland has shown serious effects of eutrophication leading to large bloom formation. The other two lakes are the small lake Vinkeveen and the large lake IJsselmeer. Ibelings *et al.* (1991) performed measurements on these lakes and reported the *Microcystis* vertical distribution variations over some 24 hour periods in the years 1988 and 1989.

2.2. Methods

The vertical column model (VC) consists of four components: 1) the $k-v$ turbulence model for the hydrodynamic component; 2) the cell-tissue density model (Visser *et al.*, 1997); 3) a model for the rising/sinking velocity of colonies in stagnant water, and 4) the Langevin-Fokker-Planck equation for the colony number concentration depending on water depth and cell-tissue density. The vertical distribution of colonies is obtained by solving the Langevin-Fokker-Planck equation (Section 2.4). To solve this equation the three models mentioned above for the rising/sinking velocity, cell-tissue density changes and turbulent diffusion are integrated in the Fokker Planck equation.

2.2.1 Hydrodynamic model

We shall neglect the role of vertical and horizontal circulation patterns in the lake and limit our analysis to vertical mixing only. For the hydrodynamic component we use a 1D vertical (1DV) version of the three-dimensional hydrostatic free-surface flow and transport solver DELFT 3D-FLOW of Deltares (Deltares, 2010). This model is based on turbulence-averaged properties and requires closures for turbulent mixing. The 1DV-model computes the vertical mixing and thermal stratification driven by atmospheric and solar conditions. For the application of the Langevin-Fokker-Planck equation, the 1DV-model provides the eddy diffusivity.

The 1DV-model solves the momentum equations (shallow water approximation) for the orthogonal horizontal velocity components (u, v) along x and y axis, averaged over turbulent motions:

$$\frac{\partial u}{\partial t} - f v + g \frac{\partial \eta}{\partial x} = \frac{\partial}{\partial z} \left\{ (\epsilon_k + \epsilon_t) \frac{\partial u}{\partial z} \right\} \quad , \quad (1)$$

$$\frac{\partial v}{\partial t} + f u + g \frac{\partial \eta}{\partial y} = \frac{\partial}{\partial z} \left\{ (\epsilon_k + \epsilon_t) \frac{\partial v}{\partial z} \right\} \quad , \quad (2)$$

where f is the Coriolis parameter, η is the water surface level, ϵ_k is the kinematic viscosity, ϵ_t is the eddy diffusivity and g is the gravitational acceleration, the z axis is positive upwards. We consider the sum of the kinematic viscosity of water and the eddy diffusivity to avoid low diffusion values whenever there is strong stratification that reduces the eddy diffusivity. Based on the dimensionless Kelvin number K , the Coriolis effect is included for the application to the 30 meter deep Lake Vlietland ($K = 0.4$) and Lake IJsselmeer ($K = 0.7$). The Kelvin number is defined as the ratio of the domain size and the Rossby radius and when it has a value much smaller than unity the Coriolis force can be neglected (Zhen-Gang, 2008). Equations (1) and (2) contain three unknown variables, in addition to these two equations the system is closed by the constraint that the depth averaged velocity for a lake should be zero. The sum of wind shear, bed shear and depth averaged velocity must cancel out because the vertical acceleration, horizontal density and horizontal velocity gradients are negligible.

The 1 DV-model uses the $k-v$ turbulence model including buoyancy effects (Rodi, 1980; Goudsmit *et al.*, 2002; Jöhnk *et al.*, 2008). The governing equations read

$$\epsilon_t = c_v \frac{k^2}{v} \quad , \quad (3)$$

$$\frac{\partial k}{\partial t} = \frac{\partial}{\partial z} \left(\frac{\epsilon_t}{\Gamma_k} \frac{\partial k}{\partial z} \right) + \epsilon_t D^2 - \frac{\epsilon_t}{\Gamma_p} N^2 - v \quad , \quad (4)$$

$$\frac{\partial v}{\partial t} = \frac{\partial}{\partial z} \left(\frac{\epsilon_t}{\Gamma_v} \frac{\partial v}{\partial z} \right) + c_{1v} k \left\{ D^2 - (1 - c_{3v}) N_{BV}^2 \right\} - c_{2v} \frac{v^2}{k} \quad . \quad (5)$$

In these equations we introduce the double contraction of the strain tensor D^2 , neglecting horizontal velocity gradients, according to

$$D^2 = \left(\frac{\partial u}{\partial z} \right)^2 + \left(\frac{\partial v}{\partial z} \right)^2, \quad (6)$$

and the Brunt-Väisälä frequency N_{BV} via

$$N_{BV}^2 = - \frac{g}{\rho_0} \frac{\partial \rho}{\partial z}. \quad (7)$$

Furthermore, k is the turbulent kinetic energy, ν is the energy dissipation and $c_p, c_{1v}, c_{2v}, c_{3v}, \dagger_p$ are well-defined constants (Rodi, 1980). These coefficients are derived from the theory for logarithmic boundary layers (Launder and Spalding, 1974). The coefficients \dagger_k and \dagger_ν are the turbulence Prandtl-Schmidt numbers for k and ν , respectively.

The density stratification in fresh water lakes is a known function of temperature for which the heat balance is solved ($H = \rho c_p T$). If stable density stratification occurs, turbulent mixing of heat and algae is suppressed. The heat distribution is described as

$$\frac{\partial H}{\partial t} = \frac{\partial}{\partial z} \left[\left(D_{mol} + \frac{\epsilon_t}{\dagger_T} \right) \frac{\partial H}{\partial z} \right] + Q, \quad (8)$$

where H is the heat content, c_p is the heat capacity of the water, D_{mol} is the molecular diffusion of heat, \dagger_T is the turbulent Prandtl number and Q represents heat sinks or sources. At the air-water interface and absorbed along the water depth (Secchi depth) the source of heat is solar radiation (short wave radiation and turbulent heat transfer through the atmospheric surface layer). The losses of heat are reflected shortwave radiation and outgoing long wave radiation whereas heat exchange occurs through free and forced convection of latent and sensible heat fluxes (Deltare, 2010).

The upper boundary conditions for the momentum are specified via surface stresses, viz.

$$(\epsilon_k + \epsilon_t) \frac{\partial u}{\partial z} = \frac{\dagger_{surf,u}}{\dots_o} \quad \text{and} \quad (\epsilon_k + \epsilon_t) \frac{\partial v}{\partial z} = \frac{\dagger_{surf,v}}{\dots_o}. \quad (9)$$

In these relations \dots_o is the reference density of water, $\dagger_{surf,u}$ and $\dagger_{surf,v}$ are the shear stresses at the lake surface parallel to the wind vector inferred from

$$\dagger_{surf} = \dots_{air} C_D U_{10}^2. \quad (10)$$

In Eq. (10) \dots_{air} is the density of air, C_D is the turbulent drag coefficient and U_{10} is the actual boundary condition given by the wind speed measured 10 m above the mean free surface (Smith and Banke, 1975). The drag coefficient C_D depends on the state of surface waves, on wind speed and on atmospheric stability. Our model includes a direct dependency on wind speed and not a dependency on atmospheric stability which would require the difficult determination of the Obukhov length scale (Arya, 2001).

The upper and bottom boundary conditions for the turbulent kinetic energy are given by

$$k_{surf} = \frac{u_{*s}^2}{\sqrt{c_-}} \quad \text{and} \quad k_{bed} = \frac{u_{*b}^2}{\sqrt{c_-}}. \quad (11)$$

Similarly, for the energy dissipation we use

$$\nu_{surf} = \frac{u_{*s}^3}{0.5 | z_s} \quad \text{and} \quad \nu_{bed} = \frac{u_{*b}^3}{| z_o}. \quad (12)$$

In these equations u_{*s} and u_{*b} are the shear velocities at the surface and at the bottom, respectively, $|$ is the Von Kármán constant ($| = 0.4$), z_s is the roughness of the surface water depending on wind and waves and z_o is the bed roughness length.

2.2.2 Model for cell-tissue density changes

Based on laboratory observations of the rate of change of *Microcystis* cell-tissue density (Fig. 2.2), Visser *et al.* (1997) approximates these rates as follows. The rate of change of the density is described by a function that increases until it reaches its maximum rate at 146 W m^{-2} and then decreases reaching negative rates (photoinhibition) when the radiation exceeds 600 W m^{-2} (Fig. 2.2a). These density changes occur under *light conditions* and the rate of change $\frac{d \dots_{cell}}{dt}$ of cell-tissue density by accumulation of carbohydrate is given by

$$\left(\frac{d \dots_{cell}}{dt} \right)_V = \frac{a}{60} I e^{-I/I_o} + d. \quad (13)$$

Wallace and Hamilton (1999) demonstrated that the accumulation of carbohydrate has a transient response time (τ_r) which is included in our model by computing the actual cell-tissue density rate of change as a weighted average of the density rate of change, according to Visser's formula, at the current and previous time step ($t, t-1$), through

$$\frac{d \dots_{cell}}{dt} = e^{-(t/\tau_r)} \left(\frac{d \dots_{cell}}{dt} \right)_V \Big|_{t-1} + (1 - e^{-(t/\tau_r)}) \left(\frac{d \dots_{cell}}{dt} \right)_V \Big|_t. \quad (14)$$

The transient response time (τ_r) in our model is chosen to be 1200 s (Wallace and Hamilton, 2000).

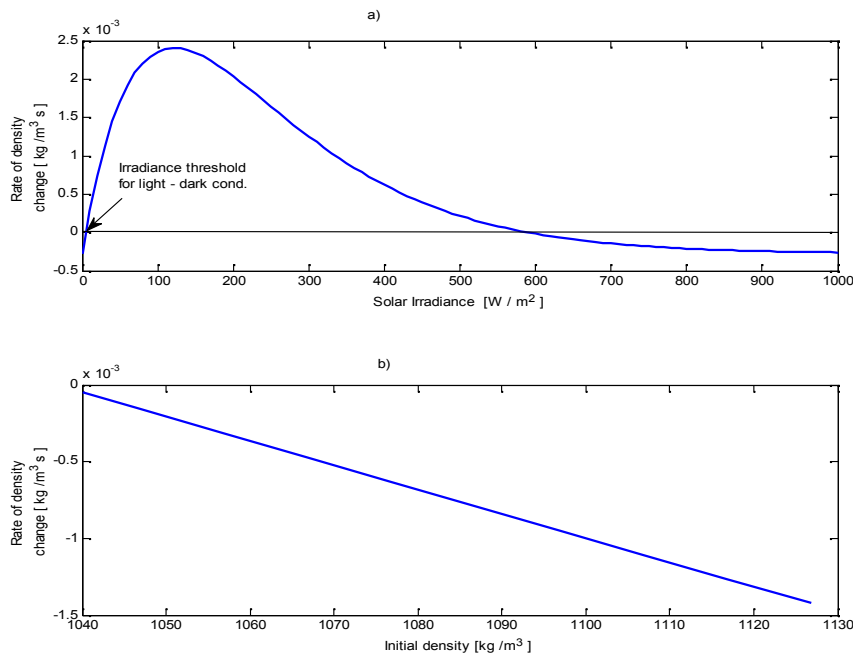


Figure 2.2: Rates of change in cell- tissue density. (a) Density changes against solar radiation (light conditions) and (b) Density changes against the initial colony density (dark conditions).

Under *dark conditions* (Fig. 2.2b) the decrease in cell-tissue density due to respiration depends on the actual cell-tissue density:

$$\left(\frac{d \dots_{cell}}{dt} \right)_V = -r (\dots_{cell} - \dots_{ref}). \quad (15)$$

In Eqs. (13), (14) and (15) $\left(\frac{d \dots_{cell}}{dt}\right)_V$ is the rate of density change in $\text{kg m}^{-3} \text{ s}^{-1}$ defined by Visser *et al.* (1997), $\frac{d \dots_{cell}}{dt}$ is the weighted average of the rate of density change, I is the irradiance, a is a normative factor, d is the rate of density change at $I=0$, I_o is the irradiance where $\dots_{cell}(I)$ is maximum, r is the slope and \dots_{ref} is the minimum cell density (1037 kg m^{-3}), below which the cells will not reduce their carbohydrate content. These constants were defined by Visser *et al.* (1997) and are listed in Table 2.1. The threshold between the light and dark regime has been defined at 5.75 W m^{-2} , corresponding to the intersection of the irradiance-response curve (Eq. 13) with the x axis at low values of photon irradiance (Visser *et al.* 1997). It is also common to convert solar irradiance, expressed in W m^{-2} to PAR (photosynthetic active radiation) expressed as $\mu \text{mol m}^{-2} \text{ s}^{-1}$ by multiplying the former by 1.895.

The light intensity along the water depth can be modeled according to the Lambert-Beer's law:

$$I(z) = I_s e^{-K_i z}, \quad (16)$$

where I_s is the irradiance at the surface and K_i is the extinction coefficient of the lake's water. We do not include the effect of self-shading (light extinction by colonies at lesser depths) although this effect could be included in Eq. (16) provided absolute colony concentrations are known.

2.2.3 The rising/sinking velocity of colonies in stagnant water

The rising/sinking velocity of a colony is estimated by Stokes' law for a sufficiently small and solid spherical particle in stagnant water:

$$\frac{dZ}{dt} = \frac{g d_c^2 (1 - \dots_{col} / \dots_w)}{18\epsilon}, \quad (17)$$

where d_c is the equivalent colony diameter (represented as a sphere), \dots_{col} is the density of the colony and \dots_w is the density of the water. For a buoyant colony $\dots_{col} < \dots_w$, Eq. (17) has a positive value, meaning that it floats upwards.

Table 2.1: Variables used in the hydrodynamic and buoyancy regulation models

Variable	Value	Unit
Extinction coefficient K_i (Vlietland)	-2 ^a	m ⁻¹
Extinction coefficient K_i (IJsselmeer)	-1.3 ^a	m ⁻¹
Extinction coefficient K_i (Vinkeveen)	-1.5 ^a	m ⁻¹
Density of water, \dots_w	998	kg m ⁻³
Minimum density, \dots_{\min}	996 ^b	kg m ⁻³
Maximum density, \dots_{\max}	1130 ^b	kg m ⁻³
Cell content in colony, n_{cell}	20 ^c	%
Gas content in cell, n_{gas}	7 ^c	%
Mucilage Density, \dots_{muc}	998+0.7 ^c	kg m ⁻³
<i>Buoyancy model</i>		
a	4.96 · 10 ⁻⁵ ^b	s ² m ⁻³
d	-2.75 · 10 ⁻⁴ ^b	kg m ⁻³ s ⁻¹
I_o	146.43 ^b	W m ⁻²
Γ	1.58 · 10 ⁻⁵ ^b	s ⁻¹
\dots_{ref}	1037 ^b	kg m ⁻³
\dagger_r	1200 ^d	s
a	from Measurements	
b	from Visser <i>et al.</i> (1997)	
c	from Reynolds <i>et al.</i> (1981)	
d	from Wallace and Hamilton (2000)	

The total mass of a single colony is the sum of cell mass, including its gas vesicles and the mass of the mucus in which the algae cells are imbedded:

$$\dots_{col} V_{col} = \dots_{cell} (V_{cell} - V_{gas}) + \dots_{gas} V_{gas} + \dots_{muc} V_{muc} \quad (18)$$

with \dots_{cell} the cell-tissue density, \dots_{muc} the mass density of the mucilage that creates the colony with *Microcystis* cells embedded, V_{col} the colony volume, V_{cell} the volume occupied by cells, V_{gas} the gas volume and V_{muc} the mucilage volume.

Considering n_{gas} equal to the ratio of gas vesicles volume to cell volume, n_{cell} the ratio of total cell volume to colony volume, and diving Eq. (18) by V_{col} we obtain the overall mass density of a colony

$$\rho_{col} = \rho_{cell} n_{cell} (1 - n_{gas}) + \rho_{muc} (1 - n_{cell}). \quad (19)$$

The values of n_{gas} and n_{cell} are kept constant for the simulations (Table 2.1).

By integrating Eqs. (13) or (15) in time, the cell-tissue density is known and after its substitution in Eq. (19) the colony mass density is dynamically determined. Substitution of the latter in Eq. (17) gives the rising/sinking velocity of the colony. This combination of models is applied in the following procedure that considers the dynamical evolution of an ensemble of colonies rather than applying particle tracking to the individual colonies.

2.2.4 The Langevin-Fokker-Planck approach applied to Microcystis colony concentrations

Firstly, we define a distribution function N being the fraction of colonies consisting of cells with cell-tissue density ρ_{cell} at depth level z and at time t . By this definition, the distribution varies along the cell-tissue density co-ordinate as well as along the physical depth co-ordinate z . For the latter, a model for the mean rising or sinking velocity is needed as well as for the turbulence mixing coefficient. The turbulence mixing diffusivity ϵ_t (see Eq. 3) is derived from the $k-v$ turbulence model given in Section 2.1. We assume that the turbulence mixing diffusivity ϵ_t is valid to estimate the dispersion of particles (colonies) having a size in the order of the Kolmogorov length scale. The rising/sinking velocity of the colonies is derived using Stokes' law (Eq. 17), valid for low particle Reynolds numbers, where the colony mass density depends on the cell-tissue density based on Visser's model (Eq. 19).

For changes along the cell-tissue density co-ordinate, the cell-tissue density model (Visser *et al.*, 1997) is applied (see Section 2.2) but without a mixing or dispersion coefficient representing different cell-tissue density rates among the colonies. The latter range is presently unknown but may be derived from the variance in the rate of change of cell-tissue density observed in the experiments of Visser *et al.* (1997).

The volumetric colony concentration number n [colonies m⁻³] at a certain depth z and time t is defined as:

$$n = \int_0^{\infty} N dz \dots \quad (20)$$

Due to mixing and vertical mobility, n varies along the depth h of the lake. Here, we introduce and include the lake's bathymetry *i.e.* depth-dependent surface area $A(z)$ (in m²). For the purpose of this study, we do not model growth, reproduction and mortality and therefore the number of colonies does not change, thus

$$\frac{d}{dt} \int_0^h n A(z) dz = 0. \quad (21)$$

This conservation of colonies limits our analysis to the vertical distribution of colonies depending on thermal stratification and relative to their volumetric concentration Eq. (20).

The Langevin - Fokker - Planck equation for the ensemble-averaged distribution function $\langle N \rangle (z, \dots_{cell}, t)$ reads (Risken, 1996)

$$\frac{\partial A \langle N \rangle}{\partial t} = - \left(\frac{dZ}{dt} \right) \frac{\partial}{\partial z} A \langle N \rangle - \left(\frac{d \dots_{cell}}{dt} \right) \frac{\partial}{\partial \dots_{cell}} A \langle N \rangle + \frac{\partial \epsilon_t}{\partial z} \frac{\partial}{\partial z} A \langle N \rangle. \quad (22)$$

The brackets operator indicates ensemble-averaging over turbulent motions as well as over cell-tissue density variations. Since N is a random function of cell-tissue density and vertical position, it is of interest to determine the average distribution function $\langle N \rangle$. The eddy diffusivity ϵ_t represents the vertical mixing of colonies by turbulence. As explained above, we neglect the dispersion of colony numbers along the \dots_{cell} axis by different density responses. $\frac{dZ}{dt}$ and $\frac{d \dots_{cell}}{dt}$ are the drift coefficients representing the mean vertical velocity (along the z - axis) and the mean density mobility (along the \dots - axis). The vertical velocity $\frac{dZ}{dt}$ is determined by Stokes' law depending on the individual colony mass density (Eq. 16). The rate of change of cell-tissue density $\frac{d \dots_{cell}}{dt}$ is given by Eqs. (13) and (15), where we used the

transient response time τ_r , see Eq. (14), to take into account some delay in carbohydrate accumulation.

For Lake Vlietland the coupled model was used to simulate the vertical distribution of 50, 200, 400 and 800 μm colony sizes. For each start of a simulation, the colony number $\langle N \rangle$ was set uniform along the vertical. The colony mass density was divided into 20 classes and varied between 996 and 1130 kg m^{-3} . The vertical distribution of *Microcystis* colonies is studied in detail with simulations for two periods of three consecutive days. The first period is characterized by high wind speeds starting on July 19 until July 21, 2009. The second period is characterized by low wind conditions starting on August 4 until August 6, 2009.

For Lake IJsselmeer we apply our model to compute the buoyancy sinking status of colonies of radii 20, 50, 70, 100, 150 and 200 μm . The vertical distribution is studied for the period September 20 – 21, 1988.

For Lake Vinkeveen we also consider colonies of radii 20, 50, 70, 100, 150 and 200 μm . The vertical distribution is studied for two periods, one in September 7 – 8, 1988 and the other one in August 23-23, 1989.

2.3 Study sites

2.3.1 Lake Vlietland

Lake Vlietland is located in the west of the Netherlands. The lake is used for recreational purposes. It consists of two basins: the northern basin which is 28 m deep (surface area: 0.8 km^2) and the south basin which is 36 m deep (surface area: 0.6 km^2). Both basins are connected by two shallow canals (see Fig. 2.3 for a map). The lake is holomictic with a seasonal cycle with a stratification period from late April until late October. The lake is connected to an extensive agricultural area providing an abundance of nutrients. Therefore, the lake is highly eutrophic and cyanobacterial blooms occur frequently and often lead to scum formation along the shores. About 80% of the cyanobacteria population during summer is composed of *Microcystis* species. No nutrient limitations occur during a *Microcystis* bloom (personal communication with Rijnland Waterboard).

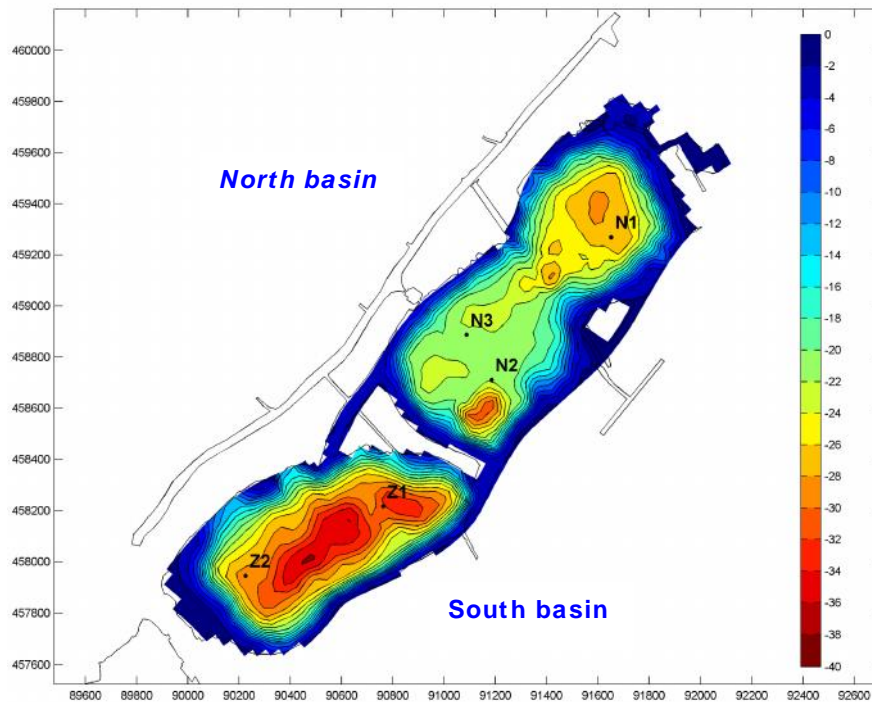


Figure 2. 3: Bathymetry of Lake Vlietland. N1, N2 and N3 are monitoring stations in the north basin. Z1 and Z2 are monitoring stations in the south basin.

Field measurements

Temperature measurements along the water depth were recorded with temperature loggers (Tidbits, HOBO). Three strings of temperature sensors were placed for continuous measurements with five minute intervals. In station N1 (see Fig. 2.3) a string of 10 tidbits located at several depths (0.5, 3.5, 6.5, 9.5, 12.5, 15.5, 18.5, 21, 24, 26 m). In station N2, 10 tidbits were located at the same depths as N1. In the south lake at Z1 a string of 8 tidbits were placed at depths of 0.5, 2.0, 6.0, 7.5, 9.0, 10, 12, 16 m, respectively. These measurements started in the middle of April and lasted until August 2009. The extinction coefficient (see Table 2.1) was computed after measuring under water light intensity on a weekly basis using a LI-COR 192 quantum meter. These measurements were performed from the beginning of May until August 2009.

Meteorological characteristics

Solar radiation, air temperature, relative humidity, cloudiness, wind speed and direction were obtained on an hourly basis from Valkenburg airport. These variables serve as input for the hydrodynamic model. The meteorological station is located 15 km from Vlietland. Fig. 2.4 shows the solar radiation and the wind speed for the two periods under investigation. The first one corresponds to high wind intensities starting on July 18 until July 21, 2009 (Fig. 2.4a). Wind intensities reach high values of 10 m s^{-1} , after midnight on July 19 wind speed reduces to 2 m s^{-1} , and then wind increases again. The solar radiation (Fig. 2.4c) shows some attenuation due to cloudiness during the first day and the other two days are characterized by clear sky conditions. The second period corresponds to low wind conditions and starts on August 4 until August 7, 2009. In this period the wind is on average less than 3 m s^{-1} (Fig. 2.4b). The solar radiation shows days with clear sky (Fig. 2.4d).

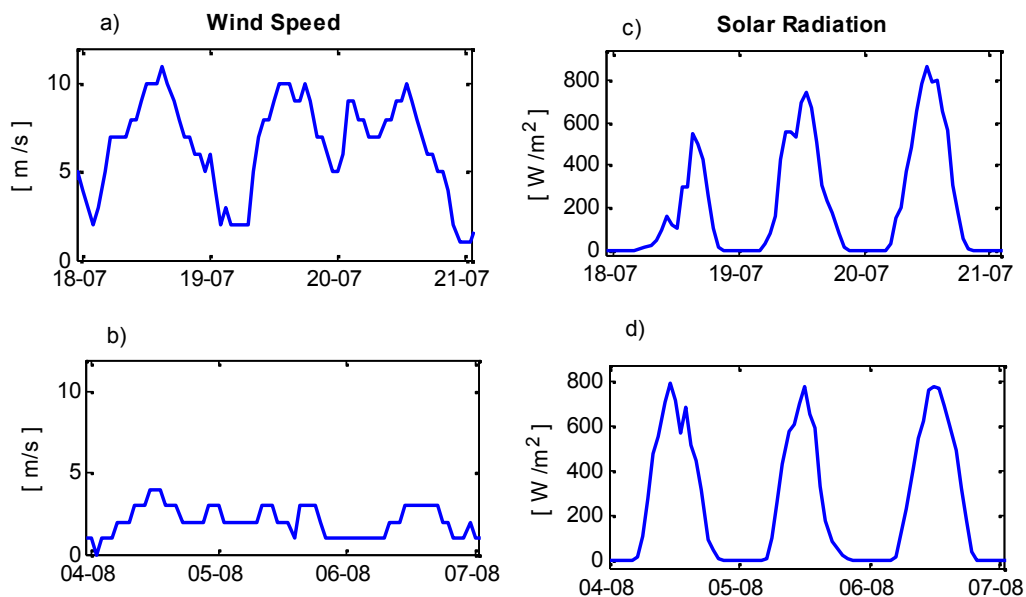


Figure 2.4: Meteorological characteristics applied to the entire Lake Vlietland. For two periods considered during summer 2009. (a) Wind speed for the period of high wind speeds [m s^{-1}], (b) Wind speed for the period of low wind speeds [m s^{-1}], (the error in the measurements reported by KNMI is 0.11 m s^{-1}) (c) Solar Radiation for the period of high wind speeds in [W m^{-2}] and (d) Solar Radiation for the period of low wind speeds in [W m^{-2}], (the error in the measurements reported by KNMI is 6 W m^{-2})

2.3.2 Lakes IJsselmeer and Vinkeveen

Lake IJsselmeer is the largest lake in the Netherlands and it has a surface area of 1190 km² (see Fig. 2.5 for a map). The average depth of the lake is 4.5 m. Ibelings *et al.* (1991) measured the buoyant status of *Microcystis* colonies during September 20 and 21, 1988. The meteorological information was obtained from Schiphol airport. The wind speeds during this period are low (max. 3.5 m s⁻¹) and the solar radiation is reduced (max. 320 W m⁻²) compared to typical summer values.



Figure 2.5: Location Map of Lake IJsselmeer.

Small - Lake Vinkeveen has an area of 0.6 km², the average depth is 3.9 m with a maximum depth of 14 m (see Fig. 2.6 for a map). Ibelings *et al.* (1991) measured several variables related to the buoyancy changes of *Microcystis* during September 7 and 8, 1988 and August 23 and 24, 1989. The meteorological information was obtained also from Schiphol airport. For the first period (September 7-8, 1988) wind speeds were equal to 4 m s⁻¹ and the solar radiation showed clear sky conditions. For the second period (August 23-24, 1989) wind speeds are low, reaching a value of zero at 3:00 am and the solar radiation shows some attenuation during the 23rd of August 1989.



Figure 2.6: Location Map of Lake Vinkeveen.

2.4. Entrainment Coefficient

The role of wind induced turbulence on the vertical distribution of colonies can be analyzed by means of the empirical entrainment coefficient \mathcal{E} (Humphries and Imberger, 1982), similar to the Rouse number for the characterization of suspended sediment,

$$\mathcal{E} = 15|w|/u_* , \quad (23)$$

where w is the vertical velocity of the sinking or buoyant colony and u_* is the friction velocity, being a characteristic scale velocity for turbulent motion (Humphries and Lyne, 1988), with,

$$u_*^2 = \frac{\rho_{air}}{\rho_w} C_D U_{10}^2 . \quad (24)$$

Here ρ_{air} is the density of the air, C_D is the drag coefficient (Smith and Banke, 1975), U_{10} is the wind speed at 10 m above the water surface and ρ_w is the density of water.

If $\mathcal{E} < 1$ then turbulent eddies are strong enough to entrain the colonies in the mixed water column, whereas if $\mathcal{E} > 1$ the distribution of the colonies is buoyancy dominated determined by their intrinsic rising/sinking velocity.

2.5. Results

2.5.1 Lake Vlietland

Temperature structure

We have modeled the temperature structure of Lake Vlietland at the deepest point from the 1st of January to the 15th of September 2009. The model did not require specific parameter calibration. Starting in the middle of April, the strong seasonal thermocline developed in the south basin. The seasonal thermocline is located approximately at 10 meters below the surface. Fig. 2.7 shows a comparison of the temperature profile modeled and measured for different days during 2009. In a qualitative sense, there seems to be a good agreement between measured and modeled water temperature, quantitatively the average Root Mean Square Deviation (RMSD) of the temperature model is 0.7 [°C]. This result gives us confidence in the model capacity to simulate the vertical characteristics of mixing within the lake. The model predicts a somewhat deeper thermocline than the measured one. This difference is usually related to the wind intensity, because the lake is surrounded by trees reducing wind intensity on its surface compared to the open area characteristics of the Valkenburg airport.

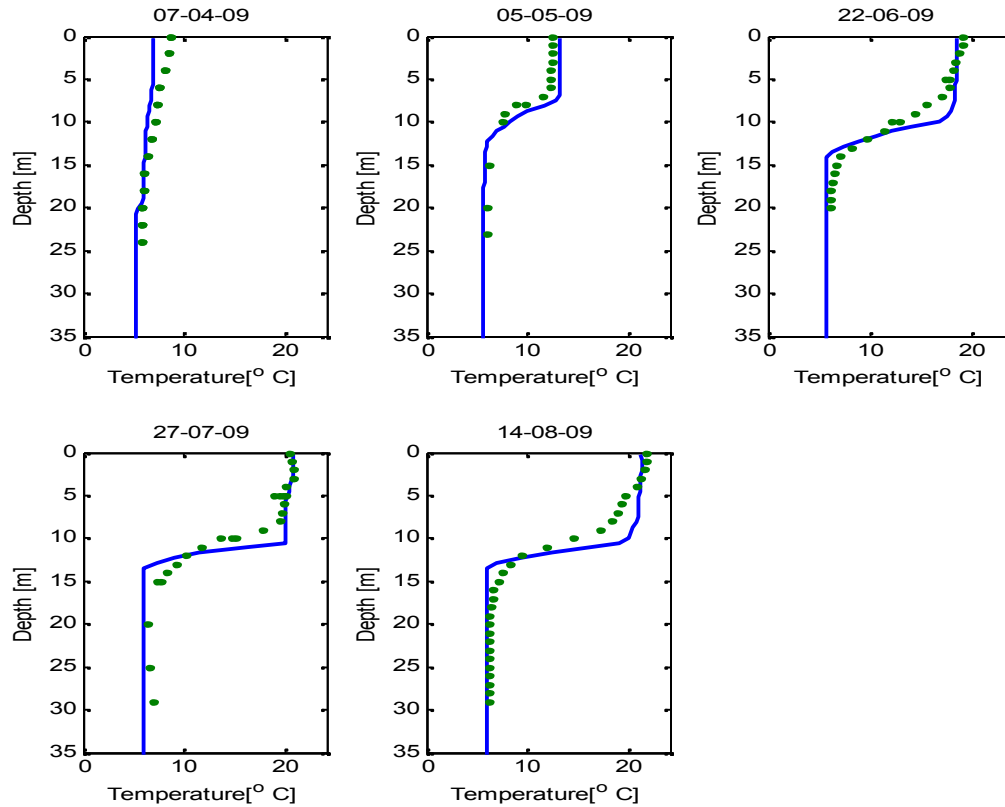


Figure 2. 7: Comparison of measured and modeled temperature profiles in Lake Vlietland. The continuous lines are the model results and the dots are measurements.

Vertical distribution of Microcystis

The parameters of the density changes model vary within ranges established in literature (Reynolds, 1981). The variation of these parameters, within their range (*e.g.* gas vesicle content), give a standard deviation lower than 5% in the resulting density variations.

The vertical migration patterns for colony sizes 50, 200, 400 and 800 μm is shown in Fig. 2.8. We have selected two scenarios to analyze the vertical distribution of *Microcystis* in relation to wind intensity:

a) High wind speeds ($> 7 \text{ m s}^{-1}$)

Figs. 2.8a, 2.8c, 2.8e and 2.8g show the vertical distribution of *Microcystis* during high wind speeds. For small colony sizes (50 μm) this means that they are well mixed over the epilimnion (Fig. 2.8a). Colonies of 200 μm show elevated concentration at the epilimnion level, following the diurnal cycle (Fig. 2.8c). Colonies

of 400 and 800 μm show subtle concentration at the epilimnion level (Figs. 2.8e and 2.8g).

b) *Low wind speeds* ($< 3 \text{ m s}^{-1}$)

Figs. 2.8b, 2.8d, 2.8f and 2.8h show the vertical distribution for low wind speeds. Colony sizes of 50 μm and 200 μm concentrate at 5 meters depth throughout the low wind period (Figs. 2.8b and 2.8d). Colonies of 400 μm show a daily pattern of movement and concentrate at the middle of the epilimnion (Fig. 2.8f), and colonies of 800 μm are dispersed over the epilimnion and concentrate temporarily just below the surface of the lake (Fig. 2.8h).

In general, the *migration depth* of the colonies with a size less than 200 μm is the same as the depth of the epilimnion. Larger colonies show a daily migration that goes deeper than the thermocline (*e.g.* 800 μm). Due to their large size and rising/sinking velocity, they are able to sink or rise through the thermocline and migrate over longer vertical distances. The *Microcystis concentration depths* also vary for the different colony diameters. Small colonies concentrate at 5 m depth (Figs. 2.8b, 2.8d, 2.8f), while colonies of 800 μm show higher concentration close to the surface (Fig. 2.8h).

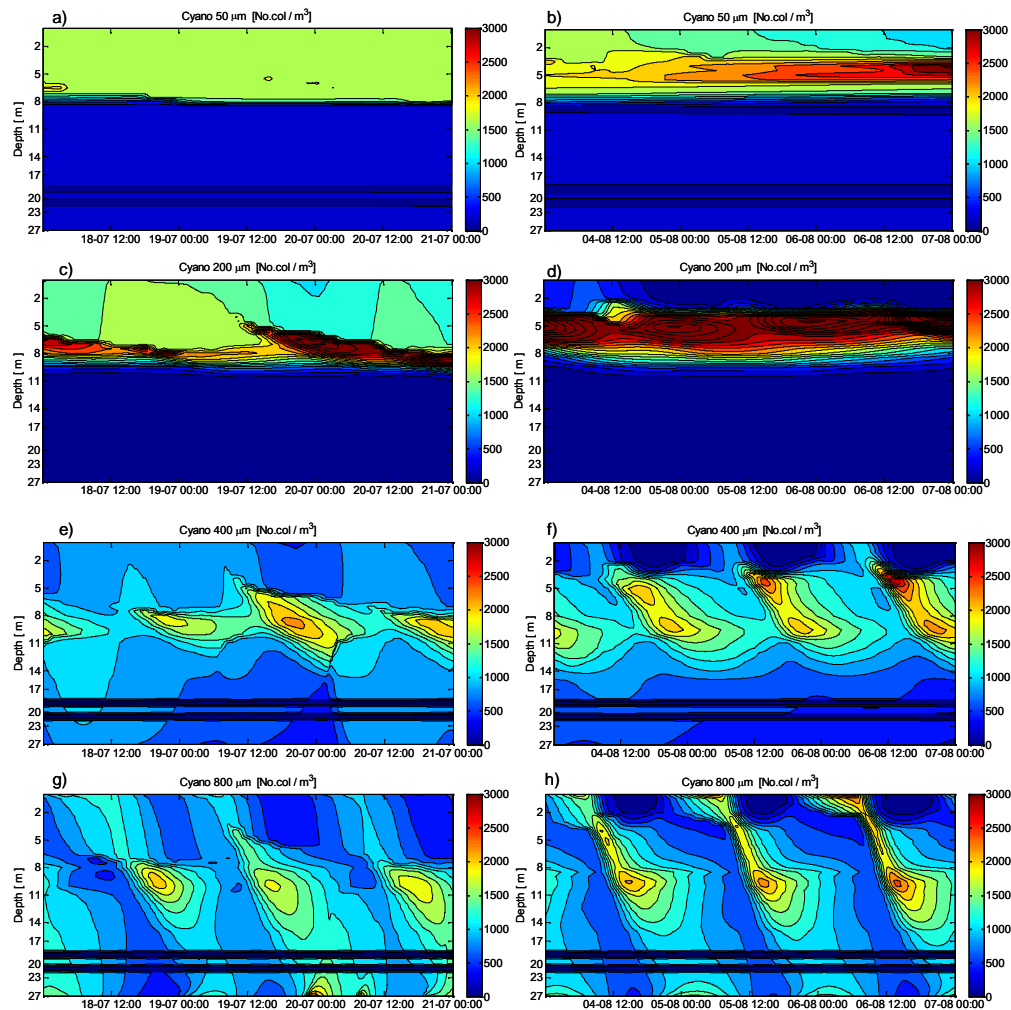


Figure 2.8: Vertical distribution of *Microcystis* colonies in Lake Vlietland. Left panels corresponds to high wind speed conditions and right panels corresponds to low wind conditions. a), b) Colonies of 50 μm , c), d) colonies of 200 μm , e), f) colonies of 400 μm , g), h) colonies of 800 μm . Color bar indicates relative colony number density. Red indicates high concentration, blue indicates low concentration.

Fig. 2.9 shows the concentration profile of different colony sizes (50, 200, 400 and 800 μm) at different times of a low wind speed day (6th of August). Colonies of 50 μm remain highly concentrated at the middle of the epilimnion increasing its concentration somewhat after receiving light during the morning. Colonies of 200 μm shows similar behavior as smaller colonies, except that their concentration peak at 5 meters depth is much higher than 50 μm colonies. Colonies of 400 μm start the day relatively uniform along the mixing depth of the lake. By midday their concentration is higher at 5 meters below the surface and this peak lowers to reach high concentrations at 10 meters by midnight. The 800 μm colonies show sharp

variations, at the beginning of the day they are distributed over the entire depth, before sunrise the concentration near the surface is high. Throughout the day the peak of the concentration lowers until the distribution becomes nearly uniform by the end of the day.

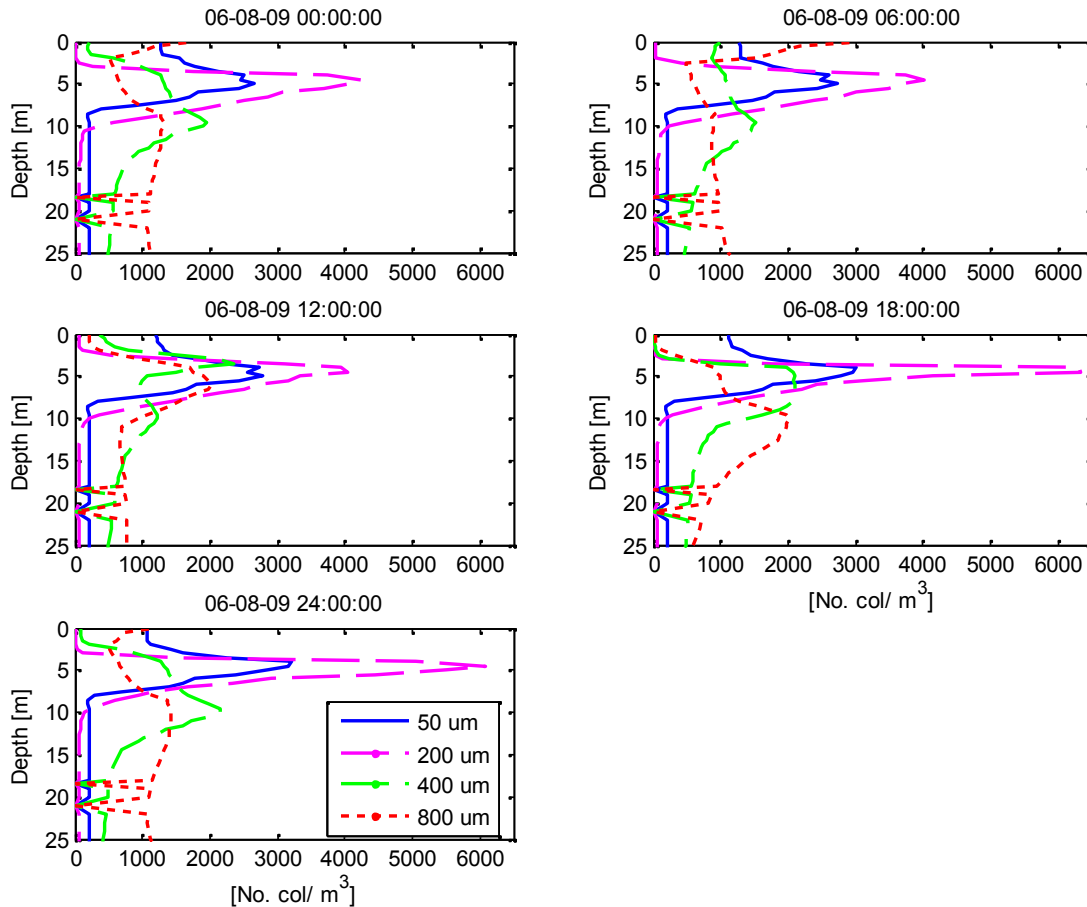


Figure 2. 9: Daily variation in concentration profiles for colonies of 50, 200, 400 and 800 μm , at four moments during the 6st of August 2009 for Lake Vlietland.

Entrainment coefficient

According to the definition of colony mass density variation in section 2.4 the density is subdivided in twenty ranges over a maximum density value of 1130 kg m^{-3} and a minimum of 996 kg m^{-3} . For each density value the respective colony vertical velocity is estimated using Eq. (17). Therefore, each colony size has one maximum and minimum speed. Fig. 2.10 shows the variation of the entrainment coefficient for colony sizes of 50 and 200 μm , based on these maximum and minimum speeds. For colonies smaller than 200 μm , the entrainment coefficient is less than unity,

suggesting that their vertical distribution is determined by the turbulent environment. Colonies of 200 μm show opposite results for its maximum and minimum density values. This means that for colonies of this size its distribution is determined by a combination of the turbulent environment and its buoyancy status. Larger colonies ($>200 \mu\text{m}$) have an entrainment coefficient exceeding unity, suggesting that their vertical distribution is determined mainly by their cell-tissue density buoyancy status.

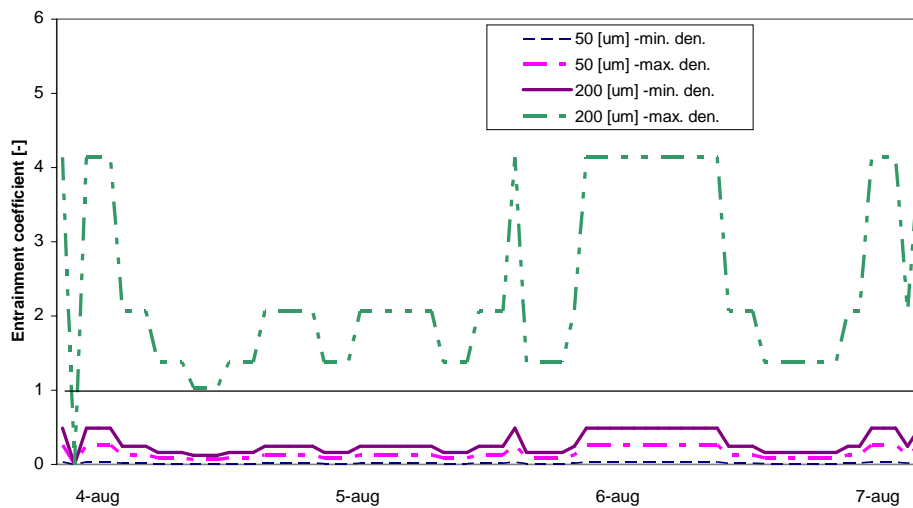


Figure 2. 10: Variation of the upward entrainment coefficient for low wind conditions. For colonies velocities corresponding to 50 and 200 μm with their maximum and minimum density. The horizontal line corresponds to the threshold of one for either turbulence or colony velocity dominated distribution.

2.5.2 Lake IJsselmeer

We modeled the temperature structure of the shallow Lake IJsselmeer over the 24 hr period of measurement (September 20-21, 1988). The temperature is nearly uniform with very subtle temporal stratification at 16:00 hrs. The shallowness of the lake, *i.e.* bed generated turbulence, reduces its possibilities to develop a seasonal thermocline.

Fig. 2.11a shows the measured percentage of sinking colonies of *Microcystis* redrawn from Ibelings *et al.* (1991) and Fig. 2.11b shows our model results for the percentage of sinking colonies. The maximum sinking colonies were measured at around 19:00 h while our model shows this peak at 16:00 h. At night from 0:00 to 8:00 h most of the colonies are in rising mode and this behavior is well represented

in our model. Such behavior corresponds to the decrease of colony mass density under dark conditions defined by Visser's model. Later in the morning, the measurements show an increment on sinking colonies at 10:00 h and our model is somewhat delayed and shows this increase at 14:00 h.

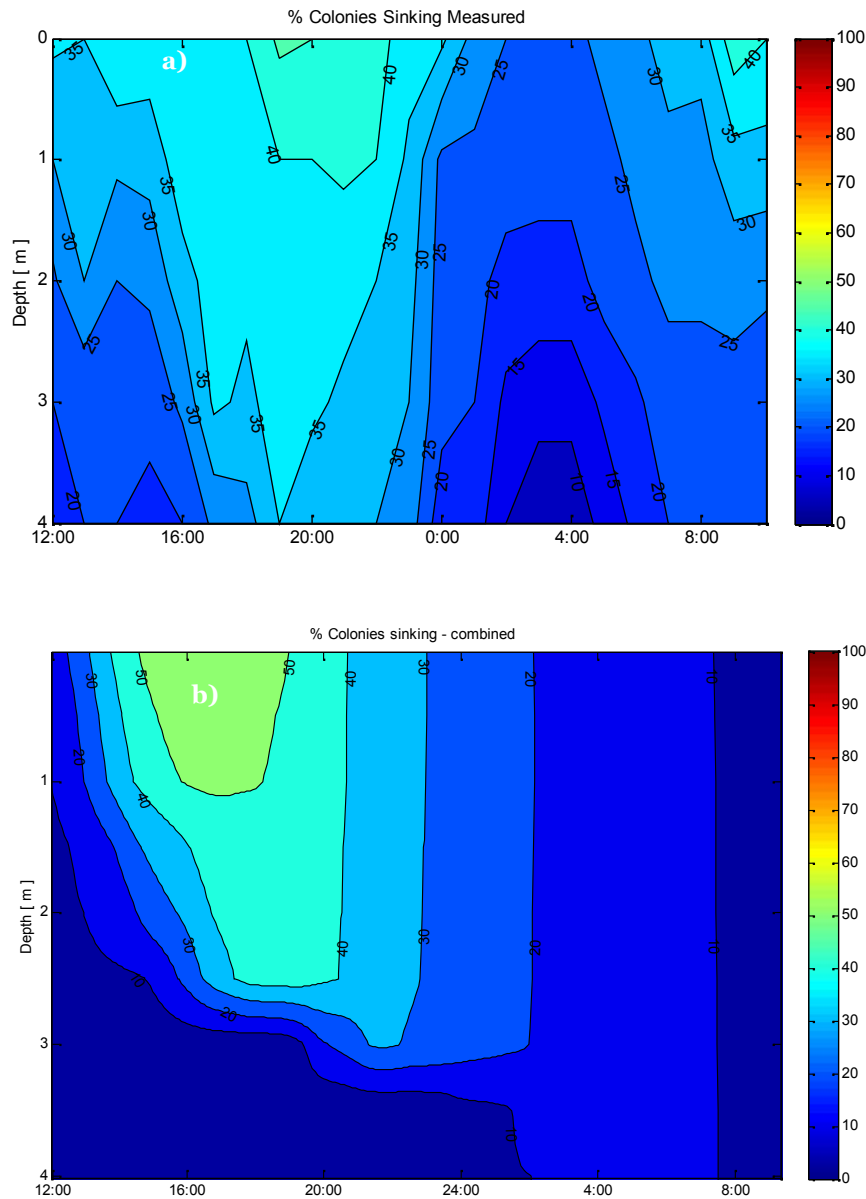


Figure 2.11: Changes of buoyancy with time and depth in Lake IJsselmeer on September 20-21, 1988. (a) Measured by Ibelings et al. (1991) and (b) modeled by the presented model.

2.5.3 Lake Vinkeveen

We have modeled the temperature of Lake Vinkeveen during September 7 -8, 1988 and during August 23-24, 1989. In September 1988 the thermocline is located at 12 meters. At this time of the year the seasonal thermocline deepens due to the lower input of solar radiation. In August 1989 the thermocline is located at 7 meters depth.

The comparison between measured and modeled temperature for two days, one in 1988 and one in 1989 is shown in Fig. 2.12. The comparison shows a good qualitative agreement and a good representation of the thermocline level which defines the mixing zone. The RMSD of the model is 1.3 [°C].

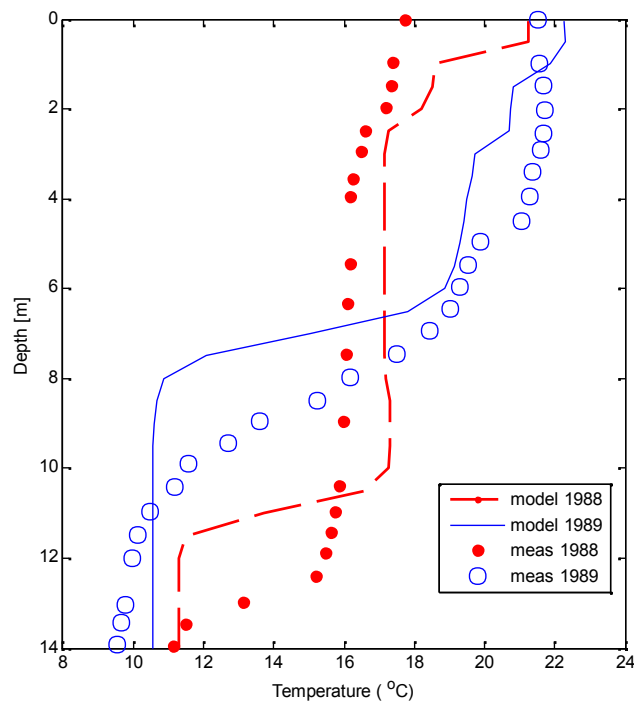


Figure 2.12: Comparison of modeled and measured temperature for September 7,1988 at 19:30 and for August 23, 1989 at 18:15.

Ibelings *et al.* (1991) measured the colony-size distribution in Lake Vinkeveen. The results are shown in Fig. 2.13 where a distinction has been made between the colony size distribution close to the surface (Fig. 2.13a) and at a depth of 8 m (Fig. 2.13b). For our computation we can not include this distribution a priori, therefore we run several simulations for representative colony sizes (20, 50, 70, 100, 150 and 200 μm) and weight them based on the size distributions shown in Fig. 2.13.

The measured percentage of sinking colonies through the period September 7-8 (1988) is displayed in Fig. 2.14a and Fig. 2.14b shows the modeled sinking colonies percentage. The higher levels of sinking percentage of colonies from 16:00 to 20:00 h is well captured by our model. Nevertheless, also some differences are visible. The measurements show the presence of sinking colonies at levels deeper than two meters while our simulations show that below two meters most of the colonies are in rising mode.

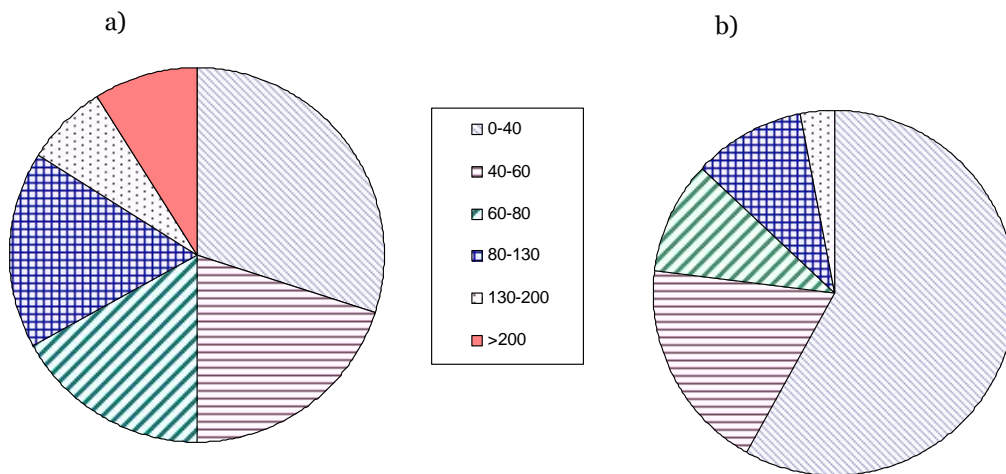


Figure 2.13: Size distribution of *Microcystis* colonies (number indicate the size in μm) measured in Lake Vinkeveen, 1988. (a) Colonies near the surface, (b) Colonies at 8 m depth. Data from Ibelings *et al.* (1991).

Fig. 2.15 shows the comparison of modeled and measured sinking colonies percentage near the surface (Fig 2.15a) and at 8 meters depth (Fig. 2.15b). In a qualitatively sense our model reproduces the variations of sinking colonies percentage well. Our model overestimates the sinking percentage close to the surface by 20% after midday and shows that during night algae are mainly on rising mode (in agreement with observations), the RMSD of the model is 16% of sinking colonies. At a depth of 8 meter the trend of observational and modeled data show reasonable agreement, the RMSD is 3% of sinking colonies (note that we are considering small percentage of sinking colonies, which gives uncertainty in the data).

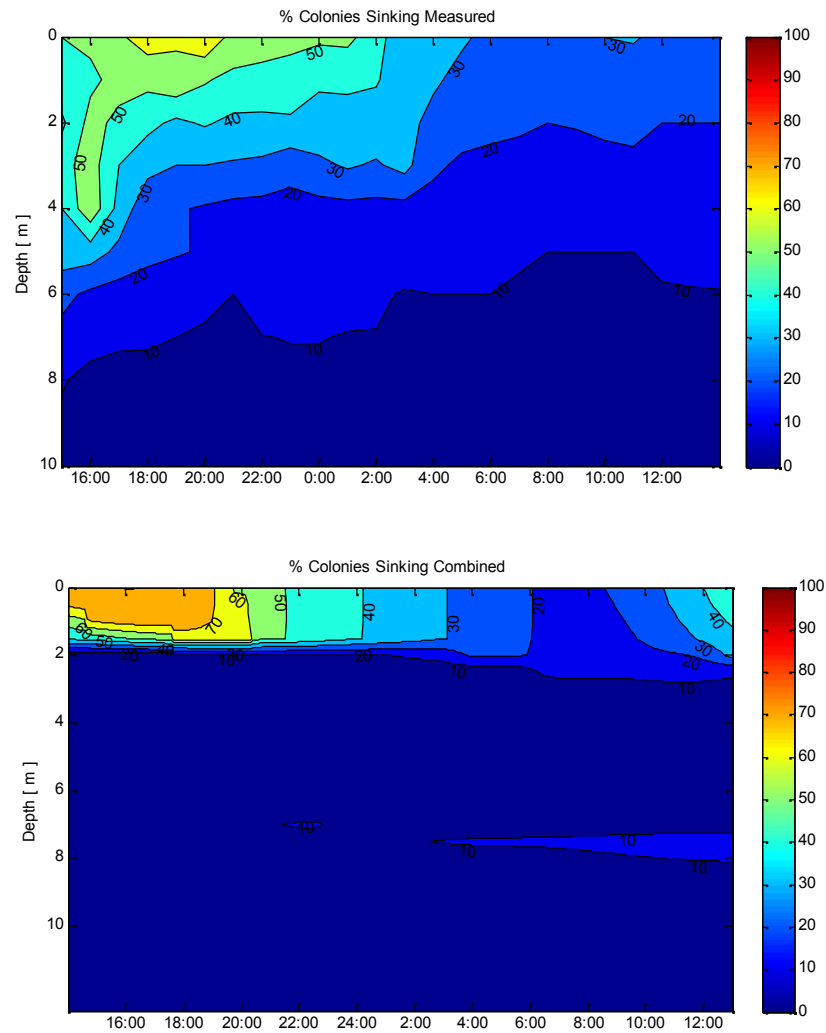


Figure 2.14: Changes of *Microcystis* buoyancy status in time and depth in Lake Vinkeveen on September 7-8, 1988. (a) Measured by Ibelings *et al.* (1991) and (b) modeled by the presented model.

Based on the data from the period of August 23-24, 1989 Ibelings *et al.* (1991) measured the vertical distribution of colonies concentration of *Microcystis*. Fig. 2.16 shows the comparison of these measurements with data from our model. Our model captures the concentration variation during this 24 hour period, except the measured peak of colonies near the surface at 3:00 h which is a result of very low wind conditions (nearly zero), the RMSD of the model is 60 colonies/ml.

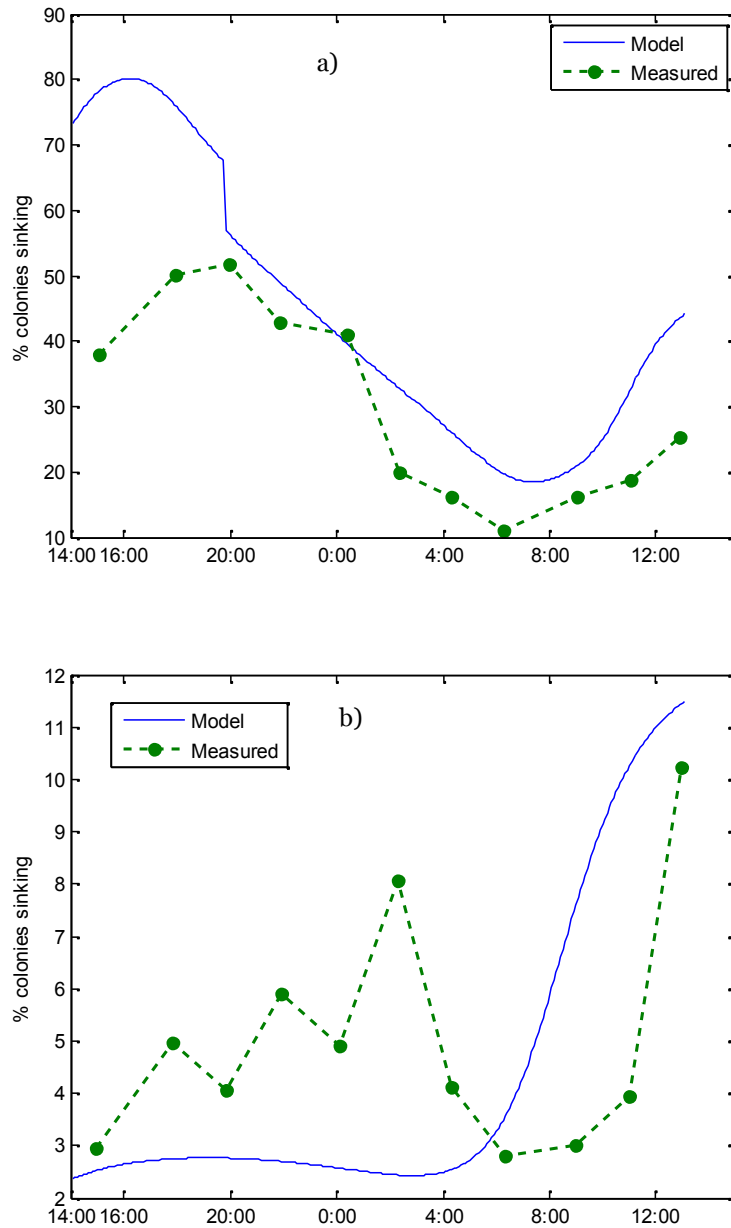


Figure 2.15: (a) Comparison of modeled and measured changes of buoyancy near the surface in Lake Vinkeveen on September 7-8, 1988. (b) Comparison of modeled and measured changes of buoyancy at 8 m depth in Lake Vinkeveen on September 7-8, 1988. (Note that it was verified that typical changes in model outcome due to realistic variations in colony composition (Reynolds, 1981) are small, $\sim <5\%$ (not shown here)).

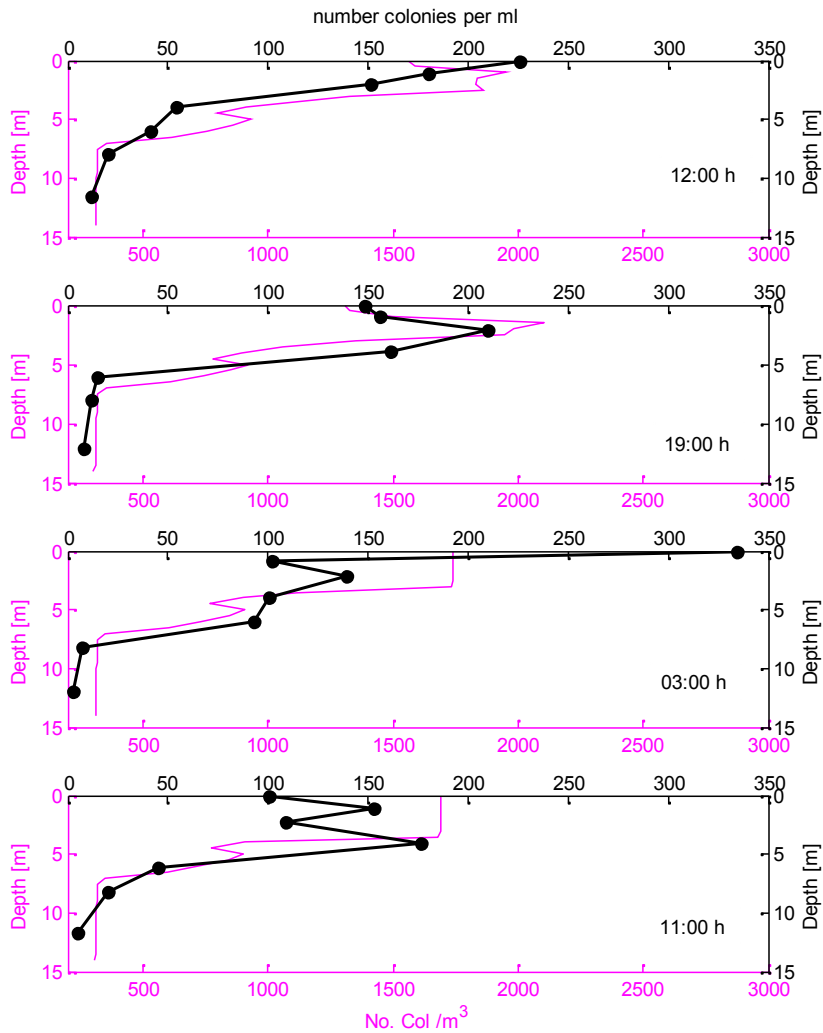


Figure 2. 16: Comparison of modeled and measured changes of vertical distribution of *Microcystis*. Lake Vinkeveen 23-24 August 1989. The dots in are measurements Ibelings *et al.* (1991) and continuous line are model results.

2.6. Discussion and Conclusions

Our model results have been compared with detailed measurements and they agree with observations that the diurnal patterns of *Microcystis* vertical distribution are different depending on colony size and wind speed.

The detailed measurements performed by Ibelings *et al.* (1991) in two lakes in the Netherlands provided a comprehensive data set to compare our model capabilities to real measurements. Through such a comparison we show that within the simplifications of our model the specific features of diurnal vertical migration of

Microcystis are captured satisfactorily. The reached agreement provides confidence to further analyze the insights of the processes responsible for the vertical distribution of colonies.

The response of colony distribution to wind speeds in Lake Vlietland leads to the following distinction. During low wind speeds (lower than 3 m s^{-1}) small colonies concentrate at the middle of the epilimnion and large colonies concentrate temporarily just below the surface. Strong wind creates entrainment and disperses the colonies of all sizes studied spread over the epilimnion. These qualitative results confirm the fast colony dispersion in response to high wind intensities as reported after field measurements by Reynolds (1976) and Moreno–Ostos *et al.* (2009) among others.

The position of large colonies ($>200 \text{ }\mu\text{m}$) is determined by their sinking/rising speeds that override turbulent entrainment velocity, this conclusion is supported by the entrainment coefficient results (Fig. 2.10). The floating and sinking speeds considered in our study were estimated using Stokes' law. For large colonies ($800 \text{ }\mu\text{m}$), sinking velocities as large as 5.5 mm s^{-1} (400 m day^{-1}) were used whereas the maximum velocity measured is 3.3 mm s^{-1} (285 m day^{-1}) (Reynolds, 1987). These large computed velocities make the colonies to travel such long distances in short times. The validity of Stokes' law is in the regime with Reynolds number less than 0.1, which holds for colony radii less than $100 \text{ }\mu\text{m}$ (Reynolds, 1984; Visser *et al.*, 1997). Applying Stokes' law for larger colony sizes leads to over prediction of actual rising/sinking speeds. Considering a non-linear drag model could help to improve determinations of colony velocities with high Reynolds numbers, for instance for a Reynolds number of 3 (*e.g.* $800 \text{ }\mu\text{m}$ colony) the terminal velocity would be reduced by 15%.

Our model provided explanations for several field observations of *stationary behavior* and *physiological suppression*. The detailed observations made by Reynolds (1973) in Crose Mere (England) showed that *Microcystis* stay at the lower epilimnion during the growth stage, when colony sizes are of order $100 \text{ }\mu\text{m}$. Reynolds (1973) attributes this concentration to an effective *stationary behavior* through buoyancy control. In our simulations we observe the same behavior for colony sizes

lower than 400 μm , suggesting that the apparent *stationary behavior* corresponds to an equilibrium depth where colonies concentrate that are continually rising and sinking. There are a few detailed observations on the colony size distributions during blooms. Wu and Kong (2009) using measurements in Lake Taihu have shown that large colonies ($> 120 \mu\text{m}$) concentrate near the surface on low wind days and they suggest that the reason is a possible suppression of their *physiological response* to light intensity. In contrast, in our model, the colony mass density changes dynamically and continuously in response to the light environment and their large concentration close to the surface is a result of its buoyancy changes and the turbulent environment.

The vertical distribution dynamics shown in our simulations suggest that there is an optimal size for colonies through their growth. At the beginning of their growth stage, colonies around 100 μm concentrate at the lower epilimnion. In later stages, due to multiplication of cells within colonies (growth), larger colonies are able to travel larger distances and access lower depths where nutrients are plenty.

Only few studies have analyzed the effects of turbulence on the vertical distribution of *Microcystis* in deep lakes. Howard *et al.* (1996) studied the vertical migration of small colony sizes (200 μm) under turbulent conditions. The model applies simple relations for carbohydrate accumulation and respiration. Their results reproduce the daily vertical migration reported after observations (Reynolds, 1984), but the influence of colony sizes was not investigated in their simulations. Wallace *et al.* (2000) simulate the vertical distribution of *Microcystis* for a shallow lake, and the emphasis of their investigation is on the importance of the delay time for carbohydrate accumulation (Wallace and Hamilton, 1999). This delay time is included in the presented model. Our results support the conclusion of Wallace *et al.* (2000) that large colonies, *i.e.* 400 μm , are able to overcome the entrainment forces of turbulence.

We conclude that the model approach presented is a step forward to previous contributions to analyze the vertical distribution of an ensemble of *Microcystis* colonies and not only its vertical depth migration. We have shown that our modeling method allows for the investigation of the vertical distribution of *Microcystis*

colonies under natural turbulent conditions. Our approach carefully allows for varying the colony composition (*i.e.* gas vesicles in cells and cells embedment in mucilage) and applies the cell-tissue density changes. We also have shown that the vertical distribution of *Microcystis* varies between colony sizes and that it is important to incorporate size distribution in realistic modeling.

Acknowledgments

This research was supported by a grant from Deltares (Deltares project numbers 1202633 and 1202837.005). We would like to thank Leo Postma and Hans Los from Deltares and Bas Ibelings from NIOO for their help and discussions. We would also like to thank to the Water Board of Rijnland for sharing data on measurements in Lake Vlietland, especially to Johan Osterbaan, Dianne Slot and Jasper Stroom.

2.7 References

- Arya, S.P., 2001. Introduction to Micrometeorology. Second Edition (International Geophysics), Academic Press.
- Chorus, I. and Bartram, J., 1999. Toxic Cyanobacteria in Water: a Guide to Public Health Significance, Monitoring and Management. Für WHO durch E & FN Spon /Chapman & Hall, London, 416 pp.
- Codd, G.A., 1999. Cyanobacterial toxins: their occurrence in aquatic environments and significance to health. In: Charpy L, Larkum AWD (eds) Marine cyanobacteria. *Bulletin de l'Institut Océanographique, Monaco, 19*, 483–500.
- Chen, Y., Qian, X., Zhang, Y., 2009. Modelling turbulent dispersion of bouyancy regulating cyanobacteria in Wind driven currents. *Bioinformatics and Biomedical Engineering* , 2009. ICBBE 2009. 3rd International Conference. Page 1-4.
- Deltares, 2010. User Manual Delft3D-Flow. Ver 3.14. Delft, The Netherlands: Deltares.
- Ganf, G.G. and Oliver, R. L., 1982. Vertical separation of light and available nutrients as a factor causing replacement of a green alga by blue green algae in the plankton of a stratified lake. *Journal of Ecology* , 70, 829-844.
- Goudsmit, G.H., H. Burchard, F. Peeters, and A. Wüest, 2002. Application of k- turbulence models to enclosed basins: The role of internal seiches, *Journal of Geophysical Research*, 107, 3230.
- Howard, A., 1997. Computer simulation modelling of buoyancy change in *Microcystis*. *Hydrobiologia*, 349, 111-117.
- Huisman, J., Arraya's, M., Ebert, U., Sommeijer, B., 2002. How do sinking phytoplankton species manage to persist? *The American Naturalist*, 159, 245– 254.
- Humphries, S., Imberger, J., 1982. The influence of the internal structure and the dynamics of Burrinjuck reservoir on phytoplankton blooms. Univ. W. Aust., Environ. Dynam. Rep. ED-82-023.
- Humphries, S., Lyne, D., 1988. Cyanophyte blooms: The role of cell buoyancy. *Limnology and Oceanography*, 33, 79-91.
- Ibelings, B. W., L. R. Mur, and A. E. Walsby, 1991. Diurnal changes in buoyancy and vertical distribution of *Microcystis* in two shallow lakes. *Journal of Plankton Research* 13, 419-436.
- Ibelings, B. W., 1996. Changes in photosynthesis in response to combined irradiance and temperature stress in cyanobacterial surface waterblooms. *Journal of Phycology*, 32, 549-557.
- Imberger, J., and P. E Hamblin, 1982. Dynamics of lakes, reservoirs and cooling ponds. *Annual Review of Fluid Mechanics*, 14, 153-187.

- Imberger, J., 1985. Thermal characteristics of standing waters: an illustration of dynamic process. *Hydrobiologia*, 125,7-29.
- Jöhnk, K.D., Huisman, J., Sommeijer, B., Sharples, J, Visser, P.M., Stroom, J., 2008. Summer heatwaves promote blooms of harmful cyanobacteria. *Global Change Biology*, 14, 495-512.
- Jöhnk, K.D. and Umlauf, L., 2001. Modelling the metalimnetic oxygen minimum in a medium sized alpine lake. *Ecological Modelling*, 136, 67–80.
- Lauder, B.E., Spalding, D.B., 1974. The numerical computation of turbulent flow. *Computer Methods in Applied Mechanics and Engeneering*, 3,269–289
- Moreno-Ostos, E., Cruz-Pizarro, L., Basanta, A., Glen, D.G., 2009. The influence of wind induced mixing on the vertical distribution of buoyant and sinking phytoplankton species. *Aquatic Ecology*, 43, 271-284.
- Oliver, R L. and Walsby, A.E., 1984. Direct evidence for the role of light-mediated gas vesicle collapse in the buoyancy regulation of *Anabaena flos-aquae* (cyanobacteria). *Limnology and Oceanography*, 29, 879-886.
- Rabouille, S. and Salencon, M.J., 2005. Functional analysis of *Microcystis* vertical migration: A dynamic model as a prospecting tool -II- Influence of mixing, thermal stratification and colony diameter on the biomass production. *Aquatic Microbiology Ecology*, 39, 281-292.
- Reynolds, C.S and Walsby, A.E., 1975. Water-blooms. *Biology Reviews*, 50, 437-481.
- Reynolds, C.S., D.A. Rogers, 1976. Seasonal variation in the vertical migration and buoyancy of *Microcystis aeruginosa* kutz . emend. elenkin in Rostherne mere, England. *Hydrobiologia*, 48, 17-23.
- Reynolds, C. S., G. H. M. Jaworski, H. A. Cmiech and G. F. Leedale, 1981. On the annual cycle of the blue-green alga, *Microcystis aeruginosa* Kutz. emend. Elenkin. *Philosophical Transactions of the Royal Society B* 293, 419–477.
- Reynolds, C. S., 1987. Cyanobacterial water-blooms. Pages 67-139 in J. A. Callow, editor. *Advances in botanical research*. Academic Press, London, UK.
- Reynolds, C.S.,1984. *The Ecology of Freshwater Phytoplankton* Cambridge University Press, Cambridge.
- Risken, H.,1996. *The Fokker Planck equation*. Springer.
- Rodi, W., 1980. *Turbulence Models and their Application in Hydraulics a State-of-the-Art Review*. IAHR Monograph. IAHR, Delft, The Netherlands.
- Sirenko, L. A., 1972. Physiological basis of multiplication of blue-green algae in reservoirs. (In Russian). Naukova Dumka, Kiev, 162 pp.
- Smith, S. D. and Banke, E. G., 1975. Variation of the Sea Surface Drag Coefficient with Wind Speed. Quart.I. *Royal Meteorological Society*, 101, 665-673.

- van Rijn, J. and Shilo, M., 1985. Carbohydrate fluctuations, gas vacuolation and vertical migration of scum forming cyanobacteria in fish ponds. *Limnology and Oceanography*, 30, 1219-1228.
- Verspagen, J. M. H., E. O. F. M. Snelder, Visser, P. M., Huisman, J., Mur, L. R., and Ibelings, B. W., 2004. Recruitment of benthic *Microcystis* (Cyanophyceae) to the water column: internal buoyancy changes or resuspension?. *Journal of Phycology* 40.
- Visser, P.M., 1995. Growth and vertical movement of the cyanobacterium *Microcystis* in stable and artificially mixed water columns. PhD Thesis, University of Amsterdam .
- Visser, P. M., J. Passarge, and L. R. Mur, 1997. Modelling the vertical migration of the cyanobacterium *Microcystis*. *Hydrobiologia* 349,99-109.
- Wallace, B. B. and D. P. Hamilton, 2000. Simulation of water-bloom formation in the cyanobacterium *Microcystis aeruginosa*. *Journal of Plankton Research*, 22, 1127–1138.
- Wallace, B.B., Bailey, M., Hamilton, D.,2000. Simulation of vertical position of buoyancy regulating *Microcystis aeruginosa* in a shallow eutrophic lake. *Aquatic Science*, 62,320–333.
- Walsby, A.E., 1994. Gas Vesicles. *Microbiological Reviews*, 58, 94-124.
- Walsby, A.E.,2005. Stratification by cyanobacteria in lakes: a dynamic buoyancy model indicates size limitations met by *Planktotrix rubescens* filaments. *New Phytologist* 168, 365-376.
- Wu, X. and Kong, F., 2009. Effects of light and wind speed on the vertical distribution of *Microcystis aeruginosa* colonies of different sizes during a summer bloom. *Hydrobiologia*, 94, 258-266.
- Zhen-Gang, J., 2008. Hydrodynamics and water quality, modelling rivers, lakes and estuaries. John Wiley & Sons.
- Zohary T. and Robarts D. ,1989. Diurnal mixed layers and the long term dominance of *Microcystis aeruginosa*. *Journal of Plankton Research*, 11, 25-48.

Chapter 3

Simulations of the diurnal migration of *Microcystis aeruginosa* based on a scaling model for physical-biological interactions¹

¹ The contents of this chapter, with minor modifications, have been submitted in the form of a paper to Theoretical Biology.

Abstract

In this study we introduce a formal scaling method for the speed up of biological assimilation/respiration processes to allow simulations of the dynamics of vertical migration of the cyanobacterium *Microcystis aeruginosa* colonies under turbulent flow conditions. We apply Direct Numerical Simulations (DNS) and the proposed scaling method allows calculation of full biological cycles within the computational constraints. The *Microcystis* colonies are subjected to homogeneous isotropic three-dimensional turbulence and their trajectories are computed with a particle tracking algorithm. The latter is based on a simplified version of the Maxey-Riley equation describing the buoyancy forces and the hydrodynamic forces on the (assumed spherical) colonies. The primary goal of this study is to analyze the influence of turbulence on the vertical displacement of *Microcystis* colonies. This cyanobacteria species has the feature to change their mass-density in response to the light climate. They become slightly heavier than water through carbohydrate assimilation under the influence of light during the day and slightly lighter due to respiration (during dark periods). Computational limitations inherent to DNS require the application of specific methodologies for simulating complete buoyancy cycles which occur on a daily time scale. We propose a normalization-scaling procedure by which biological responses of *Microcystis* cells are accelerated in order to reduce the diurnal cycle. The final coupled flow-biology model proves to capture natural diurnal migration processes of *Microcystis* colonies. Under very low turbulence conditions *Microcystis* shows a quasi-periodic daily migration where the Stokes drag and the buoyancy force are predominant in the dynamics. Higher turbulence conditions override such periodicity, and tend to mix the colonies thoroughly through the water column. Our analysis yielded a dimensionless variable: the buoyancy Stokes number St_b . This variable weighs the deterministic buoyancy dominated migration over the more chaotic random colony excursions due to the presence of turbulence.

Keywords:

Microcystis aeruginosa; biologically active particles; Direct Numerical Simulations; Lagrangian particle tracking; scaling laws for biological processes; buoyancy Stokes number; dimensionless parameters for biological processes

3.1 Introduction

The goal of this research is to study the influence of (small-scale) turbulence on the vertical migration of the cyanobacterium *Microcystis aeruginosa* colonies and to introduce a novel scaling procedure for the speed up of biological assimilation/respiration processes to allow simulations of the dynamics of vertical migration of *Microcystis* colonies under turbulent flow conditions. The method will be illustrated with several examples.

In this study, two main dynamical processes have been included. Firstly, the typical changes in *Microcystis* colony mass-density, which depend on the existing light environment, are incorporated. Secondly, we explore the effect of homogeneous isotropic turbulent flow on *Microcystis* colony vertical distribution. Turbulence is simulated via Direct Numerical Simulations (DNS) using a standard pseudospectral code based on Fourier decomposition of the dependent variables in the three coordinate directions. The trajectories of the biologically active *Microcystis* colonies are obtained with by nowadays relatively standard particle tracking algorithms (Toschi and Bodenschatz, 2009; Metcalfe *et al.*, 2012). The physical-biological coupling in a full diurnal simulation cycle is achieved by applying a normalization-scaling methodology that will be proposed here. This approach allows us to simulate vertical migration of colonies during several diurnal cycles. We explore the effects of, for example, turbulence intensity, light extinction, colony sizes and other dynamically relevant parameters. The results are translated towards realistic environmental conditions. Additionally, we want to compare our results with the outcome of a previous methodology presented in Aparicio Medrano *et al.* (2013). The latter methodology models the vertical migration of *Microcystis aeruginosa* by coupling the k - ν turbulence model and a Langevin-Fokker-Planck equation to describe the vertical distribution of the colony number concentration.

Microcystis aeruginosa is a ubiquitous species that inhabits freshwater lakes. It is a colony-forming cyanobacteria species that occasionally collect at the surface of lakes, forming fouling scums (Ibelings and Mur, 1992). Moreover, they are known to produce toxins, and therefore represent a serious health threat (Codd, 1999) that may directly affect the water recreational sector and drinking water reservoirs. The

occurrence of high concentrations of *Microcystis* (blooms) is mainly related to high nutrients loads, decrease of CO₂, high pH, stability of the water column and its resistance to grazing (Reynolds *et al.*, 1981; Sirenko, 1972).

In open waters such as lakes or oceans the distribution and survival of phytoplankton depends to a large extent on the turbulent conditions. Mixing affects phytoplankton in their access to light for photosynthesis in the upper layers and to nutrients at deeper levels, especially for those species that cannot swim. The cyanobacteria *M. aeruginosa* is typically characterized by a daily pattern in vertical migration (Visser *et al.*, 1997; Ibelings *et al.*, 1991). This pattern is the result of carbohydrates storage during exposure to light as a result of photosynthesis and carbohydrates respiration under dark conditions. The carbohydrate content variation is reflected in cell mass-density variations of the colonies. The physiological time it takes for a colony to reverse its buoyancy status (*i.e.* from floating to sinking) is defined here as a *buoyancy cycle*. The property of changing its mass-density in time implies that this species should be treated as biologically active instead of passive. Wind-driven turbulence competes with the buoyancy driven vertical migration of *M. aeruginosa* (Humphries and Lyne, 1988; Howard, 1997; Wallace and Hamilton, 2000; Aparicio Medrano *et al.*, 2013). In this study we intend to model this complex interaction between turbulent flow and buoyancy driven vertical migration over the full diurnal cycle.

Turbulence is characterized by its broad spectrum of length and time scales, ranging from the integral scale, where inertial eddies could be of the size of the (depth of the) containing body, to the dissipative scale in the order of millimeters. The latter is governed by viscosity and the turbulent kinetic energy dissipation (Imberger and Ivey, 1981). Most phytoplankton species are smaller than the smallest turbulence scales (*i.e.* the Kolmogorov length scale). Consequently, their trajectories are affected by the large-scale sweeping by the integral-scale coherent flow structures (eddies), the small-scale velocity fluctuations in the flow field and the local hydrodynamic forces of the fluid on the particles. Besides the fluid motion also inertia of the phytoplankton may influence their spatial distribution (Ross and Sharples, 2008). Here, we consider the inertial nature of the colonies by solving a simplified version of the Maxey-Riley (MR) equation (Maxey and Riley, 1983), an

equation of motion for rigid spherical particles in a nonuniform velocity field $\mathbf{u}(\mathbf{x}, t)$ with $\mathbf{x} = (x, y, z)$. The general form of the MR equation contains several hydrodynamic contributions to the force on the particles such as Stokes drag, particle buoyancy, added mass, Basset history force and Faxen corrections. For the present application of transport of almost neutrally buoyant particles it is sufficient to consider just the Stokes drag, particle buoyancy and added mass effects (see for example Babiano *et al.*; 2000).

Microcystis aeruginosa inhabits shallow and deep lakes. It outcompetes other species, especially in the presence of density-stratification because of its nearly neutrally buoyant characteristic (Reynolds *et al.*, 1981; Ibelings *et al.*, 1991; Visser *et al.* 2005). During density-stratification *Microcystis* colonies remain mainly in the mixing layer. For deep lakes the mechanisms operating in the water column are turbulence mixing, internal waves, Langmuir circulation and diffusive processes among others (Imberger, 1985). The sources of energy are identified as wind forcing, buoyancy flux related with surface cooling and internal shear production (Imberger, 1985). For shallow lakes wind forcing and buoyancy flux are the dominant drivers which create turbulent mixing within the water column (Reynolds, 2006). Strong stratification in the Northern Hemisphere usually occurs during summer periods and in the Southern Hemisphere for most of the spring, summer and autumn periods (Imberger, 1985). This difference is due to different land distribution between Northern and Southern Hemisphere. Overall, high irradiances and low wind conditions result in a mixing layer (epilimnion) with almost uniform temperature. Therefore, as a first approximation we consider the turbulence in the epilimnion as homogeneous turbulence.

In order to study the dynamics of vertical migration of *Microcystis* colonies in conjunction with turbulence we have coupled DNS of homogeneous isotropic turbulent flow with Lagrangian tracking of an ensemble of point particles. DNS allows for solving the incompressible Navier-Stokes equations at all relevant length and time scales of the flow without the need of using turbulence closure models. Particles embedded in the flow have a size usually much smaller than the smallest turbulent length scales ($d_p \ll \eta$, with d_p the particle diameter and η the Kolmogorov length scale to be defined later on). The particle Reynolds number $Re_p = d_p |\mathbf{u}$ -

$|\mathbf{u}_p|/v \ll 1$ (with \mathbf{u}_p the particle velocity and ν the kinematic viscosity of the fluid). Their dynamics can therefore be modeled with the point-particle approximation (see MR equation). The dynamics of heavy inertial particles ($\rho_p \gg \rho_f$, with ρ_p and ρ_f the particle and fluid density, respectively) in turbulence has already been well explored during the last decade. For example, it is relevant for better understanding of rain formation in clouds, turbulent aerosol transport and spray combustion (Shaw, 2003; Post, 2002). A review of the state-of-the-art in dynamics of inertial particles in turbulence can be found in Toschi and Bodenschatz (2009) and references therein. The situation is less clear for the dynamics of light inertial particles (sediment transport $\rho_p/\rho_f \sim 2.5$) or even almost neutrally buoyant particles ($\rho_p \cong \rho_f$) relevant for plankton distribution and transport in oceans and estuaries. A few efforts in this direction have been reported by Tanga and Provenzale (1994), Armenio and Fiorotto (2001), Candelier *et al.* (2004), and Van Aartrijk and Clercx (2010a, 2010b). In marine biology applications DNS has been used to study the phenomenon of preferential concentration of marine particles (Squires and Yamazaki, 1995), prey-predator contact rates (Yamazaki *et al.*, 1991) and the effects of turbulence on algae growth (Marshall and Huang, 2010). However, only few investigations included active behavior of the biological particles, the effect of gyrotaxis is a rare example (Croze *et al.*, 2013).

Yamazaki *et al.* (2002) pointed out the difficulties in applying DNS in conjunction with biology, *i.e.* the large range in time scales. The buoyancy-density changes of *Microcystis* cells occur at a time scale in the order of hours. Instead, a long DNS can span minutes of a real environmental flow simulation due to computational limitations. These two cannot be reconciled in one straightforward simulation effort.

To bridge the gap between flow and biological time scales, we therefore propose a specific scaling procedure. The scaling procedure is based on the non-dimensionalization of the system equations. The resulting non-dimensional variables include: flow Reynolds number, particle Stokes number and two ratios which compare the time-scales of biological assimilation and respiration to the typical flow time-scale. The last two are the essential ratios of our speeding-up procedure. We show that our methodology does allow simulating the fundamental interactions

between flow and biological physiology. This proof-of-principle is the main result of our paper. Next, as an illustration some possible scenarios of application are studied, by analyzing the effects of light intensity, colony size and the available hours of daylight. Finally, it will be shown that the aforementioned scaling procedure also facilitates a generalization of the results in a sense that the various individual cases of simulation can be grouped in terms of a non-dimensional parameter, the Buoyancy Stokes number. From this it appears that the typical bandwidth of vertical dispersion of colonies can be predicted.

Speeding-up physiological responses such as growth has been recently applied by few other researchers. For instance, in a study on the effect of turbulent mixing on algal growth rate, Marshall and Huang (2010) rescaled the photosynthesis time of algae in order to simulate different ratios of photosynthesis time to turbulence eddy turn-over time. A similar procedure was followed by McKiver and Neufeld (2011) who studied the dependence of a phytoplankton-zooplankton system on the ratio of biological time scale to flow time scale.

The present chapter is organized as follows. Section 3.2 describes the three modelling components of our investigation in more detail: Direct Numerical Simulations, particle tracking and biological responses. Section 3.3 elaborates the scaling procedure and Section 3.4 presents the results of the numerical simulations. Based on the derivation of the particle buoyancy Stokes number we evaluate in Section 3.5 the role of the magnitude of the terminal vertical velocity over the characteristic turbulent velocity. Finally, Section 3.6 presents a summary and conclusions of this investigation.

3.2 Modelling approach

In our computations both fluid elements and particles (colonies) are considered. Direct Numerical Simulation was used to solve the continuous phase (liquid). The *Microcystis* colonies are approximated as rigid undeformable spheres. Their trajectories are computed using a particle tracking scheme for individual point-particles (forces are based on particles size and density) in a one-way coupling to the DNS. A scheme of the model configuration is shown in Figure 3.1. The combined

methodology is intended to be representative of the epilimnion of a stratified lake, however we do not include free surface, wind forcing wave current interactions (Langmuir circulations).

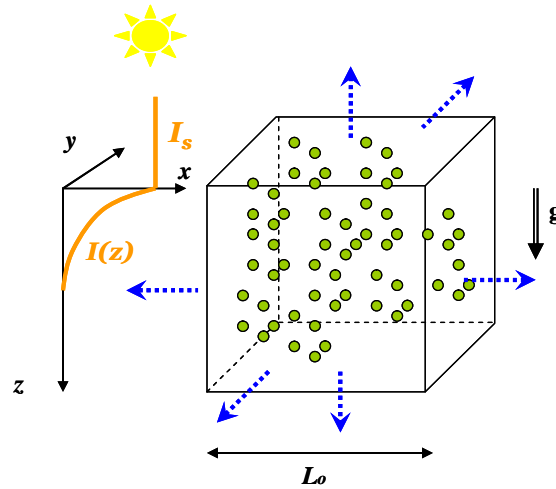


Figure 3.1: Schematic model configuration. Cubic domain with periodic boundary conditions in all three directions. Note that light intensity $I(z)$ varies in depth according to Lambert Beer's law. Particles(colonies) are initially uniformly distributed in the computational domain.

3.2.1 Direct Numerical Simulations (DNS)

The turbulent flow considered in this study is assumed to be homogeneous and isotropic, while no background density stratification is present. As such, buoyancy effects in the flow itself are excluded. The motion of the fluid is described by solving the Navier - Stokes equations

$$\frac{\partial \mathbf{u}}{\partial t} + (\mathbf{u} \cdot \nabla) \mathbf{u} = -\frac{1}{\rho_f} \nabla p + \mathbf{F}_e + \epsilon \nabla^2 \mathbf{u}, \quad (1)$$

together with the continuity equation

$$\nabla \cdot \mathbf{u} = 0. \quad (2)$$

Herein is $\mathbf{u} = (u, v, w)$ the velocity with components in the cartesian x , y and z direction, respectively. The orientation of the Cartesian coordinate system is shown in Figure 3.1. Furthermore, p is the pressure, ϵ the kinematic viscosity of the fluid, ρ_f is the reference density (here the fluid density) and \mathbf{F}_e represents any external forcing. The Navier-Stokes equations are solved using a three-dimensional parallel pseudo-spectral DNS code (Winters *et al.*, 2004; Van Aartrijk *et al.*, 2008). A cubic computational domain with side $L_o = 1$ m with periodic boundary conditions in all directions was used (Figure 3.1). Time integration of the linear viscous term is done

exactly (keeping its representation in Fourier space in mind). The non-linear, pressure and forcing contributions are integrated in time by a third-order Adams-Bashforth method.

Simulations were performed with a spatial resolution of 128^3 grid cells. Kinetic energy is continuously added to the flow in our simulations by external forcing applied in all three directions to keep the isotropic homogeneous turbulent flow statistically steady. The kinetic energy is injected at the largest scales by randomly exciting wavenumber modes in the interval $0 < k < 2k_o$, with $k_o = 2\pi/L_o$ the smallest wavenumber, and $k = |\mathbf{k}|$ the length of the wavenumber vector $\mathbf{k} = (k_x, k_y, k_z)$. The wavenumbers k_x , k_y and k_z are always multiples of k_o . For comprehensive model details, including initial conditions, implementation of the external forcing procedure, and basic testing of the turbulence data we refer to Van Aartrijk *et al.* (2008).

The fluid and (turbulent) flow properties characterizing the smallest dissipative motions are the kinematic viscosity ν and the rate of dissipation of turbulent kinetic energy (TKE) ϵ , which is estimated through $\nu = u_{rms}^3 / \epsilon$ with u_{rms} the root mean square velocity fluctuations and L_i the integral length scale of the turbulent flow, see Tennekes and Lumley (1972). Suitable combinations of these properties provide us with the Kolmogorov length scale η , time scale τ_k and velocity scale v_k , defined as: $\eta = [\epsilon / \nu^3]^{1/4}$, $\tau_k = [\epsilon / \nu^3]^{1/2}$, and $v_k = [\epsilon / \nu]^{1/4}$, respectively. The duration of the simulations is expressed in terms of the eddy-turnover time, $T_E = L_i / u_{rms}$.

3.2.2 Lagrangian particle tracking

Turbulent dispersion of particles is described here in the Lagrangian frame of reference. In the case of fluid particles the particle trajectories are then derived from $d\mathbf{x}_p/dt = \mathbf{u}(\mathbf{x}_p, t)$, with $\mathbf{u}(\mathbf{x}_p, t)$ the fluid velocity at the particle position. These particular fluid velocity data are interpolated from the DNS Eulerian velocity field. In the present study we have used cubic spline interpolation of the velocity field at the particle position. See Van Hinsberg *et al.* (2012) for a general background on interpolation schemes and comparisons between different schemes. Particle

trajectories are computed by integrating $d\mathbf{x}_p/dt = \mathbf{u}(\mathbf{x}_p, t)$ given initial conditions, *i.e.* $\mathbf{x}_p(t=0) = \mathbf{x}_0$. The same time integration scheme is used as for obtaining the Eulerian velocity field itself, *i.e.* third-order Adams-Bashforth. Because inertial particles generally do not follow the flow exactly, we have to integrate $d\mathbf{x}_p/dt = \mathbf{u}_p(t)$ (with $\mathbf{u}_p(t)$ not necessarily the same as $\mathbf{u}(\mathbf{x}_p, t)$) and introduce a separate equation of motion for those particles.

Our starting point is the deterministic equation of motion for a rigid nondeformable sphere in a non-uniform velocity field (Maxey and Riley, 1983). We therefore assume that $Re_p \ll 1$ and $d_p \ll y$. The hydrodynamic forces described by the Maxey-Riley (MR) equation are: the force exerted by the undisturbed flow on the particle (also known as the pressure gradient force of the undisturbed flow), the (viscous) Stokes drag force, the added-mass contribution which results from part of the fluid moving with the particle, and the Basset-Boussinesq history force. The MR equation includes the buoyancy force, which is the essential force for *M. aeruginosa* vertical migration. The last three hydrodynamic forces also include the Faxen corrections, which account for the spatial variation of the flow field across the particle. For our application we may assume that the Faxen corrections are negligible as the typical colony diameter is basically smaller than the Kolomogorov length scale and thus any flow field variation across the particles will presumably be small.

A *M. aeruginosa* colony consists of a cluster of cells embedded in gelatinous mucilage (traits of polysaccharide). In this study, *Microcystis* colonies are approximated as *almost* neutrally buoyant rigid spherical particles (colonies). The particle density ratios are typically $O(1)$ ($0.985 < \rho_c / \rho_f < 1.009$), with ρ_c the colony mass-density. For such a configuration it is possible to simplify the MR equation according to Babiano *et al.* (2000) where the following assumptions are made. First, the Faxen corrections are neglected for reasons mentioned above. Second, as far as dispersion properties are concerned the Basset-Boussinesq history force contribution is assumed to have no net effect for almost neutrally buoyant particles (Tanga and Provenzale, 1994; Armenio and Fiorotto, 2001; Van Aartrijk and Clercx, 2010b). However, this statement cannot be extrapolated towards individual particle velocities and trajectories (Mei *et al.*, 1991; Vojir and Michaelides, 1994). Moreover, the relative importance of the Basset force contribution with respect to the Stokes drag is

substantial (Tanga and Provenzale, 1994; Van Aartrijk and Clercx, 2010a) so that it may affect the small-scale dynamics of particles, relevant for collisions or aggregation processes of particles. As we do not consider these small-scale phenomena it seems safe to ignore the Basset history force. Besides the proposed simplifications we include the crucial buoyancy term, since *M. aeruginosa* colonies perform vertical migration due to the buoyancy or (reduced) gravity force. In the discussion we will review the relevance of the forces we consider here. Given the above assumptions, the MR equation reduces to:

$$\left(1 + \frac{1}{2} \frac{\dots_f}{\dots_e}\right) \frac{d\mathbf{u}_p}{dt} = \left(1 - \frac{\dots_f}{\dots_e}\right) \mathbf{g} + \frac{18\epsilon \dots_f}{d_p^2 \dots_e} (\mathbf{u} - \mathbf{u}_p) + \frac{3}{2} \frac{\dots_f}{\dots_e} \frac{D\mathbf{u}}{Dt}. \quad (3)$$

The quantities \dots_c , \dots_f , ϵ , \mathbf{u}_p and d_p have been defined earlier, and \mathbf{g} is the gravity acceleration pointing in the z -direction (see Figure 3.1 for the orientation of the Cartesian coordinate system). The derivative $\frac{d}{dt} = \frac{\partial}{\partial t} + \mathbf{u}_{p,j} \frac{\partial}{\partial x_j}$ is the time derivative along the trajectory of the moving particle and $\frac{D}{Dt} = \frac{\partial}{\partial t} + \mathbf{u}_j \frac{\partial}{\partial x_j}$ is the familiar convective derivative taken along the path of a fluid element at the instantaneous center of the particle. Both derivatives are almost the same when infinitesimally small neutrally buoyant (or passive) particles are considered.

In the simulations, the particles (colonies) are released when the flow has reached a statistically steady state. The particles are initiated at random positions uniformly distributed over the computational cubic domain. As we apply periodic boundary conditions, the particles that leave the domain on one side re-enter the domain on the opposite side. We consider the light intensity which varies with depth (see Section 3.2.4 for more details), in conjunction with a buoyancy regulation mechanism (see Section 3.2.3) which depends on the light intensity at the particle position z_p . As such, a particle with $z_p = L_o$ (bottom of the computational domain) does not experience the same light intensity as a particle at $z_p = 0$ (top of computational domain). We include this differentiation by defining in our model an extra coordinate p . This coordinate is simply used to compute the light intensity at depths larger than the domain vertical height. In this manner, particles that leave the

top of the domain are assigned a $\rho_p = 0$, until turbulence or the particle buoyancy status changes ρ_p to values larger than zero.²

3.2.3 Buoyancy regulation system

The biological component of our model basically consists of two empirical functions which describe the changes in mass-density of *Microcystis* cells (Visser *et al.*, 1997). Those density changes depend on the light the cells receive (Figure 3.2). Under light conditions (Figure 3.2a) the cells store carbohydrates and increase their density according to

$$\frac{d\rho_{cell}}{dt} = \beta I \exp(-I/I_o) + \gamma, \quad (4)$$

in which ρ_{cell} is the cell mass-density. Under dark conditions (Figure 3.2b) the respiration of carbohydrates leads to a cell mass-density reduction:

$$\frac{d\rho_{cell}}{dt} = -\gamma u H(u) \quad ; u = \rho_{cell} - C_{\rho}, \quad (5)$$

where H is the Heaviside step function, which is used to specify the truncation of decreasing cell mass-density below the minimum cell mass-density C_{ρ} .

² The effective fluid column height in our simulations turns out to be 3 meters deep.

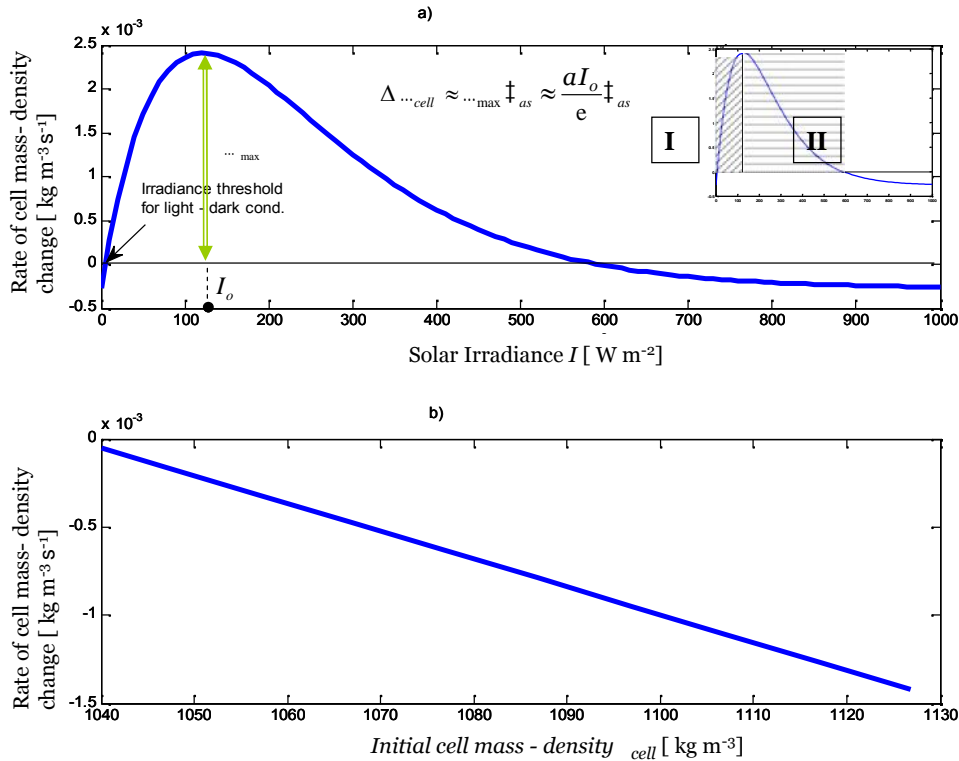


Figure 3.2: Rates of change in cell mass-density. (a) Density changes against solar irradiation (light conditions). The inset shows two regions: region I represents the positive feedback in carbohydrate assimilation at increasing light intensities. Region II shows the negative feedback region of photoinhibition in which the rate of assimilation reduces with increasing light intensity. (b) Density changes against the initial cell density (dark conditions).

The threshold between both regimes occurs when the irradiance (I) at the colony level equals 5.75 Wm⁻² (Visser *et al.*, 1997). We define the illuminated depth as the depth at which the threshold irradiance (5.75 Wm⁻²) is reached. In Eqs. (4) and (5), $d_{\dots cell}/dt$ is the rate of cell mass-density change (in kgm⁻³s⁻¹) as defined by Visser *et al.* (1997), β is a normative factor, γ is the rate of density change in absence of irradiation ($I=0$), r is the slope, C_{\dots} is the minimum cell density (1037 kgm⁻³), below which the cells will not reduce their carbohydrate content and I_o is the irradiance where assimilation is maximum. The rate of increase in cell mass-density decreases when the light irradiance exceeds I_o , this region corresponds to the photoinhibition of cells. The constants were empirically defined by Visser *et al.* (1997) for a *Microcystis* strain from Lake Nieuwe Meer, The Netherlands, and are

listed in Table 3.1. Our model also includes the delay time for assimilation τ_r (20 min) as defined by Wallace and Hamilton (2000).

A colony of *M. aeruginosa* is composed of several cells, each containing gas vesicles (Walsby, 1988), entirely covered by mucilage. Based on the volumetric composition of a colony, the relationship between colony mass-density ρ_c and cell mass-density ρ_{cell} reads: $\rho_c = \rho_{cell} n_{cell} (1-n_{gas}) + \rho_{muc} (1-n_{cell})$, where n_{cell} is the ratio of total cell volume to colony volume, n_{gas} is equal to the ratio of the gas vesicles volume to cell volume, and ρ_{muc} the density of the mucilage (Reynolds *et al.*, 1981 and Aparicio Medrano *et al.*, 2013). The values of n_{gas} and n_{cell} are kept constant during the simulations (see Table 3.1). Furthermore, the colony size is also kept constant over the diurnal cycles. Temporal integration of the cell mass-density change under light or dark conditions yields an instantaneous value for the cell mass-density ρ_{cell} . With fixed values for n_{cell} , n_{gas} and mucilage density ρ_{muc} , the density of the *Microcystis* colony can dynamically be determined.

Table 3.1: System variables for both the natural case and for values used in our DNS.

Variable Definition			Natural Case	DNS
Typical length scale / Integral length scale	L_i	[m]	1	^{*1} 0.2 ^{*3}
Typical velocity scale/ Turbulent rms velocity	$U_o = u_{rms}$	[ms ⁻¹]	2E-03	^{*2} 5E-04 ^{*4}
Viscosity		[m ² s ⁻¹]	1E-06	3E-06
Typical flow time scale	$T_{flow} = T_E$	[s]	625	400
Fluid density	ρ_f	[kgm ⁻³]	1000	1000
Gravity	g	[m s ⁻²]	9.81	9.81
Particle diameter	d_p	[m]	8E-04	8E-04
Particle density	ρ_c	[kgm ⁻³]	1010	1010
Particle response time	T_p	[s]	3E-02	1E-02
Characteristic assimilation time	τ_{as}	[s]	18000	600
Characteristic cell mass-density increment	$\Delta\rho_{cell}$	[kgm ⁻³]	48.16	48.16
<i>Biological Variables</i> ^{*5}				
	s	[s ² m ⁻³]	5.0E-05	1.5E-03
	I_o	[Wm ⁻²]	146.43	146.43
	x	[kgm ⁻³ s ⁻¹]	-2.8E-04	-8.3E-03
	α	[s ⁻¹]	1.6E-05	4.7E-04
	C	[kgm ⁻³]	1037	1037
Cell content in colony ^{*6}	n_{cell}	[%]	10	10
Gas content in colony ^{*6}	n_{gas}	[%]	5	5
Mucilage density ^{*6}	ρ_{muc}	[kgm ⁻³]	998+0.7	998+0.7
Maximum Irradiance	I_{max}	[Wm ⁻²]	800	800
Carbohydrate assimilation delay time ^{*7}	τ_r	[s]	1200	40
Light attenuation coefficient	K_i	[m ⁻¹]	0.8	4

^{*1} From Denman and Gargett (1983).

^{*2} Water turbulent velocity corresponding to a wind speed of 1 ms⁻¹ (Denman and Gargett, 1983).

^{*3} Simulation results.

^{*4} Simulation results.

^{*5} From Visser *et al.* (1997).

^{*6} From Reynolds *et al.* (1981).

^{*7} From Wallace and Hamilton (2000).

3.2.4 Lambert Beer's law - light attenuation

Light attenuation in our system is modeled through Lambert-Beer's law, where the maximum light intensity occurs at the surface and decreases exponentially with depth according to

$$I(z) = I_s \exp(-K_i z), \quad (6)$$

where I_s is the irradiance at the surface of the water column, z is the depth (see definition of the coordinate system in Figure 3.1), and K_i is the extinction coefficient. The irradiance at the surface is modeled here as a sinusoidal function with a maximum irradiance of 800 Wm^{-2} (Figure 3.3a). The sinusoidal function is shifted and truncated to zero for simulating the hours of daylight and day-night cycles. For particles that leave the top of the computational domain their vertical coordinates are assigned $p = 0$ (Section 3.2.2). The light intensity that these particles (colonies) receive is truncated to the maximum irradiance at the surface I_s (Figure 3.1). Solar irradiance can be expressed in Wm^{-2} and also in PAR (photosynthetic active radiation) expressed as $\mu\text{mol m}^{-2} \text{ s}^{-1}$ by multiplying the former by 1.895.

3.3. Scaling procedure

The main goal of our investigation is to analyze the influence of turbulence on the vertical migration of *Microcystis* colonies including their changing buoyancy status. Here we consider a scaling procedure such that DNS is applicable for daily variation of *Microcystis* vertical migration. The time scale for changes in the colony buoyancy status (from floating to sinking or vice versa) is in the order of hours (Reynolds *et al.*, 1987). Furthermore, mixing time scales for the applications of interest to us (wind-driven turbulent mixing layer in lakes, for example) are in the order of minutes (Denman and Gargett, 1983). Conductivity-temperature-depth (CTD) profile measurements (Etemand-Shahidi and Imberger, 2001) showed that under moderate wind conditions ($3\text{-}4 \text{ ms}^{-1}$) the rate of dissipation of turbulent kinetic energy ϵ has an order of magnitude of $10^{-8} \text{ m}^2\text{s}^{-3}$ and the buoyancy frequency N has an order of magnitude of 10^{-3} s^{-1} . For these values we can estimate an eddy turnover time T_E of 10^2 s and a Kolmogorov time scale τ_k of 10^1 s (see Section 3.3.3). DNS is limited by computational resources. It has to resolve the full band width of length scales up to the Kolmogorov scale and the time stepping should even be smaller than the typical

Kolmogorov time scale. In our simulations the time step is kept at least 100 times smaller than the Kolmogorov time scale for particle handling purposes. Let us consider a DNS with the following characteristics: bulk Reynolds number $Re_b = O(10^3)$, cubic computational domain $L_o = 1\text{m}$, spatial resolution of 128^3 , turbulence kinetic energy dissipation $\nu = O(10^{-5} \text{ m}^2\text{s}^{-3})$, integral length scale $L_i = 0.15 \text{ m}$ and root-mean-square velocity $u_{rms} = 0.01 \text{ ms}^{-1}$. With relatively moderate computational resources this exercise would complete 60 eddy turnover times ($T_E=L_i/u_{rms}$) approximating 15 minutes of real flow time. However, within the described DNS coverage of one full *buoyancy cycle* would require at least 1200 eddy overturns (T_E), hence a factor of 20 larger. Providing suitable statistics requires at least several (but preferably many) of these cycles, and any attempt to explore the variability over many weeks requires even hundreds of buoyancy cycles. Accordingly, and as a first step, we propose to speed up the algae assimilation/respiration rate to less than $60T_E$ and thus decrease the time scale of the buoyancy cycle. In the following paragraphs we elaborate on the steps taken.

3.3.1 Definition of the system scale parameters and nondimensionalization of the equations

As a first step we need to choose the proper scaling parameters for nondimensionalization of the relevant length, time and velocity scales. Similarly, we need to arrive at dimensionless expressions for the particle dynamics, fluid and colony-density variations and the height-dependent irradiance in the water column. For this purpose the following parameters have been selected regarding the buoyancy regulation of *Microcystis* cells. The characteristic assimilation time of the *M. aeruginosa* cells is \dagger_{as} [s], the biological optimal irradiance (see Figure 3.2a) is I_o [Wm^{-2}], and the characteristic cell mass-density increment (see Figure 3.2a) is $U_{\dots cell} = \beta I_o \dagger_{as} e^{-1}$ [kgm^{-3}], with e Euler's number. Regarding the turbulent flow the following scaling parameters will be used: the typical length scale L_i [m], the typical flow time scale $T_{flow}=T_E$ [s], and for the typical velocity scale we use the turbulent root-mean-square velocity: $U_o=u_{rms}$ [m s^{-1}].

The nondimensional variables (denoted with an asterisk) related with the Navier-Stokes and MR equations are then:

$$\mathbf{u} = U_o \mathbf{u}^*, \mathbf{u}_p = U_o \mathbf{u}_p^*, t = L_i t^*/U_o, \mathbf{x} = L_i \mathbf{x}^*, p = \dots f (U_o)^2 p^*,$$

$$\mathbf{F}_e = (U_o)^2 \mathbf{F}_e^*/L_i, \dots f = U \dots cell \dots f^*, \mathbf{g} = (U_o)^2 \mathbf{g}^*/L_i,$$

and those related with the buoyancy regulation process are:

$$\dots c = U \dots cell \dots c^*, \dots cell = U \dots cell \dots cell^*, I = I_o I^*, I_s = I_o I_s^*, C_{\dots} = U \dots cell C_{\dots}^*.$$

By replacing the non-dimensional variables in the formulae (1-6), and subsequently removing the asterisks everywhere, we obtain the following non-dimensional equations:

$$\nabla \cdot \mathbf{u} = 0, \quad (7)$$

$$\frac{\partial \mathbf{u}}{\partial t} + (\mathbf{u} \cdot \nabla) \mathbf{u} = -\nabla p + \mathbf{F}_e + \frac{1}{1} \nabla^2 \mathbf{u}, \quad (8)$$

$$\left(1 + \frac{1}{2} \frac{3}{\dots c}\right) \frac{d \mathbf{u}_p}{dt} = \left(1 - \frac{3}{\dots c}\right) \frac{1}{4} (\mathbf{u} - \mathbf{u}_p) + \frac{3}{2} \frac{3}{\dots c} \frac{D \mathbf{u}}{Dt}, \quad (9)$$

$$\frac{d \dots cell}{dt} = \dots 5 (I \exp(1 - I) + \dots 6), \quad (10)$$

$$\frac{d \dots cell}{dt} = - \dots 7 u_d H(u_d); \quad u_d = \dots cell - \dots 8, \quad (11)$$

$$I = I_s \exp(- \dots 9 z). \quad (12)$$

The dimensionless equations which govern our complete system are: the continuity equation (Eq. 7), the Navier-Stokes equation (Eq. 8), particle motion based on the reduced MR equation (Eq. 9), cell mass-density changes (Eq. 10 and 11) and thus indirectly, via $\dots c = \dots cell n_{cell}(1 - n_{gas}) + \dots muc(1 - n_{cell})$, the colony mass-density changes, and the equation for the distribution of light along the water column (Eq. 12).

3.3.2 Characterization of the non-dimensional numbers 1 to 9

The Navier-Stokes equations and the reduced MR equation contain four dimensionless numbers 1 to 4. The first dimensionless number, $\dots 1 = U_o L_i / \epsilon l \equiv Re_i$, is actually the integral-scale flow Reynolds number as it relates the inertial forces to

the viscous forces (Re_i should be distinguished from the particle-based Reynolds number Re_p which is always very small). The magnitude of Re_i is related to the level of turbulence activity of the flow and the integral flow scale. A high Reynolds number corresponds to more turbulence. The second dimensionless number represents the ratio of the particle relaxation time $T_p = d_p^2 \rho_c / (18 \epsilon_{..f})$ to the intrinsic flow time scale $T_{flow} = L_i / U_o$, and is known as the particle Stokes number: $St = T_p / T_{flow} \equiv St$. It provides an estimate of the particle inertia, particles will closely follow fluid parcel dispersion at very small particle Stokes number. The characteristic cell mass-density increment during one buoyancy cycle is denoted by $\beta \dagger_{as} = \epsilon_{..f} e / (I_o \beta \dagger_{as}) \equiv \epsilon_{..f} / U_{..cell}$. Note that the product $\beta \dagger_{as}$ determines the actual characteristic change in cell mass-density $U_{..cell}$ via $e^{-1} \beta \dagger_{as} I_o = U_{..cell}$. The next dimensionless quantity is a vector constant, the normalized gravity: $\mathbf{g}_4 = \mathbf{g} L_i / U_o^2$. Here, only the z-component is nonzero.

The dimensionless numbers γ_5 to γ_8 are directly related with the relevant biological carbohydrate assimilation and respiration processes and appear in the rate-of-change equations of the cell mass-density. The first one is the flow-biological assimilation time scales ratio $\gamma_5 = T_{flow} / \dagger_{as}$, which relates the flow time scale with the time scale for biological carbohydrate assimilation and hence colony mass-density increase. Eq. (10) contains also the normalized rate of density change at $I=0$ which is $\gamma_6 = e / \beta \dagger_{as} I_o$. The flow-biological respiration time scales ratio is $\gamma_7 = T_{flow} / T_{res}$ where $T_{res} = 1 / \Gamma$. The normalized respiration constant is $\gamma_8 = C_{..i} / U_{..cell}$. Finally, we have to introduce a dimensionless extinction coefficient in the normalized Lambert Beer's Law: $\gamma_9 = K_i L_i$. The extinction coefficient is proportional to the inverse of the euphotic depth. The euphotic depth is taken as the depth at which the light intensity is 1% of the surface intensity I_s .

3.3.3 Definition of external variables for a realistic case, *natural case*

In view of the non-dimensional parameters introduced previously we need to establish a reference value for the length and velocity scales in a *natural case*. The natural case refers to the upper layer of a lake. This surface layer is subject to mixing generated by the prevailing atmospheric conditions, *e.g.* wind speed and solar irradiation.

We first address the natural length scale. There are several alternatives for choosing a characteristic length scale depending on the degree of density-stratification in a lake. If density stratification is absent, the vertical length scale could be taken as the depth of the lake. However, due to solar irradiation a temperature gradient can build up and wind-driven turbulence mixes the upper part resulting in a uniform temperature in the top layer and a thermocline at a certain depth. In this case the vertical length scale could be represented by the mixed-layer thickness (epilimnion bounded below by the thermocline). However this appears not to be the optimal length scale. *M. aeruginosa* is abundant during summer when relatively deep lakes are density-stratified. Stratification restricts the vertical motions to less than the extent of the mixed layer and therefore a different length scale is needed. It was pointed out by Denman and Gargett (1983), that in a stratified surface layer and close to the surface, the eddies feel the boundary. Thus, this region is controlled by surface stresses where the rate of dissipation can be expressed as $\nu = u_*^3/L_i$, with u_* the friction velocity. The friction velocity u_* is a function of atmospheric conditions. Here, we take $\rho_{air} C_D (U_{10})^2 = \rho_f u_*^2$, where ρ_{air} is the density of air, C_D is the turbulent drag coefficient and U_{10} is the wind speed measured 10 m above the mean free surface (Smith and Banke, 1975). The integral length scale we consider is derived for the case $\nu/l = O(10^{-8})$ and a friction velocity for a wind speed $U_{10} = 2 \text{ ms}^{-1}$. For the characteristic velocity scale we take the turbulent root-mean-square velocity u_{rms} . It can be related to the friction velocity in the surface layer via $u_{rms} \cong 2u_*$ (Denman and Gargett, 1983).

In Table 3.1 we have summarized the relevant system variables for the natural case (and those used in the DNS). The values presented in Table 3.1 only represent characteristic values that could occur in nature. In reality a broad range of characteristic scales exists for the surface layer of a lake.

3.3.4 Choice of the numerical values for the non-dimensional numbers τ_1 to τ_9

Table 3.2 summarizes the numerical values for the non-dimensional variables τ_1 to τ_9 as estimated for the natural case (epilimnion) and as used in our DNS. Ideally, in a formal similarity exercise, the non-dimensional variables in a simulation correspond to the natural system. However, computational constraints demand some

tolerance. We have set up our non-dimensional variables for a case with relatively low turbulence levels $\nu_l = O(10^{-10}) \text{ m}^2\text{s}^{-3}$, because in this almost no-turbulence scenario it is where *Microcystis* colonies perform their characteristic vertical migration. This low turbulence level involves large eddy turnover times compared to a high turbulence intensity case. For a low turbulence level case and given our computational resources, we are able to simulate up to $10 T_E$. However, a complete buoyancy cycle would occur typically after $200 T_E$. Therefore, in order to simulate a full buoyancy cycle in one DNS we should increase the ratio T_{flow}/τ_{as} (5) by a factor 20. In our simulations we have chosen the values for T_{flow} and L_i somewhat smaller than in the natural case (*i.e.* T_{flow} in the DNS is 0.64 times T_{flow} in the natural case and L_i in the DNS is 0.2 times L_i in the natural case). Therefore, the assimilation time τ_{as} is reduced by a factor 30.

Our main interest is maintaining $\rho_3 = \rho_f e/(I_0\beta\tau_{as})$ similar for the natural case and the simulations. We keep the values for the fluid density ρ_f and the irradiance I_0 in the DNS the same as in the natural case (Table 3.1). In other terms, to keep the typical density increase U_{cell} equal to 50 kgm^{-3} we need to maintain the product $\beta\tau_{as}$ constant in order to preserve ρ_3 constant ($U_{cell} = I_0\beta\tau_{as}e^{-1}$). Since τ_{as} is reduced by a factor of 30, the assimilation constant β needs to be increased by the same factor as to keep ρ_3 constant. In order to preserve the shape of the assimilation curve, the constant γ is reduced proportionally to β . As such $\rho_6 = e\gamma/\beta I_0$ remains constant. Assimilation and respiration should change proportionally. Therefore, T_{flow}/T_{res} (7), similar as 5, is also increased by a factor of about 20 such that the ratio T_{res}/τ_{as} is kept constant (T_{res} is reduced by a factor of 30 just as τ_{as}).

Computational constraints not only limit similarity in the assimilation/respiration processes but also in the Reynolds number Re_1 and the particle Stokes number St_2 . Here, we restrict our simulations to rather low values of the Reynolds number. Achieving strict Reynolds number similarity is usually rather demanding for DNS in geophysical flow configurations. Nevertheless, it will be shown that both extreme cases of weak and strong mixing can be represented by the simulations. The particle Stokes number St_2 , is much smaller than unity for both the

natural case and the simulations. Consequently the particles inertial behavior remains similar.

Finally, the light extinction coefficient is adjusted to maintain γ_9 the same. The latter similarity effectively creates higher turbidity in the simulation. By keeping γ_9 constant the ratio between euphotic depth and integral length scale L_i is preserved. The remaining non-dimensional variable representing gravity (γ_4) has the same order of magnitude for both the natural case and the simulations. Alternatively, the particle (colony) settling velocity could be used for interpretation (Table 3.2).

Table 3.2: Overview of the non-dimensional variables γ_1 to γ_9 for both the natural case as the values used in our simulations with the default parameter settings. The integral Reynolds number $Re_i = L_i u_{rms}/\nu$ is based on the integral length scale L_i . The bulk Reynolds number $Re_b = L_o u_{rms}/\nu$ is based on the domain length L_o . The two normalized gravities ($\gamma_4 = \mathbf{g} L_i / U_o^2$) correspond to normalization with the dimensional flow velocity u_{rms} and the dimensional terminal colony velocity w_s respectively. Grey rows denote the non-dimensional variables in the DNS which are different than in the natural case.

Parameter Definition	NDV	Natural Case	Simulation
Integral Reynolds Number (Bulk Reynolds Number)	1	1230 (1 E+04)	37 (1 E+3)
Particle Stokes Number	2	4E-05	3E-05
Characteristic cell mass-density increment	3	20.8	20.8
Gravity (flow velocity) Gravity (settling velocity)	4	1.4E+06 4E+06	1.1E+06 8E+06
Flow - Biological Assimilation	5	0.035	0.67
Assimilation constant	6	-0.1	-0.1
Flow - Biological Respiration	7	0.01	0.19
Respiration Constant	8	21.53	21.53
Extinction Coefficient	9	0.80	0.80

3.4 Application of the scaling procedure

3.4.1 Overview

Previous analysis introduces a formal method as to speed up biological assimilation/respiration in a consistent way. Next, it will be shown that this method indeed allows simulation of full biological cycles within the computational

constraints. This will be illustrated with some typical examples with various parameters permutations (sensitivity analysis), *e.g.* to study the effect of turbulence intensity, the role of the light extinction coefficient, the influence of the colony size, the length of the day and the effect of the presence of a free water surface (using irradiation as a proxy). The parameters characterizing the simulations carried out during this investigation (and reported here) are given in Table 3.3. The intensity of turbulence is characterized here, with the turbulent kinetic energy dissipation rate ε diagnosed from the simulations. In this investigation, we take $\varepsilon = 2 \times 10^{-6} \text{ m}^2 \text{ s}^{-3}$, $\varepsilon = 3 \times 10^{-7} \text{ m}^2 \text{ s}^{-3}$ and $\varepsilon = 5 \times 10^{-10} \text{ m}^2 \text{ s}^{-3}$ to represent the high, intermediate and low turbulence-intensity cases, respectively. The associated Kolmogorov length scales are $y = 2 \text{ mm}$, $y = 3 \text{ mm}$ and $y = 13 \text{ mm}$, respectively (and Kolmogorov time scales $\tau_k = 1 \text{ s}$, $\tau_k = 3 \text{ s}$ and $\tau_k = 77 \text{ s}$, respectively). Table 3.4 presents an overview of the turbulent properties for the simulations performed to analyze the effect of turbulence. Comparison of the Kolmogorov scale and the typical colony diameter used in the present study (0.6, 0.8 and 1.0 mm) shows that we met the condition $d_p < y$. Previous studies by Van Aartrijk and Clercx (2010b) have shown that this condition, although not strictly $d_p < y$, is sufficient for applying the (reduced) MR equation to describe particle dynamics.

Table 3.3: Parameters of the different simulations presented in this paper (grey row is the default case; default values for the other cases are indicated by the asterisk *).

Case	Description	$[\text{m}^2 \text{ s}^{-3}]$	K_i $[\text{m}^{-1}]$	d_p $[\text{m}]$	Day - night cycle
C1	Low Turbulence	5E-10	4	8E-04	16 h - 8h
C2	Intermediate Turbulence	1E-07	*	*	*
C3	Higher turbulence	1E-06	*	*	*
C4	Turbid water	*	5	*	*
C5	Clearer water	*	3	*	*
C6	Larger Colony size	*	*	1E-03	*
C7	Smaller Colony size	*	*	6E-04	*
C8	Shorter day-night cycle	*	*	*	12 h - 12 h
C9	No - water surface	*	*	*	*

Our results are based on 1000 particles for all the simulations due to computational expensiveness. One run with 10000 particles is performed and used to check the accuracy of our results based on tracking 1000 particles only. All of our results are presented in physical units in order to establish direct comparison with previous modelling research and field measurements.

In this study three statistical parameters are used to characterize the simulations. Firstly, the mean-squared colony path $\mu_z(t)$ in the z direction. Secondly, the standard deviation $\sigma_z(t)$ which is used to characterize the spreading of the colonies around the mean vertical path $\mu_z(t)$. Thirdly, the concentration standard deviation μ_σ that is the time average of $\sigma_z(t)$. The later parameter is used for quantitative comparison between simulations.

Table 3.4: Turbulent properties of simulations with different turbulence intensities: C1 – LT refers to the low turbulence simulation, C2 – IT refers to the intermediate turbulence simulation, and C3 – HT refers to the high turbulence simulation. $Re_\lambda = u_{rms} \lambda / \nu$ is the Reynolds number based on the Taylor length scale $\lambda = u_{rms} / ((\partial \mathbf{u} / \partial \mathbf{x})^2)^{1/2}$. $Re_i = L_i u_{rms} / \nu$ is the Reynolds number based on the integral length scale L_i . $Re_b = L_o u_{rms} / \nu$ is the bulk Reynolds number based on the domain length L_o . η , τ_k and v_k are the Kolmogorov length, time and velocity scales respectively (the grey column shows the default values used for cases C4 to C9).

Property		C1 - LT	C2 - IT	C3-HT
Re_λ		23	80	116
Re_i		37	189	394
Re_b		1E+03	2E+03	3E+03
λ	[m]	0.12	0.06	0.04
η	[mm]	13.4	2.8	1.6
τ_k	[s]	69.4	3.1	1.1
v_k	[mms ⁻¹]	0.19	0.92	1.58

3.4.2 Reference case C1: Low turbulence

The reference case C1 focuses on low turbulence conditions where the buoyancy cycle of *Microcystis* colonies should clearly be present. Figure 3.3 shows that our simulations successfully couple flow and biological interactions. Complete buoyancy cycles can be simulated by the DNS tool within a limited number of eddy turnover times. This is the principal result of our research.

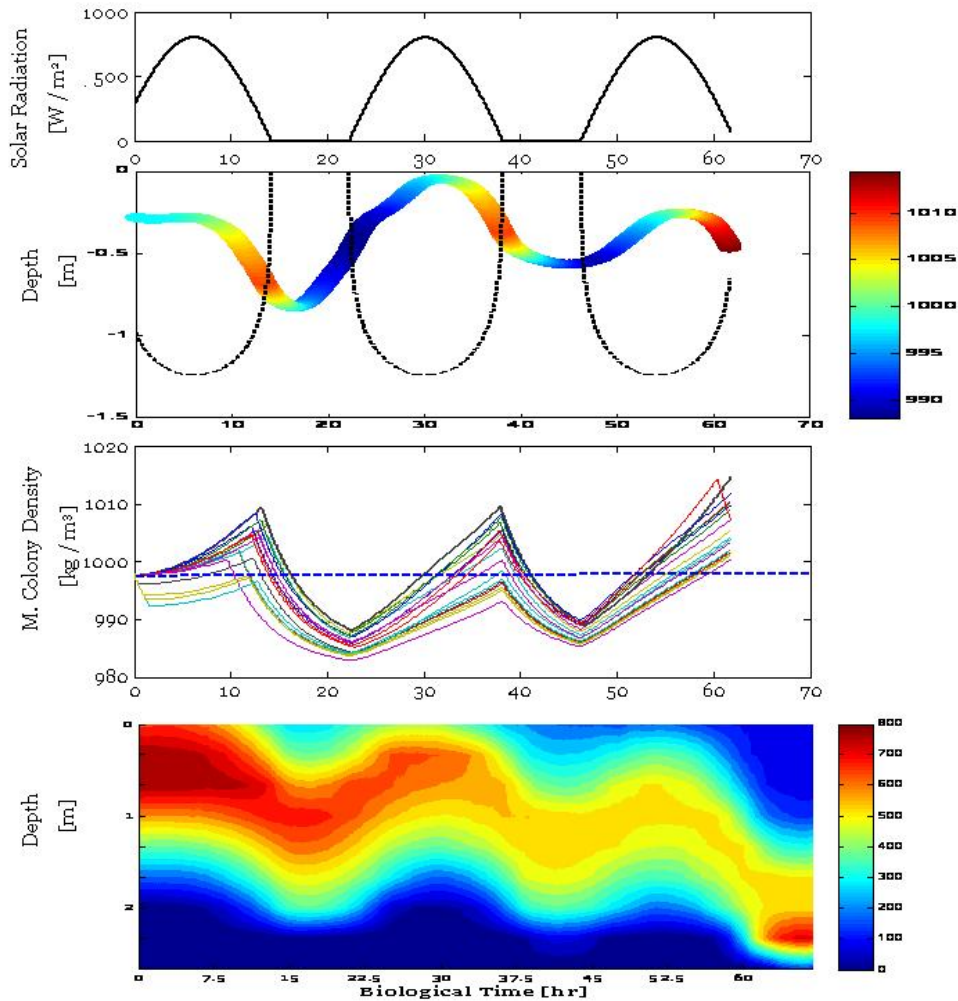


Figure 3.3: The evolution with time of a) the solar irradiation at the surface of the domain, b) the vertical path of a single colony and at the same time its changes in colony mass-density, the color of the markers represent the density of the colony and the dashed line corresponds to the illuminated depth at which the dark regime starts (5.75 Wm^{-2}), c) the response of the colony mass-density to the light cycle (density increases in light and decreases in dark environments). The horizontal dashed line represents the density of water. d) The colony concentration as function of the depth.

Figure 3.3a shows the evolution of the solar irradiation at a hypothetical surface of the domain. Here, we consider a day-night cycle of 16 hours versus 8 hours. Figure 3.3b shows the vertical path of a single colony and at the same time its changes in colony mass-density. As soon as the colony leaves the illuminated depth the colony mass-density reduces. Observe the inflection points in the colony path after crossing the illuminated depth (dashed line), this shows the delay time for a colony to change its buoyant status from sinking to rising. Figure 3.3c shows the response of the colonies mass-density to the daylight cycle. The colony mass-density

increases during light and decreases during dark periods. The colony mass-density varies around the reference density of water. Figure 3.3d shows the evolution of the colony concentration along the depth. In this figure we can see the “cyclic” behavior of the center of mass emulating the pattern observed in nature (Reynolds *et al.*, 1981; Walsby, 1988; Ibelings *et al.*, 1991). The discrete data of colony position is transformed into a concentration field by the number concentration N_p [number of colonies m^{-3}]. This method simply counts the numbers of colony in predefined volume intervals. The volume interval we define is $1 \times 1 \times 0.2 \text{ m}^3$. Note that other computations for the concentration field are possible (Dunsbergen, 1994). Here, the resulting concentration field allows a visual interpretation of the vertical migration of the *Microcystis* colonies. However, the simulation period is too short to display stationary conditions. To analyze the sensitivity of our results to horizontal dispersion, we have divided the horizontal domain in four regions. Consequently, the cubic domain is divided in four columns and the volume interval for the determination of the concentration is $0.5 \times 0.5 \times 0.2 \text{ m}^3$ in each column. Overall, the results of each column show a similar deterministic pattern as the one presented in Figure 3.3d. The mean vertical path $\mu_z(t)$ in any of the four columns deviates 6% compared to the mean vertical path $\mu_z(t)$ when the whole domain is considered. Additionally, the concentration spreading $\sigma_z(t)$ deviates 10% compared to the spreading for the whole domain (one column).

Compared to the simulation with 10000 particles our results with 1000 particles showed a 3% deviation in the mean vertical colony path. For the purpose of the present investigation this result gives us confidence in the choice of tracking only 1000 particles for the rest of the scenarios that we will present in the following sections.

3.4.3 Effect of Turbulence Intensity

Turbulence affects the vertical distribution of the colonies. When the turbulence intensity is very low ($\varepsilon = 5 \times 10^{-10} \text{ m}^2\text{s}^{-3}$), the particle (colony) motion is rather deterministic revealing a quasi “harmonic” behavior (Figure 3.3d). In the low turbulence regime the velocity of the colonies is similar to their terminal settling or rising velocity. After analyzing the forces acting on the particles (colony) we found

indeed that the Stokes drag force is largely proportional to the buoyancy force and that the contribution of the other forces is small. Figure 3.4a shows the evaluation of the colony concentration for intermediate turbulence levels ($\varepsilon = 3 \times 10^{-7} \text{ m}^2\text{s}^{-3}$). The dispersion around the mean vertical colony path is higher than the low turbulence case shown in Figure 3.3d. Figure 3.4b shows that for higher turbulence intensity ($\varepsilon = 2 \times 10^{-6} \text{ m}^2\text{s}^{-3}$) the colonies are largely dispersed over the water column. For this higher turbulence intensity scenario we found that the pressure gradient and added mass forces increase in average by two orders of magnitude. Compared to the Stokes drag force, the added mass and the pressure gradient forces are nevertheless twenty and ten times smaller, respectively. The magnitude of the added mass and the pressure gradient we compute here compare with those reported in Van Aartrijk and Clercx (2010a). The turbulent dispersion and in a smaller extent the influence of these two forces affect the velocity and displacement of the colonies which then differ from the “deterministic” behavior shown in the low turbulence case.

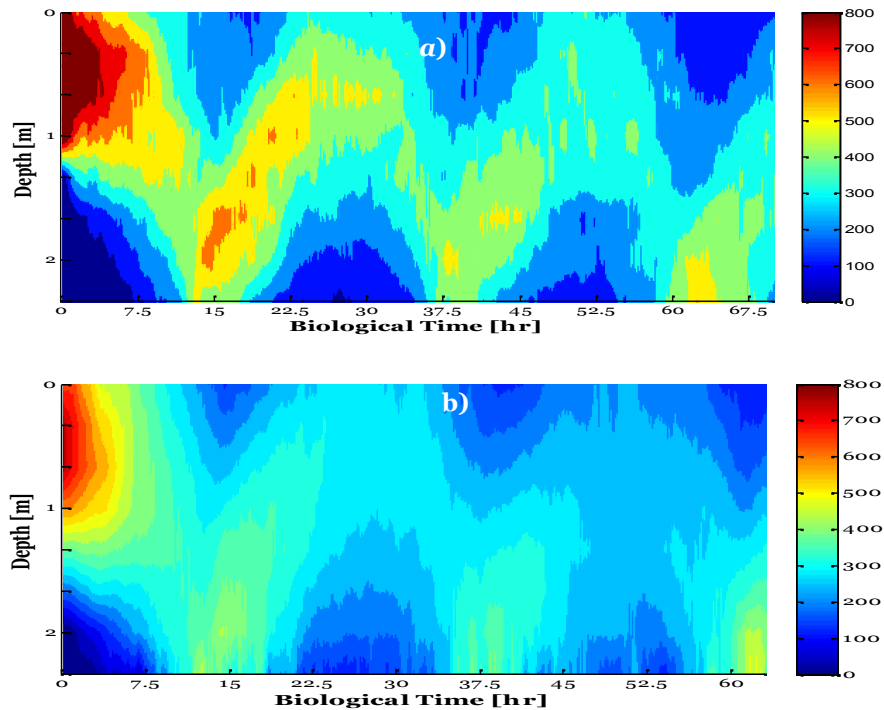


Figure 3.4: The evolution of colony concentration for different turbulence intensities a) medium turbulence intensity with $\varepsilon = 10^{-7} \text{ m}^2\text{s}^{-3}$ and b) high turbulence intensity with $\varepsilon = 10^{-6} \text{ m}^2\text{s}^{-3}$. The default level is $\varepsilon = 10^{-10} \text{ m}^2\text{s}^{-3}$ and its colony concentration evolution is shown in Figure 3.3d.

3.4.4 Effect of colony size

As shown in (Aparicio Medrano *et al.* 2013) the colony size influences the colony vertical distribution. In particular, their characteristic size determines the maximum distance that colonies can travel. We consider the role of colony size on vertical excursions in a low turbulence regime compared to the default size in our simulations ($d_p=800 \mu\text{m}$). Two colony sizes are simulated: $d_p=600 \mu\text{m}$ (scenario C7) and $d_p=1200 \mu\text{m}$ (scenario C8). Large colony size results in larger terminal velocities as the settling velocity is proportional to the colony diameter squared. This leads to larger vertical migration distances (Figure 3.5a). As such, a 50 percent increase in colony size results in more than 100 percent increase in vertical migration distance. Smaller colony sizes have a somewhat smaller migration depth than found in our reference case (the migration depth of scenario C7 is approximately 20% smaller than reference case).

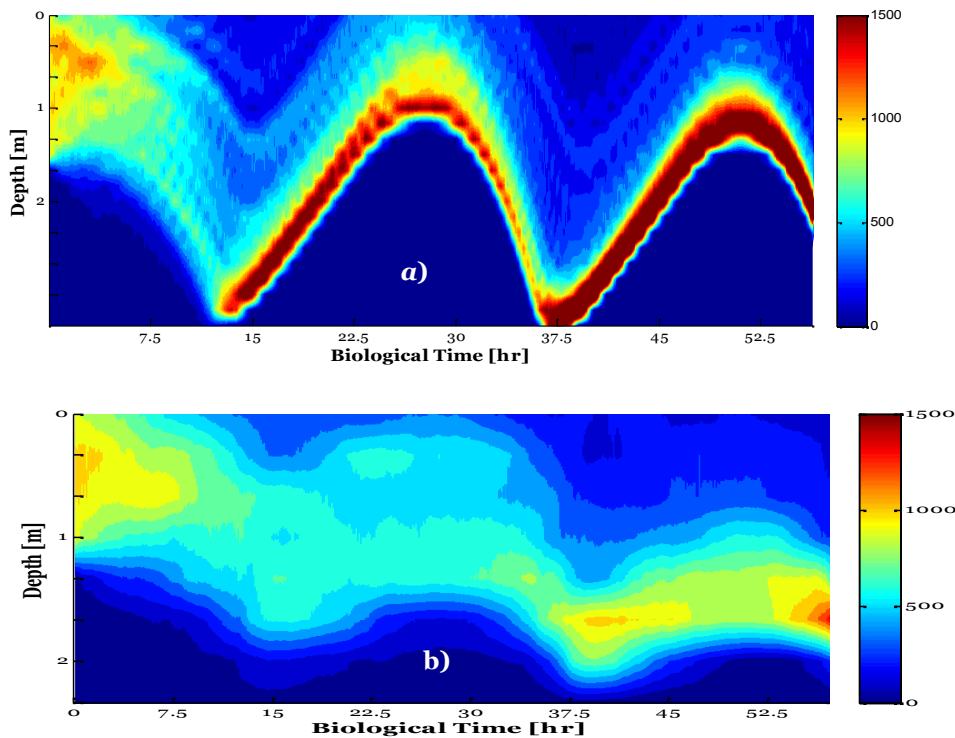


Figure 3.5: The evolution of colony concentration for different colony sizes; the default colony size is $800 \mu\text{m}$ and is shown in Figure 3.3d. a) Large colony size $1200 \mu\text{m}$ and b) small colony size $600 \mu\text{m}$. Note that the patchy behavior in Figure 3.5a is due to the resolution used for the determination of the volumetric concentration.

Moreover, smaller colony sizes result in a relatively larger influence of turbulent diffusion on the migration of colonies over the water column (despite the relatively low turbulence intensity), see Figure 3.5b. This diffusive effect will be discussed in more detail in Section 3.5.

3.4.5 Light attenuation effect and day-night cycle

The light attenuation in the water column changes the migratory behavior of the *Microcystis* colonies (Reynolds *et al.*, 1981). A smaller extinction coefficient ($K_i=3\text{m}^{-1}$ versus $K_i=4\text{m}^{-1}$ in the reference case) increases the euphotic depth and enhances the chances for the colony to receive more light and become heavier, see Figure 3.6a. Then, for most of the colonies, only night time hours will correspond to darkness. The darkness time will be insufficient for the colonies to reposition themselves in the light region for the next day (Figure 3.6a). On the other hand a larger extinction coefficient ($K_i=5\text{m}^{-1}$) assures that the depth of vertical motion reversal is shallower, such that the colonies can reach the top layer within a single daily period. This enables *synchronization* within the diurnal light cycle (see Figure 3.6b). Field observations of vertical migration of *Microcystis* under different extinction coefficients are scarce. The available measurements show that *Microcystis aeruginosa* is mostly abundant when the extinction coefficient is relatively large (similar as the reference case) (Reynolds *et al.*, 1981; Ibelings *et al.*, 1991).

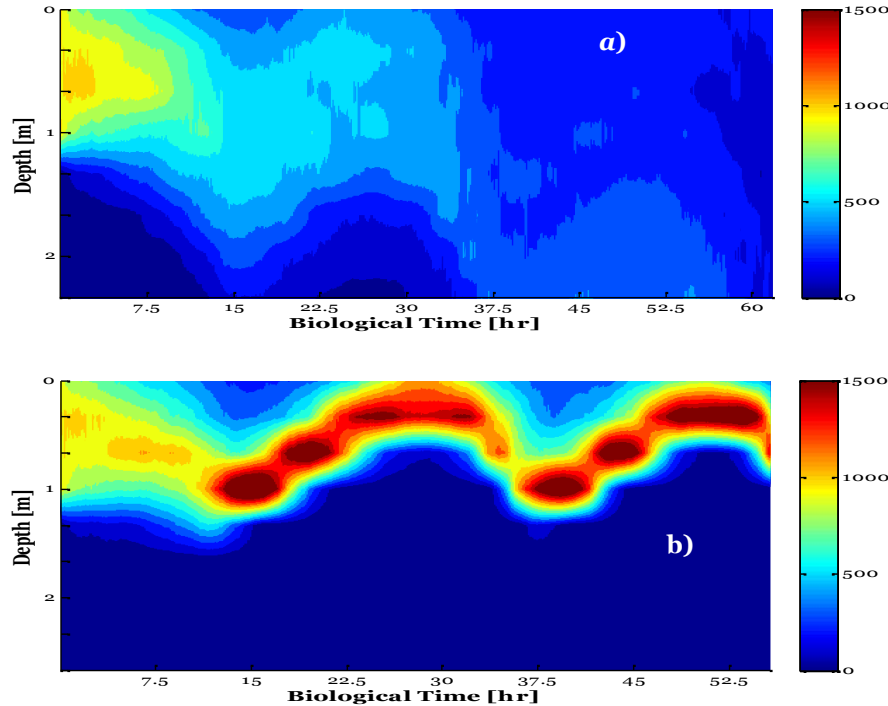


Figure 3.6: The evolution of colony concentration for different extinction coefficients; the default value of the extinction coefficient is $K_i=4 \text{ m}^{-1}$ and is shown in Figure 3.3d. a) Small extinction coefficient $K_i=3 \text{ m}^{-1}$ and b) large extinction coefficient $K_i=5 \text{ m}^{-1}$. Note that the patchy behavior in Figure 3.6b is due to the rough resolution used for the determination of the volumetric concentration.

The daylight length also plays a role in the concentration behavior of *Microcystis* colonies. The daylight length is a function of latitude and the day of the year. The reference case C1, represents a daylight length for either the Northern or the Southern Hemisphere in early summer. We consider here a day-night cycle of 12 versus 12 hours and all simulations are in the low-turbulence regime. This regime represents a daylight length for either Hemisphere in late summer. Shorter periods of daylight stimulate higher algae concentrations near the surface, see Figure 3.7. Although Figure 3.7 suggests that the colonies remain close to the surface, a closer look into the colonies path show that after a few hours most of the colonies leave the surface (not shown in Figure 3.7). In this scenario (C8) there is a longer time of darkness (12 hr) in which colonies respire and become lighter so that their density becomes smaller than the (reference) water density. Additionally, less hours of daylight lead to smaller positive differences between colony mass-density and water density. For comparison let us consider once again Figure 3.3d which shows our reference case of 8 hr of darkness. Besides the differences in the pattern of

concentration, the case with longer dark periods shows a subtly larger concentration spreading around the mean displacement than our reference case. As mentioned before, the differences between colony mass-density and water density are smaller, resulting in density-ratios between colonies and water closer to unity. Consequently, the particles are more influenced by the turbulent dispersion (behavior similar to fluid particles).

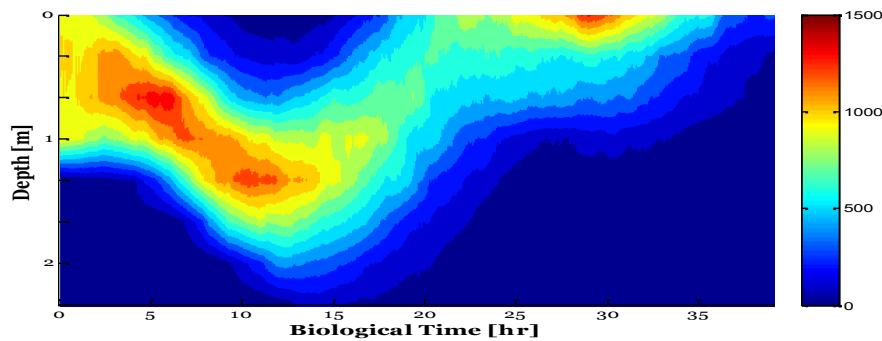


Figure 3. 7: Influence of the daylight cycle on the colony distribution. The daylight is equal to 12 hours. The default daylight equals to 16 hours and is shown in Figure 3.3d.

3.4.6 Domain without water surface

We have also considered the hypothetical scenario in which particles (colonies) could leave the domain at the surface ($p < 0$). In this area they would receive the maximum surface irradiance I_s . This scenario clearly shows the effect of photoinhibition. Figure 3.8 shows the vertical path of 20 colonies under this scenario. A *bifurcation* appears: the lower region I where colonies perceive less than the surface irradiance due to light extinction, and the upper region II, where colonies perceive full surface irradiance. Colonies in region II assimilate carbohydrates at lower rates (due to photoinhibition) than colonies in region I. These two regions correspond to the assimilation areas defined in the inset of Figure 3.2. It is important to notice that strong photoinhibition could promote longer accumulation of colonies close to the surface. However, even low rates of assimilation (due to photoinhibition) will make colonies heavier than water and therefore eventually sink (not shown in Figure 3.8).

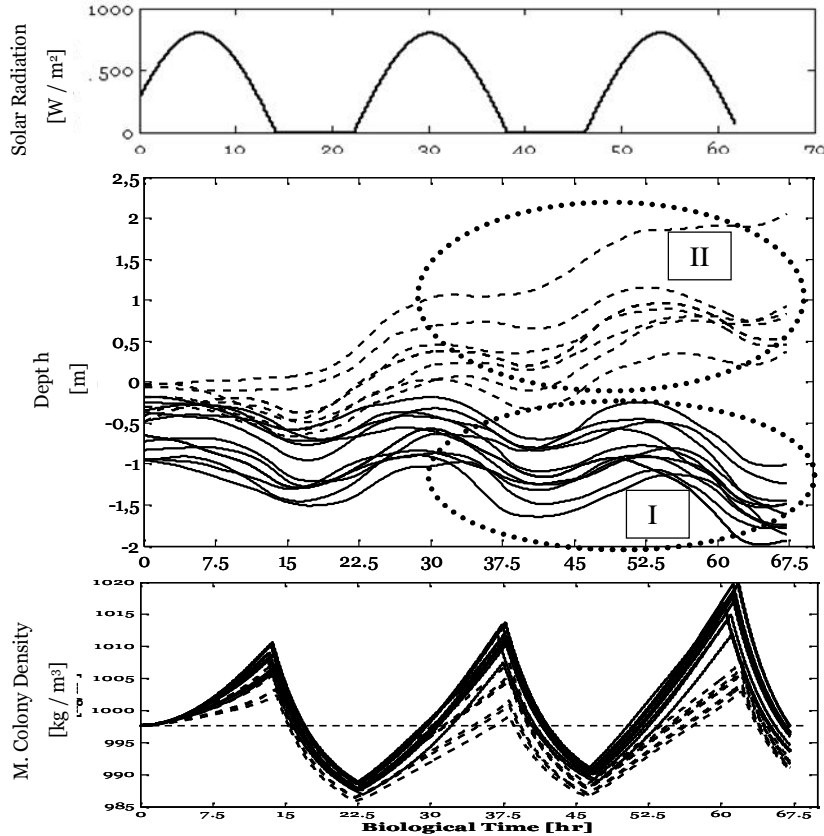


Figure 3.8: a) The evolution with time of the solar irradiation at the surface of the domain. b) Trajectories of 20 colonies simulated under the hypothetical scenario of a domain without a water surface case (C9). Region I shows the colonies that perceive less than the surface irradiance due to light extinction, and region II shows colonies that receive full surface irradiance. c) The response of the colony mass-density to the light cycle (the dashed lines corresponds to region II). The horizontal dashed line represents the density of water.

3.5. The Buoyancy Stokes Number

The default case (C1 - Figure 3.3d) and the high turbulence case (C3- Figure 3.4b) show that basically two processes compete with each other in determining the vertical distribution of algae. The first process is the buoyancy driven vertical motion, which tends towards an approximately deterministic path of rising and sinking colonies. The second process is the externally driven turbulence tending to a more uniform distribution by turbulent mixing over the water column. Next, we elaborate on this by analyzing the particle equation of motion and showing that the outcome of this competition is determined by a parameter that we will call the “buoyancy Stokes

number”. The starting point is the dimensionless reduced MR particle equation of motion (Eq. 9) rewritten as

$$\left(1 + \frac{1 - \beta}{2 \dots c}\right) \frac{d\mathbf{u}_p}{dt} - \frac{3 - \beta}{2 \dots c} \frac{D\mathbf{u}}{Dt} = \frac{1}{2} (\mathbf{u} - \mathbf{u}_p) + \left(1 - \frac{\beta}{\dots c}\right) \mathbf{g}, \quad (13)$$

with β the particle Stokes number St , β the dimensionless fluid density $\dots f$ and \mathbf{g} the dimensionless gravity. In the first place, we consider that the particles (colonies) are almost neutrally buoyant. In that case $\beta/\dots c = \dots f/\dots c \cong 1$, so that $(1 + \beta/(2\dots c)) \cong 3/2$. Secondly, the particle Reynolds number is small, $Re_p = d_p |\mathbf{u} - \mathbf{u}_p|/\nu \ll 1$. Finally, we assume infinitesimally small and almost neutrally buoyant particles such that we are allowed to make the approximation $D\mathbf{u}/Dt = d\mathbf{u}/dt$. This actually means that the rate of change of the ambient velocity as observed at the center of the sphere in the absence of the body ($D\mathbf{u}/Dt$) is approximately the same as the rate of change of the ambient fluid following the moving body ($d\mathbf{u}/dt$), see Van Aartrijk (2008). Then, Eq. (13) is considerably simplified:

$$\frac{d}{dt} (\mathbf{u}_p - \mathbf{u}) = -\frac{2}{3} \frac{1}{2} (\mathbf{u}_p - \mathbf{u}) + \frac{2}{3} \left(1 - \frac{\beta}{\dots c}\right) \mathbf{g}. \quad (14)$$

Eq. (14) is a first-order homogeneous ordinary differential equation and we take the particular solution $\mathbf{u}_p - \mathbf{u} = St_b \mathbf{e}_z$ with \mathbf{e}_z the unit vector in the z -direction where the buoyancy Stokes number St_b is

$$St_b = \frac{2}{3} \left(1 - \frac{\beta}{\dots c}\right) \frac{d_p^2 g}{18 \epsilon U_o} = w_s, \quad (15)$$

where w_s is the dimensionless settling velocity (normalized by $U_o = u_{rms}$). With the homogeneous solution we arrive at the general solution, which takes the form: $\mathbf{u}_p - \mathbf{u} = St_b \mathbf{e}_z + \mathbf{A} \exp(-2t/3\beta)$ with \mathbf{A} a constant.

The buoyancy Stokes number St_b , relates the competition between the “deterministic” gravitational terminal settling or rising velocity and the “randomness” of externally forced turbulent mixing. For large t , only the particular solution $\mathbf{u}_p - \mathbf{u} = St_b \mathbf{e}_z$ of Eq. (15) becomes relevant. Two limiting cases emerge: for $St_b \ll 1$ we obtain $\mathbf{u}_p \cong \mathbf{u}$ thus the particle (colony) velocity closely follows the fluid velocity. The *Microcystis* colony distribution is then more disperse due to turbulent motions. For $St_b \gg 1$ and $\mathbf{u} = \mathbf{0}$, we obtain $\mathbf{u}_p \cong St_b \mathbf{e}_z = w_s \mathbf{e}_z$ and the particle (colony) velocity will be similar to the terminal settling or rising velocity. Then, the particles

(colonies) distribution is more deterministic and shows less spreading in the vertical direction.

Now we analyze the buoyancy Stokes number for the simulations presented in the previous section. The low turbulence simulation (C1, see Figure 3.3d) has a buoyancy Stokes number $St_b = 2$ and the concentration plot shows the more “deterministic” behavior resulting mainly from the terminal sinking and rising velocities of the *Microcystis* colonies. In contrast, the high turbulence simulation (C3, see Figure 3.4b) has $St_b = 0.2$ and the vertical colony distribution is more “random-like”. The simulations exploring the colony size effect (C6, shown in Figure 3.5a and C7 in Figure 3.5b) have both a larger than unity buoyancy Stokes number of 1.5 and 6, respectively. Figure 3.9 shows the variation of the standard deviation of the mean vertical displacement μ_σ (spreading) for simulations C1 - Low turbulence, C2 - Intermediate turbulence, C3 - High turbulence, C6 - Larger colony size and C7 - Smaller colony size. As the buoyancy Stokes number increases the spreading of the concentration field reduces (reflecting dominance of deterministic behavior).

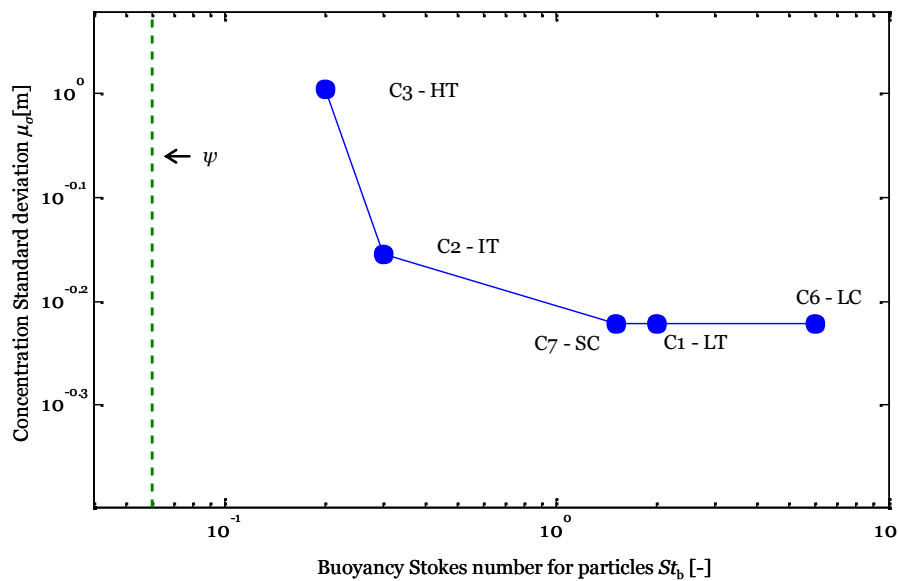


Figure 3.9 : The standard deviation of the concentration field μ_σ versus the buoyancy Stokes number St_b . HT refers to the high turbulence simulation C3, IT refers to the intermediate turbulence simulation C2, SC refers to small colony size simulation C7, LT refers to low turbulence simulation C1, LC refers to larger colony size simulation C6 and the dashed line represents the entrainment coefficient $j = 1$ distinguishing between turbulence-dominated and buoyancy-dominated vertical transport defined by Humphries and Lyne (1988).

The buoyancy Stokes number derived here corresponds to the empirical equivalent defined by Humphries and Lyne (1988) for natural systems as the entrainment coefficient $j = 15w_s/u_{rms}$, with w_s dimensionfull terminal vertical velocity and u_{rms} the dimensionfull root mean square turbulent velocity. This parameter defines the threshold for colonies distribution dominated either by turbulence ($j < 1$) or by the intrinsic rising/sinking colony velocity ($j > 1$). The non-dimensional variable j arises either from a comparison between diffusivities or time scales. Let us first consider the comparison based on diffusivities. Then, we define $j = 15D_B/D_K$, the ratio between the ‘apparent diffusion’ D_B , due to the buoyant character of the colony ($D_B = w_s z_m$, with w_s the dimensionfull terminal colony velocity and z_m the dimensionfull mixed layer depth), and the empirically determined turbulence diffusion coefficient $D_K = u_{rms} z_m/15$, with u_{rms} the dimensionfull root mean square turbulent velocity. Similarly, the time scale comparison T_K/T_B , is made between the time scale for diffusion in the mixed layer $T_K = z_m^2/D_K$, and the time scale for sinking or rising over the mixed layer $T_B = z_m/w_s$. Note that z_m refers to the characteristic depth to which the colonies migrate. In the present investigation this characteristic depth is defined as the integral length scale L_i .

From the preceding definition of the empirical entrainment coefficient j it is clear that all of the previous scenarios would be buoyancy dominated. The larger colony size simulation C6 has a $St_b = 6$ and $j = 190$, the low turbulence simulation C1 has a $St_b = 2$ and $j = 40$, the smaller colony size simulation C7 has a $St_b = 1.5$ and $j = 23$, the intermediate turbulence simulation C2 has a $St_b = 0.3$ and $j = 15$ and the high turbulence simulation C3 has a $St_b = 0.2$ and $j = 13$. The threshold defined by $j = 1$ is included in Figure 3.9 and it is indicated by the dotted line at the left end of the curve.

The discrepancy between St_b and j may lie in the fact that our critical buoyancy Stokes number was derived for isotropic turbulence and the entrainment coefficient j was determined from laboratory experiments of open channel flows (Jobson and Sayre, 1970). The anisotropic turbulence present in channel flows would delay the critical transition to a well-mixed regime.

The framework for the derivation of the buoyancy Stokes number can be interpreted as for passive particles. Other parameters related to abiotic components such as light availability, also influence the deterministic behavior of the colonies by limiting or expanding the effective domain available for diffusion. In Figure 3.9 all cases have similar euphotic depth. However, this depth is not constant for some other cases. For instance, scenario C5 has a deeper euphotic depth and scenario C4 has a shallower euphotic depth. Therefore, we included the euphotic depth as a scaling parameter to quantify the non-dimensional spreading of the concentration field of *Microcystis* colonies. Figure 3.10 shows the latter non-dimensional spreading against the buoyancy Stokes number. It clearly shows that the threshold defined by the buoyancy Stokes number $St_b = 1$ is consistent for all of our simulations. However, in order to draw definitive conclusions more simulations would be required. In particular simulations should have even higher turbulence intensities than our scenario C3.

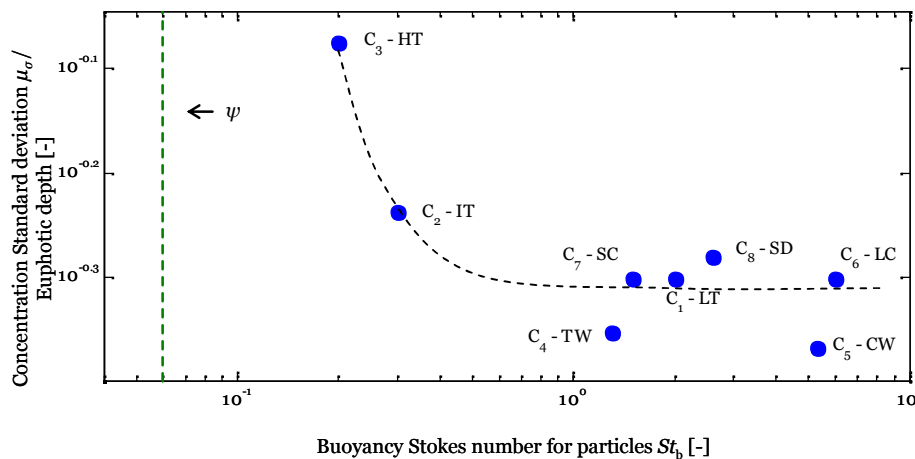


Figure 3.10: The ratio of the standard deviation of the concentration field μ_σ with the euphotic depth versus the buoyancy Stokes number St_b . HT refers to the high turbulence simulation C3, IT refers to the intermediate turbulence simulation C2, SC refers to small colony size simulation C7, LT refers to low turbulence simulation C1, LC refers to larger colony size simulation C6, TW refers to the turbid water case C4, CW refers to the clearer water case C5, SD refers to shorter day length case C8 and the dashed line represents the entrainment coefficient $j = 1$ distinguishing between turbulence-dominated and buoyancy-dominated vertical transport defined by Humphries and Lyne (1988). The dashed line is intended simply to guide the eye.

3.6. Discussion and conclusions

The vertical migration of *Microcystis* colonies in lakes is affected by physical and biological processes with distinctly different dynamical time scales: the characteristic flow time scale of the order of seconds to minutes and the assimilation and respiration time scales of *Microcystis* cells that determine a buoyancy cycle time scale of several hours. We propose a new approach for numerical studies of vertical migration of *Microcystis* colonies reconciling the different dynamical time scales by a proper scaling procedure.

The physical-biological coupled simulations are performed with a combination of different modelling approaches. A straightforward application of DNS for physical-biological coupling is usually not recommended due to computational limitations arising from the effort needed to solve the flow up to the Kolmogorov length and time scales (Yamazaki *et al.*, 2002). These limitations are reflected in smaller physical domains and relatively shorter computational times. Especially when the interest is on seasonal biological variations DNS would not be the first option. We are concerned with the effect of (small-scale) turbulence fluctuations on vertical migration of *Microcystis* colonies and therefore we choose for DNS instead of a turbulence closure model. Our time scale of interest is not monthly but daily variations. However, DNS has limitations and also particular computational hardware capabilities restricted our research. To overcome these differences we presented a normalization-scaling procedure.

The normalization-scaling approach proposed in this investigation contributes to bridge the gap between time scales of flow and physiological responses. The proposed methodology shows that realistic migratory behavior of *M. aeruginosa* can be simulated with DNS.

The results of this study support the outcome presented in Aparicio-Medrano *et al.* (2013). The daily pattern of *Microcystis* vertical migration that we are capable to simulate here, compares qualitatively well with the results presented in Aparicio-Medrano *et al.* (2013). The modelling approach presented in the latter study is different than the current one in two major aspects. First, turbulence is simulated by

applying a k - ϵ turbulence model instead of solving directly the Navier Stokes equations as done in this investigation. Second, the vertical mobility of the *Microcystis* colonies is studied by applying a Langevin-Fokker-Planck equation which is solved for an ensemble of particles (colonies) while in the present study we follow a Lagrangian approach for the simulation of colony transport by solving a particular equation of motion for each of the particles (colonies). In order to study seasonal variations of *Microcystis* vertical migration the Langevin-Fokker-Planck methodology seems more suitable.

The buoyancy Stokes number we have introduced in Section 3.5 appears to be a potential candidate in order to predict the strength of turbulence in relation with settling/rising terminal velocity of the colonies. Similar ratios have been proposed by Humphries and Lyne (1988) and MacIntyre (1993), with the difference that those were based on heuristic arguments rather than our formal analysis. Hence, the added value of this dimensionless number relies on its explicit derivation which results from the reduced dimensionless MR equation of motion instead of empiricism. At the same time, it is expected that the analysis of the buoyancy Stokes number will largely profit from additional simulations with mixing rates that are more vigorous (higher turbulence intensities than $\nu = 10^{-6} \text{ m}^2\text{s}^{-3}$). The vertical migration of the colonies is to a certain degree bounded by the ratio of the euphotic depth and the depth of the mixed layer. For intense turbulence in a density-stratified domain the colonies will be dispersed within this region and the spreading will remain limited by the depth of the mixed layer (plateau).

In natural temperate systems, most phytoplankton blooms usually occur in spring and summer. At this stage temporary or even permanent density stratification may be present. Here, only the neutral case is considered as a first approximation to the coupling problem. Although in general DNS is widely applied for evaluating models and theories (Marshall and Huang, 2010; Toschi and Bodenschatz, 2009; Moin and Mahesh, 1998; Squires and Yamazaki, 1995). We should emphasize that the present flow configuration is still rather academic, but it allows already preliminary evaluation of the role of turbulence intensity, light extinction effects, colony diameter and daylight hours on the vertical distribution of *Microcystis aeruginosa* colonies in the water column.

In this study we included the delay time for assimilation of carbohydrates defined by Wallace and Hamilton (2000). They also mention the importance of biochemical processes involved in the acclimation of the delay time. From a mathematical point of view, a biochemical response time would give continuity and differentiability of the rate of cell mass-density. Currently, the rate of change of cell mass-density abruptly changes sign when the threshold of minimum Irradiance is reached. However, these processes have not been quantified yet and are not included in the present study. This topic represents a challenge for future research.

We have proposed a methodology with which further fundamental analysis could be carried out, *e.g.* incorporating other species for competition studies, prey-predator physical interactions and particle flocculation. The last two studies would require the inclusion of the Basset history force in the reduced equation of motion as pointed out in Van Aartrijk and Clercx (2010a). Additionally, there are other aspects that would play an important role and are not incorporated here. These are the fluid density-stratification in the presence of a thermocline and free surface wall-bounded flow. Further research based on the normalization-scaling procedure proposed in this study should consider the latter aspects.

Acknowledgments

This research was supported by a grant from Deltares (Deltares project numbers 1202633 and 1202837.005). We wish to acknowledge the Stichting Nationale Computerfaciliteiten (National Computing Facilities Foundation (NCF)) for the use of supercomputer facilities, and the Netherlands Organization for Scientific Research (NWO). We would like to thank Marleen van Aartrijk for providing the pseudospectral code and Michel van Hinsberg for scientific discussions and for helping us with the implementation of several particle tracking upgrades of the code.

3.7 References

- Aparicio Medrano, E., Uittenbogaard, R.E., Dionisio Pires, L.M. van de Wiel, B.J.H. and Clercx, H.J.H. (2013). Coupling hydrodynamics and buoyancy regulation in *Microcystis aeruginosa* for its vertical distribution in lakes. *Ecological Modelling*, 248 : 41-56.
- Armenio, V. and Fiorotto, V. (2001). The importance of the forces acting on particles in turbulent flows. *Physics of Fluids*, 13, 2437-2440.
- Aartrijk, M. van, Clercx, H.J.H. and K.B. Winters, K.B. (2008). Single-particle, particle-pair and multi-particle dispersion of fluid particles in forced stably stratified turbulence. *Physics of Fluids*, 20, 025104.
- Aartrijk, M. van (2008). Dispersion of inertial particles in stratified turbulence. Ph.D. thesis, Technical University of Eindhoven.
- Aartrijk, M. van and Clercx, H.J.H. (2010a). The dynamics of small inertial particles in weakly stratified turbulence. *Journal of Hydro-environment Research*, 4, 103–114.
- Aartrijk, M. van and Clercx, H.J.H. (2010b). Vertical dispersion of light inertial particles in stably stratified turbulence: the influence of the Basset force. *Physics of Fluids*, 22, 013301.
- Babiano, A., Cartwright J. H. E., Piro, O. and Provenzale, A. (2000). Dynamics of a small neutrally buoyant sphere in a fluid and targeting in Hamiltonian systems. *Physical Review Letters*, 84, 5764-5767 .
- Candelier, F., Angilella, J.R. and Souhar, M. (2004). On the effect of the Boussinesq-Basset force on the radial migration of a Stokes particle in a vortex. *Physics of Fluids*, 16, 1765-1776.
- Codd, G.A. (1999). Cyanobacterial toxins: their occurrence in aquatic environments and significance to health. In: Charpy, L., Larkum, A.W.D. (Eds.), *Marine Cyanobacteria*, 19. *Bulletin de l'Institut Océanographique*, Monaco, 483–500.
- Croze, O.A., Sardina G., Ahmed M., Bees M. A. and Brandt L. (2013). Dispersion of swimming algae in laminar and turbulent channel flows: theory and simulations. *Journal of the Royal Society Interface*, 10, 81.20121041.
- Denman, K. L. and Gargett, A. E. (1983). Time and space scales of vertical mixing and advection of phytoplankton in the upper ocean. *Limnology and Oceanography*, 28, 801-815.
- Dunsbergen, D. (1994). Particle Models for transport in three-dimensional shallow water flow. Ph.D. Thesis, Delft University of Technology.
- Etemad-Shahidi, A. and Imberger, J. (2001). Anatomy of turbulence in thermally stratified lakes. *Limnology and Oceanography*, 46, 1158–1170.

- Hinsberg, M.A.T. van, Thije Boonkamp, J.H.M. ten, Toschi, F. and Clercx, H.J.H. (2012). On the efficiency and accuracy of interpolation methods for spectral codes. *SIAM Journal on Scientific Computing*, 34, B479-B498.
- Howard, A. (1997). Computer simulation modelling of buoyancy change in *Microcystis*. *Hydrobiologia*, 349, 111-117.
- Humphries, S. and Lyne, D. (1988). Cyanophyte blooms: the role of cell buoyancy. *Limnology and Oceanography*, 33, 79-91.
- Ibelings, B.W., Mur, L.R. and Walsby, A.E. (1991). Diurnal changes in buoyancy and vertical distribution of *Microcystis* in two shallow lakes. *Journal of Plankton Research*, 13, 419-436.
- Ibelings, B.W. and Mur, L.R. (1992). Microprofiles of photosynthesis and oxygen concentration in *Microcystis* scums. *FEMS Microbiology Ecology*, 86, 195-202.
- Imberger, J. (1985). Thermal characteristics of standing waters: an illustration of dynamics processes. *Hydrobiologia*, 125, 7-29.
- Imberger, J. and Ivey, G. N. (1991). On the nature of turbulence in a stratified fluid. Part II: Application to lakes. *Journal of Physical Oceanography*, 21, 659-679.
- Jobson, H.E. and Sayre, W.W. (1970). Vertical transfer in open channel flow. *Journal of Hydraulics Division, ASCE*, 96, 703-724.
- Marshall, J.S. and Huang, Y. (2010). Simulation of light-limited algae growth in homogeneous turbulence. *Chemical Engineering Science*, 65, 3865-3875.
- Maxey, M. R., and Riley, J. J. (1983). Equation of motion for a small rigid sphere in a nonuniform flow. *Physics of Fluids*, 26, 883-889.
- MacIntyre, S. (1993). Vertical mixing in a shallow, eutrophic lake: Possible consequences for the light climate of phytoplankton. *Limnology and Oceanography*, 38, 798-817.
- McKiver, W.J. and Neufeld, Z. (2011). Resonant plankton patchiness induced by large-scale turbulent flow. *Physical Review E*, 83, 016303.
- Mei, R., Adrian, R.J. and Hanratty, T.J., 1991. Particle dispersion in isotropic turbulence under Stokes drag and Basset force with gravitational settling. *Journal of Fluid Mechanics*, 225, 481-495.
- Metcalf, G., Speetjens, M.F.M., Lester, D.R. & Clercx, H.J.H. (2012). Beyond passive: chaotic transport in stirred fluids. *Advances in Applied Mechanics*, 45, 109-188.
- Moin, P. and Mahesh, K. (1998). Direct Numerical Simulations. A tool in turbulence research. *Annual review of Fluid Mechanics*, 30, 539-578.
- Post, S. and Abraham, J. (2002). Modelling the outcome of drop-drop collisions in Diesel sprays. *International Journal of Multiphase Flow*, 28, 997-1019.

- Reynolds, C. S., Jaworski, G. H. M., Cmiech H. A. and Leedale G. F. (1981). On the Annual Cycle of the Blue-Green Alga *Microcystis Aeruginosa* Kütz. Emend. Elenkin. *Philosophical Transactions of the Royal Society of London. Ser. B*, 293, 419-477.
- Reynolds, C.S., Oliver, R.L. and Walsby, A.E. (1987). Cyanobacterial dominance: The role of buoyancy regulation in dynamic lake environments. *New Zealand Journal of Marine and Freshwater Research*, 21, 379-390.
- Reynolds, C.S., (2006). Ecology of Phytoplankton. Cambridge University Press, Cambridge, UK.
- Reynolds, C.S., Oliver, R.L. and Walsby, A.E. (1987). Cyanobacterial dominance: The role of buoyancy regulation in dynamic lake environments. *New Zealand Journal of Marine and Freshwater Research*, 21, 379-390.
- Ross, O.N. and Sharples, J. (2008). Swimming for survival: the role of phytoplankton motility in turbulent environments. *Journal of Marine Systems*, 70, 248–262.
- Shaw, R. (2003). Particle-turbulence interactions in atmospheric clouds. *Annual Review of Fluid Mechanics*, 35, 183-227.
- Sirenko, L. A., 1972. Physiological basis of multiplication of blue-green algae in reservoirs. (In Russian). Naukova Dumka, Kiev, 162 pp.
- Smith, S.D. and Banke, E.G. (1975). Variation of the sea surface drag coefficient with wind speed. *Quarterly Journal of the Royal Meteorological Society*, 101, 665–673.
- Squires, K. and Yamazaki, H. (1995). Preferential concentration of marine particles in isotropic turbulence. *Deep-sea Research*, 42 , 1989-2004.
- Tanga, P. and Provenzale, A. (1994). Dynamics of advected tracers with varying buoyancy. *Physica D*, 76, 202-215.
- Tennekes, H. and Lumley, J. L. (1972). A First Course in Turbulence, MIT Press, Cambridge, MA.
- Thorpe, S. A. (1977). Turbulence and mixing in a Scottish loch. *Philosophical Transactions of the Royal Society of London*, 86, 125–181.
- Toschi, F., and Bodenschatz, E. (2009). Lagrangian properties of particles in turbulence. *Annual Review of Fluid Mechanics*, 41, 375–404.
- Visser, P. M., B. W. Ibelings, L. R. Mur, and A. E. Walsby. 2005. The ecophysiology of the harmful cyanobacterium *Microcystis*: features explaining its success and measures for its control, p. 109–142. In J. Huisman, H.C.P. Matthijs, and P.M. Visser (ed.), Harmful cyanobacteria. Springer, Dordrecht, The Netherlands.
- Visser, P. M., J. Passarge, and L. R. Mur. (1997). Modelling the vertical migration of the cyanobacterium *Microcystis*. *Hydrobiologia*, 349, 99-109.
- Vojir, D.J. and Michaelidis, E.E., 1994. Effect of the history term on the motion of rigid spheres in a viscous fluid. *International Journal of Multiphase Flow*, 20, 547-556.

- Wallace, B. B. and D. P. Hamilton, (2000). Simulation of water-bloom formation in the cyanobacterium *Microcystis aeruginosa*. *Journal of Plankton Research*, 22, 1127–1138.
- Walsby, A.E. (1988). Buoyancy in relation to the ecology of freshwater phytoplankton. in: F.E. Round (ed.), *Algae and the aquatic environment*. Biopress Ltd., Bristol, 125-137.
- Winters, K.B., MacKinnon, J.A., and Mills, B. (2004). A spectral model for process studies of rotating, density-stratified flows. *Journal of Atmospheric and Oceanography Technology*, 21, 69–94.
- Yamazaki, H., Osborn, T. R. and Squires, K. D. (1991). Direct numerical simulation of planktonic contact in turbulent flow. *Journal of Plankton Research*, 13, 629-643.
- Yamazaki, H, Mackas, D. and Denman, K. (2002). Coupling small-scale physical processes to biology: towards a Lagrangian approach. In: A.R. Robinson, J.J. McCarthy and B.J. Rothschild (eds.). *The Sea: Biological-Physical Interactions in the Ocean*, 12, 51-112.

Chapter 4

Could cyanobacterial scum formation be explained by oxygenic photosynthesis?¹

¹ The contents of this chapter, with minor modifications, have been submitted in the form of a paper.

Abstract

The cause of persistent cyanobacteria scum formation in lakes is an unresolved subject. Scum refers to the event in which cyanobacteria remain at the water surface of a lake or reservoir. The general notion is that the combination of low turbulence levels, long day-light and high water temperatures plays a role in the occurrence of scums. In literature the buoyancy capacity of cyanobacterial cells (see Chapter 2 and 3) is usually given as the major reason for these scum formations. However, daily cycles of buoyancy change result in continuously sinking and rising of cyanobacteria colonies without permanent accumulation at the surface and this therefore cannot explain persistent scums at the water surface. In this study, we present an alternative explanation: irreversible buoyancy of cyanobacterial colonies leads to more persistent scums (*i.e.* colonies do not sink due to photosynthesis).

The hypothesis we present here is that irreversible buoyancy of cyanobacteria colonies is created by the growth of gas bubbles on or in the mucilage of the colonies. These bubbles grow under oxygen super-saturation conditions. At low wind speed and high chlorophyll levels the dissolved oxygen (DO), produced during photosynthesis by cyanobacteria, cannot escape sufficiently fast to the atmosphere thereby creating DO super-saturation in the water. At that stage, growth of oxygen bubbles may occur inside or attached to the mucilage.

We present results of compression experiments (using the Riebesell chamber) to support our hypothesis. In the chamber, the pressure on lake water containing a natural cyanobacteria population is increased. At 3 and 4 bars the cyanobacteria colonies were not able to float anymore and sank. This pressure is lower than the 10 bar needed to collapse all gas vesicles inside the cyanobacteria cells (Walsby, 1994). The observed change from floating to sinking colonies due to increased water pressure suggests that gas bubbles were present inside the colonies. In lakes, these gas bubbles may lead to permanent buoyancy, *i.e.* a scum.

4.1 Introduction

In this study the formation of cyanobacteria scums will be discussed. At present a comprehensive understanding of cyanobacteria scum formation appears to be lacking. We focus on the transition from a bloom to a scum, *i.e.* the stage of scum formation itself. In literature a number of alternative explanations for cyanobacterial scum formation are given and these will be discussed below. Next, we present our hypothesis *i.e.* scum formation (colonies overbuoyancy) due to oxygen bubble growth in the mucilage of cyanobacteria under oxygen supersaturated conditions. To support our hypothesis we present the results of compression experiments (abbreviated as Riebesell experiments) suggesting that oxygen bubbles are present in recently formed cyanobacteria scums.

Generally, eutrophication (elevated contents of nutrients in the water column) has a negative consequence for water quality and the aquatic life. A common symptom of eutrophication is the formation of cyanobacteria blooms. Blooms are often composed by species that produce toxins. Such toxins can cause damages to animals and humans (Codd *et al.*, 2005). Blooms can also be precursors for scum formation. The most common cyanobacteria species that form nuisance scums are *Microcystis* spp., *Planktothrix* spp., *Anabaena* spp., *Aphanizomenon* spp. (Reynolds and Walsby, 1975). Although these genera differ in form, they all appear as colonies composed of cells with gas vesicles embedded in mucilage. An important feature of cyanobacteria, also known as blue green algae, is their ability to perform vertical migration (rising/sinking) within the time span of a daily cycle via buoyancy regulation (Reynolds and Walsby, 1975). Their ability to regulate their buoyancy is mainly the result of the cell composition (cells contains gas vacuoles all embedded in mucilage). The cyanobacteria cells produce carbohydrates (so called carbon assimilation in which carbon from CO₂ is incorporated in the newly produced carbohydrates) when exposed to light and respire carbohydrates under dark conditions. In deep stratified lakes this capability of buoyancy regulation contributes to the success of cyanobacteria in the competition with green algae for light. The oxygen gas bubbles (a consequence of oxygen supersaturation) described in this study are *not the same* as the gas vesicles inside the cells of cyanobacteria. Gas vesicles are rigid structures *i.e.* hardly compressible, fully permeable by diffusion to

the surrounding gases and capable to withstand considerable pressures (Walsby, 1994).

A distinction has to be made regarding the definition of a cyanobacteria bloom and a scum. The word bloom is commonly used to refer to high concentrations of cyanobacteria in the upper layers of water bodies and to their accumulation at the surface of lakes and reservoirs (Reynolds and Walsby, 1975). In this study we exclusively refer to *scums* as the extremely high concentration of cyanobacteria that accumulate at the surface of a lake or reservoir and persist for more than a day (Ibelings *et al.*, 1991).

In this study, the species of interest is *Microcystis aeruginosa*. *Microcystis* is a well know species which occurs worldwide. The processes of photosynthesis and supersaturation of dissolved oxygen in surface water not only correspond to cyanobacteria but more generally to plants and algae. Nevertheless, the combination of vertical mobility and oxygen supersaturation is reserved to cyanobacteria only. A *Microcystis* colony is composed of cells embedded in mucilage which is mainly composed by polysaccharides. The composition of the polysaccharides is reported by De Philippis and Vincenzini (1998) and mainly consists of monosaccharides (acidic and neutral sugars). The most frequently found monosaccharide is glucose, mannose and rhamnose. The mucilage has a high water content that reduces its overall mass density to nearly the same density as water, in spite of the high density of the polysaccharides (1500 kg m^{-3}) (Reynolds, 2007). Each cell has vacuoles and each vacuole contains gas vesicles. The gas vesicles are hollow and rigid and filled with air (Walsby, 1994). Gas vesicles are a common feature of several cyanobacteria *e.g.* *Anabaena*, *Microcystis*, *Planktothrix*, *Gloeoetrichia*. After destruction of the gas vesicles, the space originally occupied by gas is partially filled with water (Walsby, 1980).

According to Aparicio Medrano *et al.* (2013) it is convenient to consider the total mass of a colony as the sum of specific elements with its own specific weight and volume. Including the contribution of gas bubbles the total mass of a colony reads:

$$\dots_{col} (V_{col} + V_{bub}) = \dots_{cell} (V_{cell} - V_{ves}) + \dots_{ves} V_{ves} + \dots_{muc} V_{muc} + \dots_{bub} V_{bub} \quad (1)$$

with \dots_{col} the colony mass-density, \dots_{cell} the cell-tissue density, \dots_{muc} the mass-density of the mucilage plus interstitial water, \dots_{ves} the gas vacuoles density, \dots_{bub} the air density inside the bubble, V_{col} the colony volume ($V_{col} = V_{cell} + V_{muc}$), V_{cell} the volume occupied by cells, V_{ves} the gas vesicles volume, V_{muc} the mucilage volume and V_{bub} the volume occupied by the gas bubbles. The mass-density of a colony can be expressed as

$$\dots_{col} = \dots_{cell} \frac{n_{cell}(1-n_{ves})}{1+n_{bub}} + \dots_{muc} \frac{(1-n_{cell})}{1+n_{bub}} + \dots_{ves} \frac{n_{ves}n_{cell}}{1+n_{bub}} + \dots_{bub} \frac{n_{bub}}{1+n_{bub}}, \quad (2)$$

where n_{ves} equals to the ratio of gas vesicles volume to cell volume, n_{cell} the ratio of total cell volume to colony volume and n_{bub} is the ratio of bubbles volume to colony volume. The mucilage mass-density can be expressed as $\dots_{muc} = \dots_w(1-n_{pol}) + \dots_{pol}n_{pol}$, with n_{pol} the ratio of polysaccharides to mucilage volume, \dots_{pol} the mass-density of the polysaccharides and \dots_w the density of water. Considering that \dots_{muc} is nearly constant and that \dots_{ves} and \dots_{bub} are negligible, expression 2 shows that the following four variables can lead to a change in colony mass-density: the cell mass-density, the effects of colony composition n_{cell} , n_{ves} and n_{bub} . Table 4.1 summarizes common values for *Microcystis*.

Table 4.1: Measured values of biological parameters for *Microcystis* (Reynolds *et al.*, 1981). ρ_{col} is the mass-density of a colony, ρ_{muc} is the density of the mucilage, ρ_w is the density of water (998 kg m⁻³), n_{cell} is the ratio of cell volume to colony volume and n_{ves} is the ratio of gas vesicles volume to cell volume.

	Min	Max	
ρ_{col}	995	1015	kg m ⁻³
$\rho_{muc}(\rho_w + 0.7)$	998.7	998.9	kg m ⁻³
n_{cell}	20	26	%
n_{ves}	5	8	%

4.2 Literature review of scum formation mechanisms

The formation of scums has long been attributed to the vertical migration of cyanobacteria. At present it is known that the phenomenon of buoyancy regulation (vertical migration leading to temporally elevated cyanobacteria concentration levels at the surface) occurs mainly due to two factors. The first factor is the biological processes of carbohydrates accumulation and respiration as shown by Reynolds *et al.*, 1987, Ibelings *et al.*, 1991 and Visser *et al.*, 1997. The second factor is the composition of a cyanobacteria colony (including gas vacuoles, mucilage), that brings the density of a colony to a nearly neutral mass-density. The processes of carbon assimilation and respiration for *Microcystis* have been measured in laboratory experiments (Visser *et al.*, 1997). Figure 4.1 shows the rate of change in cell mass-density as function of solar irradiation. It has been shown that assimilation and respiration of carbohydrates do not lead to the formation of scums (Aparicio Medrano *et al.*, 2013). Photoinhibition is marked as the shaded area in the figure.

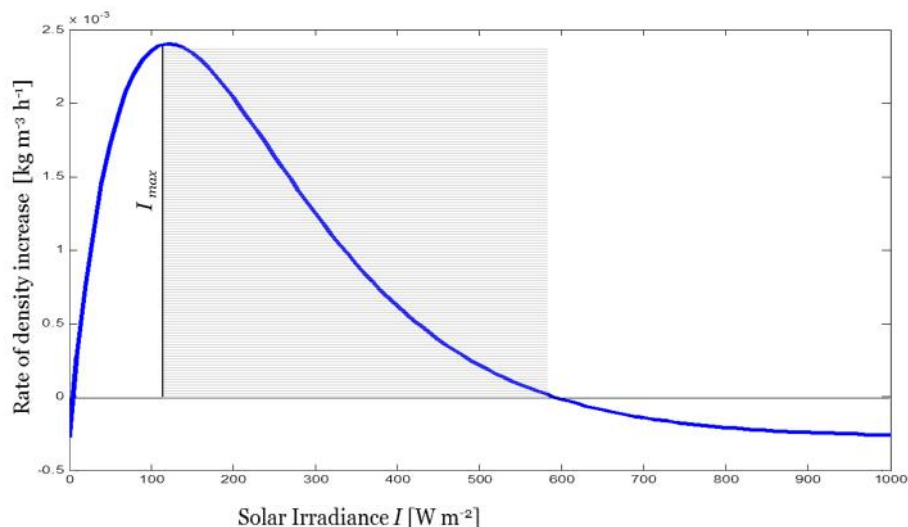


Figure 4.1: Rate of change in cell mass-density as a function of light intensity. The shaded area represents light intensities resulting in photoinhibition (slightly modified from Visser *et al.*, 1997).

Previous research identified three conditions that allow the formation of a scum (Ibelings *et al.*, 2003). These are: 1) an existing population of cyanobacteria (bloom); 2) the presence of buoyant colonies in the bloom and 3) stability of the water column (stratified) combined with low turbulence intensities.

Different hypotheses for cyanobacterial scum formation have been suggested. They are: 1) the photoinhibition hypothesis, 2) the self-shading hypothesis, 3) the carbon depletion hypothesis, 4) the extra gas vesicles hypothesis, 5) the superbuoyancy hypothesis, 6) the dead-stage hypothesis, 7) the sudden bloom at the surface hypothesis and, 8) the apparent scum hypothesis. These hypotheses are discussed here below.

The *photoinhibition* hypothesis

Photoinhibition refers to a reduction in the photosynthetic capacity of cyanobacteria due to high light intensities (Figure 4.1). Cyanobacteria become so strongly photoinhibited at the water surface that they are unable to synthesize carbohydrates or carbohydrates accumulation is far below optimal levels: therefore, potentially, colonies remain at the surface (Reynolds and Walsby, 1975).

Indeed photoinhibition is a common feature of the photosynthetic process. Very strong photoinhibition has been measured in several phytoplankton species (Long *et al.*, 1994). Considering *M. aeruginosa*, Visser *et al.* (1997) measured a positive but slow rate of carbohydrate accumulation even when the cells underwent photoinhibition. This implies that eventually a colony will sink, provided no other buoyant mechanisms is available (see Chapter 3). More arguments against the photoinhibition hypothesis exist. It has for instance been shown that cells subjected to high irradiances enhance their carotenoid content and thus can resist higher irradiation without damaging their photosynthetic apparatus (Paerl *et al.*, 1995). Moreover, the possibilities for a colony to reach the surface abruptly and receive a shock of irradiance impairing its photosynthetic apparatus are low. If we consider a colony that has been respiring (in the dark) and has a mass-density (ρ_{col}) lower than water, then as it rises (because of its mass-density) and crosses the euphotic layer towards the surface it will experience an increase in irradiance ΔI . An increase in irradiance ΔI is proportional to an increase in cell mass-density $\Delta\rho_{cell}$. As a result, the colony mass-density will increase. Next, the colony vertical velocity will change leading to a change in vertical position z . Therefore, the colony will experience a gradual accumulation of carbohydrates causing its gradual transition towards sinking mode rather than appearing suddenly at the surface.

The *self-shading* hypothesis

Colonies near the surface of a lake reduce the light availability below and create dark conditions for the colonies under it. The cyanobacteria colonies in the dark would be respiring (getting lighter than water) and not able to photosynthesis and accumulate carbohydrates. The light colonies would act like an air cushion thereby keeping heavy colonies on top (Ibelings and Mur, 1992).

The experiments performed by Ibelings and Mur (1992), to support their hypothesis, consisted on collecting a cyanobacteria sample early in the morning. The colonies were left in the dark and allowed to float to the surface. Next, the sample received light pulses and oxygen profiles were recorded. The results show that high oxygen supersaturation levels (>300 %) exist on the top millimeters of the scum. This implies that the colonies at the top are photosynthesizing (becoming heavier) but they remain at the surface. According to Ibelings and Mur colonies at the surface were kept there because the deeper located lighter colonies were pushing upwards. However, this explanation is not physically likeable because heavier particles on top of lighter particles represent a hydrodynamically unstable convective state. The oxygen levels measured would suggest that oxygen gas bubbles would be present. The oxygen bubbles may be the reason for the colonies to remain at the surface.

For a considerable reduction in light availability (less than 1% of surface irradiance) a very thick scum must already be formed (> 5 cm). Therefore the self-shading mechanism cannot be considered as an initiator for scum formation. As an illustration, Figure 4.2 shows the vertical profile of irradiance under a scum. The measurements were taken in Lake Vlietland (The Netherlands) during *Microcystis* scum formation in the summer of 2009. According to the measurements of Visser *et al.* (1997) a light intensity higher than 6 W m^{-2} yields sufficient light for *Microcystis* cells to accumulate carbohydrates. Figure 4.2 shows that up to a depth of 1 meter it is the case even when a scum is present.

Summarizing, we believe that the self-shading hypothesis is not responsible for initiating scum formation.

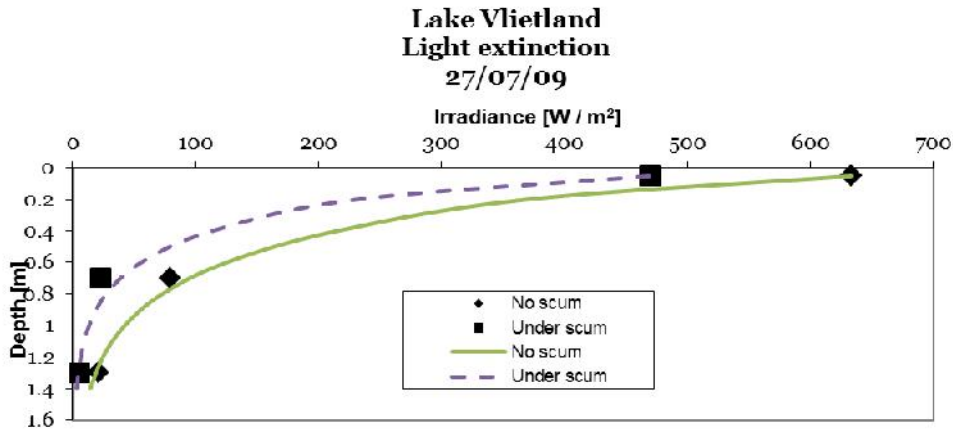


Figure 4.2: Light availability measured in Lake Vlietland during scum in August 2009. The markers represent the measurements. The lines are drawn based on the computed extinction coefficients from the measurements. The filled line shows the light intensity in clear water and the dashed line shows the light intensity under a scum.

The carbon depletion hypothesis

Large biomass of cyanobacteria (high productivity) results in reduction of carbon dioxide (CO_2) in the epilimnion of a lake (as detected by $\text{pH} > 10$). The shortage of CO_2 causes the cyanobacteria colonies to move to the air-water interface in order to capture atmospheric CO_2 directly (Paerl and Ustach, 1982). A shortage of CO_2 and other inorganic carbon causes respiration to be higher than carbon uptake and therefore the colonies are highly buoyant.

In most natural lakes CO_2 shortage rarely occurs (Shapiro, 1997; Cole *et al.*, 1994). However, in water poorly buffered against low pH, Maberly (1996) measured carbon-depletion ($\approx 0.01 \text{ mg l}^{-1}$ of CO_2) in productive waters together with high pH values (> 10). We do not rule out that in some lakes or reservoirs CO_2 depletion may occur and drive cyanobacteria to reach the air-water interface. Nevertheless, for the studied Lake Vlietland we found normal pH levels ($\text{pH} \sim 8.5 \approx 2.2 \text{ mg l}^{-1}$ of CO_2) throughout the summer period of 2009 in which *Microcystis* scums occurred (Annex A). We agree that the availability of CO_2 may determine the dominance of cyanobacteria over green algae in lakes as suggested by Shapiro (1997) but it does not explain the formation of a scum.

If the colonies of cyanobacteria float to the surface because C-uptake possibilities are lacking, they will resume their accumulation of carbohydrates when they reach the surface. Eventually the colonies will become heavier than water (approximately a few hours) and therefore sink provided no oxygen bubbles are formed. Therefore, under the carbon depletion hypothesis the colonies will not remain at the surface for several hours and form a scum.

The *extra gas vesicles* hypothesis

Walsby(1980) proposed that scum formation occurs due to extra growth of gas vesicles within the cells. Careful observations however, showed that in several hours no significant change in gas vesicles content occurs (Walsby, 1994). Ibelings *et al.* (1991), performed measurements for the changes of gas vesicles during a diurnal cycle of *Microcystis*. These authors concluded that the changes in gas vesicle content were too low (< 2%) to be responsible for the vertical migration observations.

The *superbuoyancy* hypothesis

This hypothesis states that scum is formed by colonies which remained at low irradiances (at night or in dark layers) and have become highly buoyant (colony mass-density much lower than water density). These highly buoyant colonies will slowly accumulate carbohydrates and will become entrapped at the surface (Walsby *et al.*, 1997).

If at the beginning of daylight a colony is at the surface with very low cell mass-density (*e.g.* 1037 kg m^{-3}) it takes approximately one hour before the cell mass-density reaches values in order of 1050 kg m^{-3} , such that the total colony mass-density exceeds the density of the surrounding water and sinks. The latter calculation uses the coefficients for accumulation of carbohydrates measured by Visser *et al.* (1997) for *Microcystis aeruginosa*. The superbuoyancy hypothesis therefore cannot explain a persistent scum in the field because colony mass-density increases rapidly when the colonies become exposed to sunlight.

The *dead-stage* hypothesis

This hypothesis assumes that a scum is a form of cyanobacteria colonies senescence (dying cells) (Reynolds and Walsby, 1975). Measurements on early formed scums

showed that there is still much photosynthetic activity in the top layer of a scum (Ibelings and Mur, 1992). The photosynthetic activity implies that the process of carbon assimilation and respiration is active. After a scum has been formed and is transported and collected on the lake shores the colonies at the top will desiccate (dry out). This phenomenon of desiccation occurs in what we call hyperscums (*i.e.* following a scum) and therefore is outside the scope of this investigation.

The sudden *bloom at the surface* hypothesis

This hypothesis assumes excessive growth of colonies that suddenly collect and stay at the surface. This possibility has been discarded considering the growth rate of cyanobacteria species (Reynolds and Walsby, 1975). To reach concentrations encountered during scums it is necessary to have a growing time (time after which the population has doubled) of two hours. However, most cyanobacteria have a doubling time of at least one day (Reynolds and Walsby, 1975).

The *apparent scum* hypothesis

Scum is an apparent manifestation of colonies arriving alternately close to the surface (Kromkamp and Walsby, 1990). We consider this apparent accumulation not a scum but just a temporarily accumulation. A scum refers to the *persistent* accumulation at the surface for more than a day (Ibelings *et al.*, 1991). The temporal accumulation, if it occurs, would be a consequence of vertical migration and that does not explain scum formation lasting more than 24 hours.

4.3 Hypothesis for the formation of Cyanobacteria scum

4.3.1 Sequence resulting in scum formation

Our hypothesis is that irreversible buoyancy of cyanobacteria colonies occurs due to growth of gas bubbles in or on the mucilage of the colonies. In water treatment plants the technology referred to Dissolved Air Flotation (DAF) has some resemblance to our hypothesis. In DAF air is dissolved in pressurized water until saturation concentrations are reached and subsequently released to normal pressure in water tanks containing algae. In that way gas bubbles are formed. Additionally, flocculants are added to the algae which reduce their electric charge to zero, thus promoting the

binding (flocculation) of bubbles and algae. The final floc plus gas bubbles rise to the surface for further removal (Edzwald, 1995). The technology is expensive and as an alternative another technique has been proposed which uses the same principle: *autoflotation*. In autoflotation the minute gas bubbles trapped in algae flocs are responsible for collecting algae at the surface (Vuuren *et al.*, 1965; Arbalaez *et al.*, 1983; Jodolowski, 2002). The latter researchers assumed that the origin of the minute bubbles is high dissolved oxygen (DO) levels from photosynthesis. Autoflotation follows from high DO production of pre-flocculated algae.

As mentioned in the Introduction a scum may occur following a bloom (or several blooms). Favorable conditions for bloom formation are mild wind, moderate or strong irradiances and in the case of deep lakes the existence of stratified water column (Ibelings *et al.*, 2003). In addition, we consider the pre-existence of a cyanobacteria bloom as a first essential condition for a scum to occur.

A cyanobacteria bloom (high concentrations of cyanobacteria) is usually reflected in high chlorophyll concentrations. The result of the photosynthetic activity is oxygen production and an increase in dissolved oxygen (DO) concentrations (provided consumption is weak). Although during respiration DO is consumed (Ibelings and Maberly, 1998; Plough, 2008), several days of blooms and DO production may increase the DO to supersaturation levels. DO supersaturation could only occur due to the presence of a bloom, which is why we consider a bloom as the essential first condition. Figure 4.3 shows the cycle of oxygen and carbon due to assimilation, respiration and vertical migration by cyanobacteria. When the colony resides in the upper illuminated layers near the surface it will take up carbon and release oxygen due to photosynthetic processes. As a consequence, the heavier colonies sink lower in the epilimnion where due to respiration carbon is released and oxygen is consumed. This vertical mobility creates a distribution of high oxygen concentrations near the surface and low concentrations at deeper and darker water layers of the epilimnion.

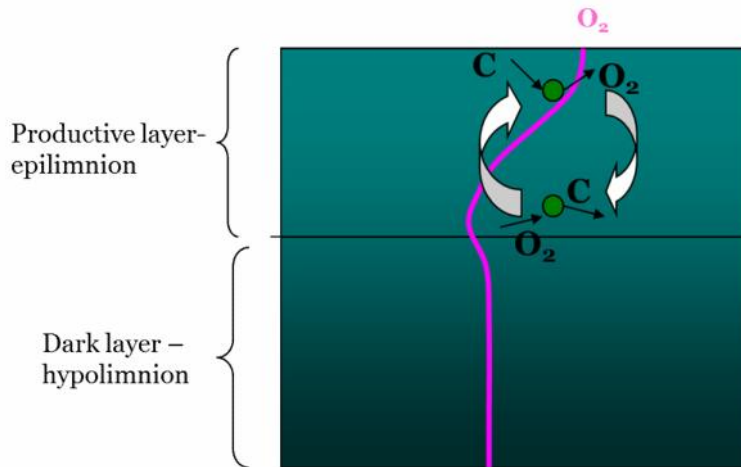


Figure 4.3: Schematic representation of the oxygen and carbon pump caused by vertical mobility of cyanobacteria. Close to the surface there is carbon uptake by the colonies and production of oxygen, the colonies transported at the bottom of epilimnion respire carbon and consume oxygen.

When the forcing of wind on the lake is weak, this may have two important consequences for scum formation. The exchange of oxygen with the atmosphere will be reduced (Wanninkhof and Bliven, 1991) and the wind-driven turbulent mixing intensity in the water tends to be low (see Chapter 3). As a second essential condition for scum formation we consider DO supersaturation in lakes accompanied with low wind intensities so that vertical mobility dominates.

As a third essential condition we assume the existence of nucleation sites for bubble growth (Yount, 1982), probably both in or on the mucilage. There are two possibilities for nucleation (formation of a nucleus): homogeneous and heterogeneous. Homogeneous nucleation requires very high reduction in pressure (100 atm. or in equivalent saturation levels $\gg 1000\%$) that do not occur in lakes. Heterogeneous nucleation can occur on existing surface impurities, nuclei and small supersaturation levels that occur in the top layers of lakes (Ramsey, 1962). Therefore heterogeneous nucleation is feasible on for example a solid surface with gas filled cracks. If the DO supersaturation is such that the partial pressure in water is higher than the pressure inside the bubble (Section 4.3.3), bubble growth may occur (Ramsey, 1962). The required and feasible level of supersaturation ($\approx 140\%$) occurs near the surface of a lake (Section 4.3.2) (Ramsey, 1962), mostly cyanobacteria due to vertical migration reach this layer (see Chapter 3).

Finally, the presence of gas bubbles inside colonies will bring the cyanobacteria colonies to an irreversible highly buoyant state ending at the surface and forming scums (Figure 4.4). Figure 4.5 shows bubbles in a *Microcystis* scum sample taken on an early morning in Lake Vlietland. The measured supersaturation oxygen level was higher than 150%.

Below I provide an explanation for scum formation using physical arguments based on principles of oxygenic photosynthesis.

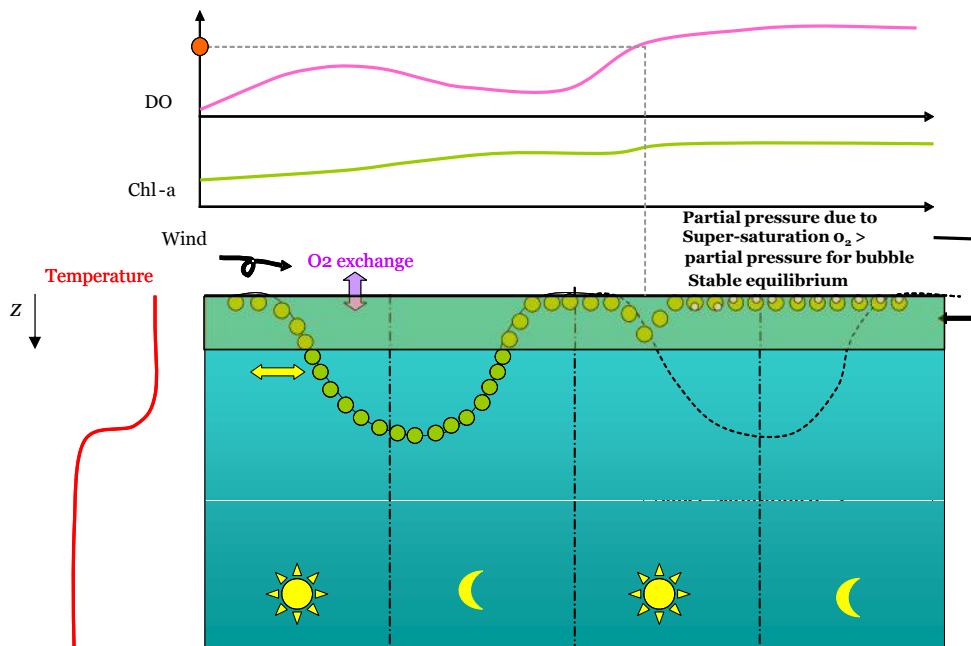


Figure 4.4: Schematic representation of the formation of a scum by oxygenic photosynthesis. The top figure shows the increase in DO levels until a point of supersaturation is reached (red point). The figure in the middle shows the increase in chlorophyll-a concentrations which is responsible for the increase in DO concentrations. The lower figure shows a cyanobacteria colony, performing vertical migration due to the buoyancy regulation, eventually floating to the surface where it will remain when oxygen bubbles are formed and attached to the mucilage.

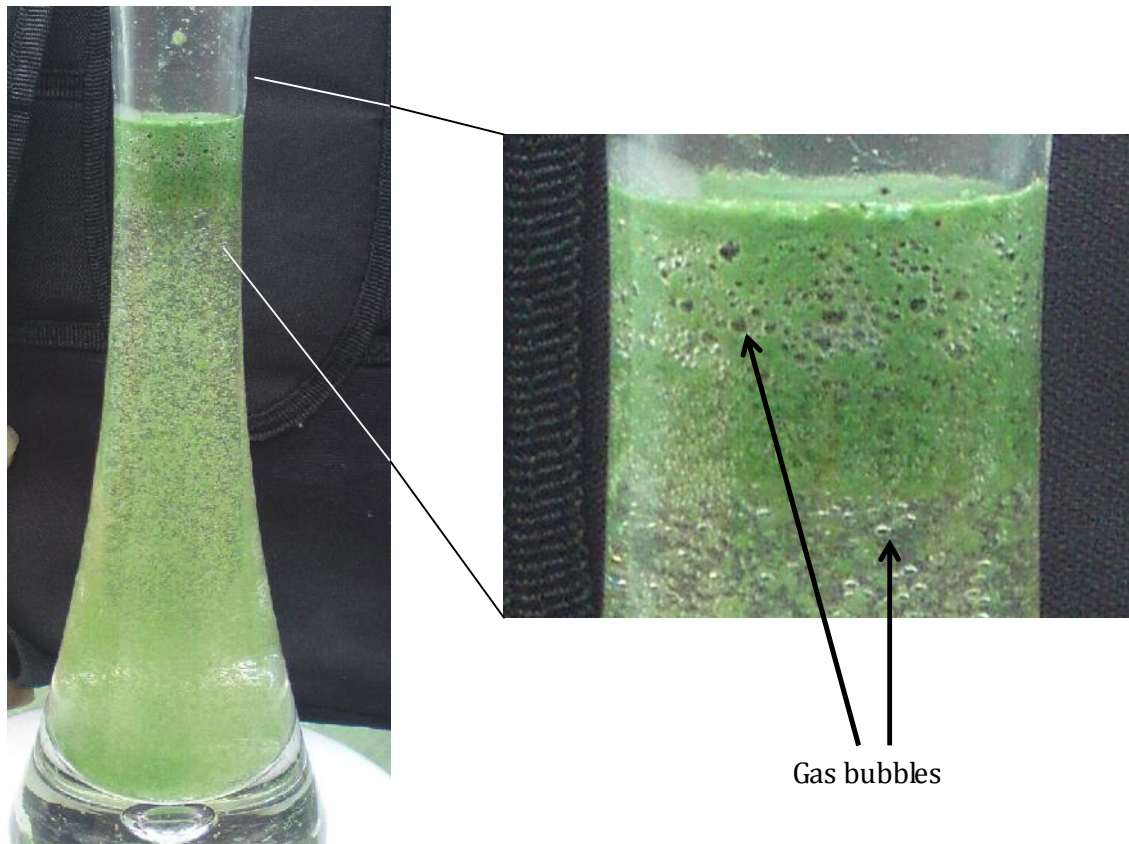


Figure 4.5: Visible gas bubbles in a *Microcystis* scum collected from the surface of Lake Vlietland during the summer of 2009.

4.3.2 Photosynthetic oxygen supersaturation

In the past, oxygen saturation levels often have not been considered as a highly significant parameter in the study of cyanobacterial scum formation (*e.g.* Soranno, 1997; Reynolds and Walsby, 1975; Ibelings *et al.*, 1991). Plough (2008) measured oxygen levels in the millimetric region surrounding an aggregate (surface scum) showing high O₂ supersaturation levels (210% O₂ supersaturation). These microenvironments of O₂ supersaturation have also been measured in benthic species (Revsbech *et al.*, 1983). The oxygen saturation levels leading to bubble growth are not necessarily measured remote (in the water column) from the cyanobacteria scum.

The basics of photosynthesis can be summarized as conversion of CO₂ (and other elements such as nitrogen and phosphorus) into biomass and molecular oxygen (O₂). The produced dissolved oxygen gas is diffused through the cell tissue

increasing the dissolved gas level in the surrounding water (Ploug, 2008). Some oxygen is consumed during respiration. However, consecutive bloom events or one single large bloom will gradually bring the O₂ levels to supersaturation levels (> 140%) (Figure 4.4). DO supersaturation is commonly described in literature as a consequence of the presence of large blooms (150 µg/L of chlorophyll-a leading to 120% of O₂ supersaturation) (Robarts *et al.*, 2005; Marks and Pytel, 2011), but the connection with scum formation has not been made explicitly.

4.3.3 Conditions for bubble growth

Bubbles inside the aggregates have been observed in marine seston formed by detrital-fecal material and living phytoplankton (Riebesell, 1992; Stachowitsh *et al.*, 1990). The growth of gas bubbles in cyanobacteria colonies requires firstly a source of gas production that leads to supersaturation, in this case the natural source would be oxygen (O₂) by photosynthesis. Secondly, given that the surrounding water is supersaturated the diffusion of gas towards the water column will be low.

We assume the pre-existence of microbubbles (micronuclei) (Ramsey, 1962; Yount, 1982) because the pressures required for the homogeneous growth of bubbles in surface water are very high (100 atm.) and unrealistic for natural conditions. As stated by Ramsey (1962) a variety of sources may exist explaining the presence of microbubbles in water. In the sea it may arise from gas seepage from the sea floor, air entrapment as a result of breaking waves, or adsorption of atmospheric gasses on the surface of particulate matter (forming gaseous films on the particles which subsequently form stable microbubbles while the particle is sinking). Biological sources in the sea and lakes include decomposition of detritus (which generally occurs on the bottom) and, more indirectly from biological activity like photosynthesis and respiration by cells as discussed in the section above. However, for these latter processes an environment allowing heterogeneous nucleation is required.

Bubbles inside aggregates and colonies are assumed to be grown out of the microbubbles which are a result of heterogeneous nucleation. The bubble growth must be due to supersaturation of gasses dissolved in the water column, in particular O₂ which is released in the water column around the cyanobacteria due to

photosynthesis resulting in dissolved oxygen supersaturation. Other candidate gasses for bubble growth might be carbon dioxide (CO_2) and nitrogen (N_2). Nitrogen is less soluble in water compared to oxygen but does not take part in the relevant chemical processes related with photosynthesis and respiration (with carbon and oxygen as main contributors) (Ramsey, 1962). Therefore, local supersaturation is not expected and the dissolved nitrogen concentration in the water column will not differ significantly from its value for water in equilibrium with the atmosphere. Nitrogen will thus not promote bubble growth. As we assume that near the surface photosynthesis is the main driver for gas production it is reasonable to assume that also no supersaturation of carbon dioxide will occur as respiration and photosynthesis will not take place simultaneously at the same location (at the surface layer). Moreover, the solubility of CO_2 is approximately twenty times higher than that of O_2 , thus CO_2 as a source for bubble growth can also be excluded.

The rate of solution of gas bubbles by diffusion for undersaturated liquid-gas solutions, or the growth of bubbles by the same mechanism in the case of supersaturation, has been studied by Epstein and Plesset (1950). They assumed that the bubbles have no translational motion and the motion of the medium is also neglected. Epstein and Plesset (1950) also included the effect of surface tension in the analysis of bubble growth or bubble dissolution. Surface tension is particularly relevant for the evolution of the radii of small (nano) bubbles. Next we will briefly introduce the Young-Laplace and Henry's law.

Consider a spherical vapour bubble with radius r in a liquid (consisting of the same pure substance). Standard ambient pressure condition ($P_{amb}=1$ bar at 298 K) is assumed and gravity is absent for the moment.² The difference between the pressure in the gas bubble (P_{int}) and the ambient pressure P_{amb} balances the surface tension which is described by the Young-Laplace equation, $\Delta P=P_{int}-P_{amb}=2\gamma/r$, with γ the surface tension at the vapour-liquid interface (see Figure 4.7). The smaller the bubble the larger the internal pressure will be (assuming that the surface tension remains approximately constant over the range of radii). The vapour-liquid interface is

² The presence of gravity results in an additional hydrostatic pressure contribution depending on the distance of the bubble from the free surface. Moreover, buoyancy will result in rising bubbles, but following Plesset and Epstein (1950) they do not substantially affect bubble growth or dissolution.

permeable in the sense that vapour molecules leave the bubble and end up in the liquid, and the other way around.

Let's now consider a slightly different system. Suppose we have a non-volatile liquid B and a gas bubble entirely consisting of gas A embedded in the liquid. The gas is soluble in the liquid. The net transport of gas molecules through the gas-liquid interface depends on the gas solubility in the liquid and the amount of gas already dissolved in the liquid. The relation between the gas solubility in the liquid and the pressure p of the gas in the bubble is given by Henry's law which states that $p=k_H c$, with c the concentration of the solute in the liquid and k_H a constant of proportionality. Besides the fact that the solubility of the gas in the liquid depends on the pressure it also varies with the temperature. Typical values for k_H of some gases in water at room temperature are: $k_H[\text{O}_2]=769$ L atm/mol, $k_H[\text{CO}_2]=29$ L atm/mol, and $k_H[\text{N}_2]=1639$ L atm/mol confirming the statements about the relative solubility of N_2 and CO_2 compared to that of O_2 mentioned above. (Note that 1 atm is equivalent to 1,01325 bar.)

I now briefly discuss two non-equilibrium situations, thus not satisfying Henry's law. In both cases we consider a bubble consisting of gas A with pressure p (satisfying Young-Laplace equation). The equilibrium solubility of the gas according to Henry's law is: $c_o = p/k_H$. The actual concentration of the gas dissolved in the liquid is now $c < c_o$ (undersaturation). As a result a net flux of molecules of A from bubble to liquid across the interface will take place, thus gas leaves the bubble by diffusive processes to restore equilibrium (*i.e.* to enhance the solute concentration near the bubble). As a result the bubble size decreases but the internal pressure has to increase to satisfy the balance between pressure and surface tension. Increased pressure results in further diffusion of gas molecules into the liquid as the equilibrium value c_o also increases due to Henry's law. We actually have here a positive feedback cycle which results in dissolution of the gas bubble. The other case $c > c_o$ (supersaturation) results in a feedback cycle the other way around and the bubble starts to grow. The classical paper by Epstein and Plesset (1950) provides expressions for the bubble radius as function of time for both cases.

Consider now large gas bubbles consisting of several components, say A, B and C, in water. The size of the bubbles is sufficiently large that surface tension

effects may be ignored. For the bubble in equilibrium with the water the internal pressure P equal to the hydrostatic pressure P_h that varies along the depth in the water column is then the sum of the water vapor pressure p_w and the partial pressures p_{oA} , p_{oB} and p_{oC} :

$$P_h = p_w + p_{oA} + p_{oB} + p_{oC} = p_w + k_H[A]c_{oA} + k_H[B]c_{oB} + k_H[C]c_{oC} . \quad (3)$$

The concentration of substance A in the liquid is then:

$$c_{oA} = (P_h - p_w - k_H[B]c_{oB} - k_H[C]c_{oC})/k_H[A] = (P_h - p_w - p_{oB} - p_{oC})/k_H[A] . \quad (4)$$

Bubble growth may occur for supersaturation of one of the substances, say A, thus when $c_A > c_{oA}$. Define the supersaturation degree by $S_o = c_A/c_{oA} = p_A/p_{oA}$. Applying this relation for air bubbles in the water column supersaturated with oxygen we arrive at the expression introduced by Ramsey (1962),

$$S_o = p(\text{O}_2\text{-water})/p(\text{O}_2\text{-air}) = (P_h - p_w - P_{og})/p(\text{O}_2\text{-air}) , \quad (5)$$

where $p(\text{O}_2\text{-water})$ is the partial pressure of oxygen in water, $p(\text{O}_2\text{-air})$ is the partial pressure of oxygen in air, P_h is the hydrostatic pressure that varies along the depth (z) and P_{og} is the partial pressure of other gases than oxygen (nitrogen, argon and carbon dioxide).

Figure 4.6 shows the DO supersaturation requirement for bubble growth. Measured oxygen saturation values in lakes (130-180 %) suggest that only in the first meter below the water surface (0.5 – 1 m) bubble growth could occur (Bosak *et al.*, 2010).

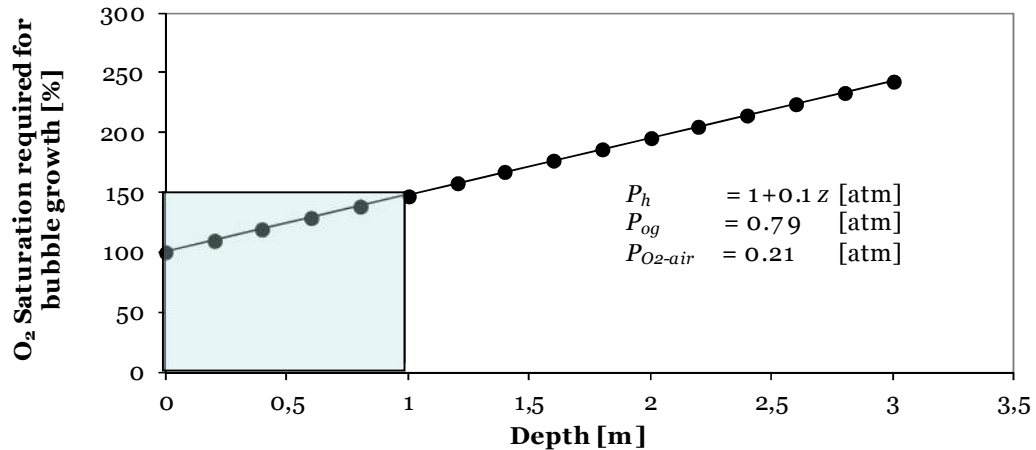


Figure 4.6: Oxygen supersaturation, excluding surface tension, necessary to allow bubble growth. The shaded area shows the more likely supersaturation level reached in natural lakes. Modified from Ramsey (1962).

4.3.4 Stability of gas bubbles

In this study we assume the gas bubbles to be attached to the mucilage. In the previous section we described the conditions promoting bubble growth. The next addressed issue is how these bubbles can be stable for periods of days. In the case of, for example, filamentous benthic cyanobacteria oxygen rich bubbles have been observed to be stable for periods as long as weeks (Bosak *et al.*, 2010).

The mechanical stability of a bubble depends on the equilibrium of the three forces acting on a bubble which are discussed in the previous Section: the internal pressure, the ambient pressure and the surface tension (Figure 4.7). In addition to the mechanical stability the bubbles must be thermodynamically stable.

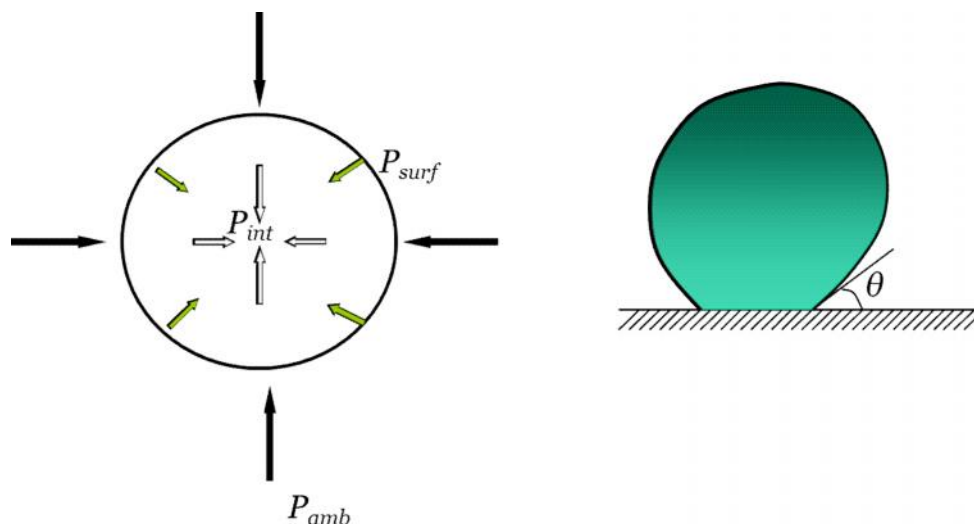


Figure 4.7: Left figure: Pressures acting on a bubble. P_{int} is the internal pressure, P_{surf} is the surface tension pressure, and P_{amb} is the pressure outside the bubble. Right figure: Sketch of a gas bubble attached to a surface where θ is the contact angle.

The Young-Laplace equation apparently does not hold for nanobubbles because at such dimensions the surface tension should lead to rapid dissolution, as the internal pressure will be so high that satisfying Henry's Law will result in a net flux of gas from the bubble to the liquid, see the brief overview in the previous Section. Epstein and Plesset (1950) provided some estimates for the dissolution of air bubbles in water for still relatively large initial bubble radii (1, 0.1 and 0.01 mm, respectively). For the smallest bubble radius ($r=10^{-5}$ m) they considered, and also assuming that initially Henry's Law was satisfied, Epstein and Plesset predicted that dissolution time (with surface tension effects included) is of the order of seconds. For nanobubbles the dissolution time will then be in the range of microseconds. However, there are several observations that nanobubbles remain stable for longer than the microseconds they should last. We should distinguish here between spherical nanobubbles with radii of the order of 100 nm in the bulk, surface nanobubbles with heights and widths of order 10 and 100 nm, respectively (and typical radii of curvature of 100-1000 nm). Some recent insightful (mini)reviews on nanobubbles are those by Seddon and Lohse (2011), Craig (2011) and Seddon and coworkers (2012), all addressing several aspects of the nanobubble puzzle (see also the references in these reviews). The theoretical explanation for stability of nanobubbles is still under investigation (Seddon and Lohse, 2011; Seddon *et al.*, 2012; Papadopoulou *et al.*, 2013; Petsev, Shell and Leal, 2013). A possible explanation for

the stability of surface nanobubbles is put forward by Brenner and Lohse (2008) and called the “dynamic equilibrium model”. In this model the diffusive outflux of gas molecules through the spherical cap is balanced by a gaseous influx at the contact line (demarcation between the solid-liquid and the solid-gas interface). The source of the influx would come from an enhanced gas concentration near the walls (Dammer and Lohse, 2006), which may exceed more than two orders of magnitude above the concentration in the bulk. The enrichment would occur because there is a potential attracting solute molecules to the wall. Solute molecules at a gas-liquid interface are attracted to the wall and driven inside the bubble. This model also predicts that hydrophobic substrates are preferred as nucleation sites for surface nanobubbles over hydrophilic substrates. The “dynamic equilibrium model” moreover predicts a typical size of the stable surface nanobubble. Another possibility for the nanobubble to be stable is because of the presence of surfactants that lower the surface tension (Yount, 1979). In absence of consensus over a theoretical explanation we assume the presence and stability of bubbles of nano-size (Borkent *et al.*, 2007) as a working hypothesis.

Considering the nanobubbles to be stable (although not yet well understood in the physics community) and under DO supersaturation conditions we assume the bubbles will grow until they reach a stable size (millimetric size). The grown bubble could remain stable because it is attached to a wall (Kralchevsky, 1996). This would occur if the nucleus is out of diffusive equilibrium (there is a diffusional transport between water and the bubble) and if the contact angle is acute (Figure 4.7). Other possibility is that the bubble stability comes from the tissue elasticity (surrounding material) (Goldman, 2009). Bosak (2010) also suggests that the stability of bubble formed in cyanobacteria mats comes from biofilms around the bubbles.

4.4. Experimental evidence of scum formation

To test our hypothesis (*i.e.* oxygen bubbles attached to the colonies mucilage are responsible for scum formation) we analyzed field scum samples from three lakes. The laboratory experiments consist of placing the samples in a compression chamber. For that we have constructed a controlled pressure chamber (Fig. 4.8). We call this chamber the Riebesell chamber since it is a copy of the chamber used by

Riebesell in marine snow studies (Riebesell, 1992). To determine the rising velocity of the colonies we have constructed another chamber called still chamber.

The Riebesell chamber consists of a 60 cm transparent long plexi-glass tube, with a diameter of 15 cm and a wall thickness of 6,6 mm. The cylinder can be closed at both extremes (airtight) and placed in a frame in the laboratory. A pressure gauge is connected to the upper cap to measure the pressure inside the tube. The cylinder is connected to an air pressure tank to increase the pressure inside the tube.

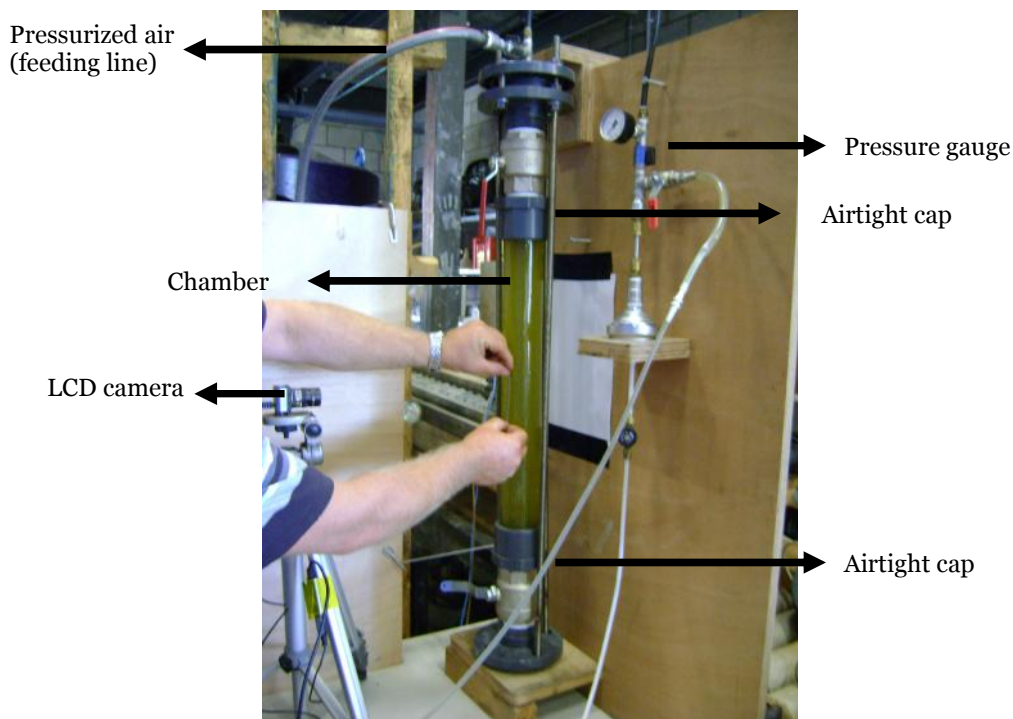


Figure 4.8: Photography of the Riebesell chamber.

4.4.1 Sites description

During the summer of 2011 and 2012 we collected three scum samples from three different shallow lakes in the Netherlands: Delftse Hout, Prinsenbos and Kralingse Plas.

Delftse Hout

Delftse Hout is a shallow lake located close to Delft, with an area of 0.23 km² and an average depth of 2.5 m. Since several years it suffers from scum formation during summer. The genera that are usually abundant in this lake are *Microcystis*,

Anabaena and *Aphanizomenon*. During the summer of 2011 a large bloom followed by scum occurred (the scum was mainly formed by *Microcystis*). For the purposes of our study we collected scum on the 5th of September 2011. Figure 4.9 shows the location from where the scum was collected.



Figure 4.9: Satellite picture of Deltse Hout. The circle shows the northern location for the scum sample collection (the satellite image was obtained from Google earth).

Prinsenbos

Prinsenbos, located close to The Hague, is a shallow lake with an average depth of 1.6 m. It covers an area of 0.055 km². The species that usually appear in this lake belong to *Microcystis*, *Anabaena*, *Aphanizomenon* and *Planktothrix*. During the summer of 2012 a scum of *Planktothrix* was reported. On the 7th of August that year we collected a scum sample (Figure 4.10).

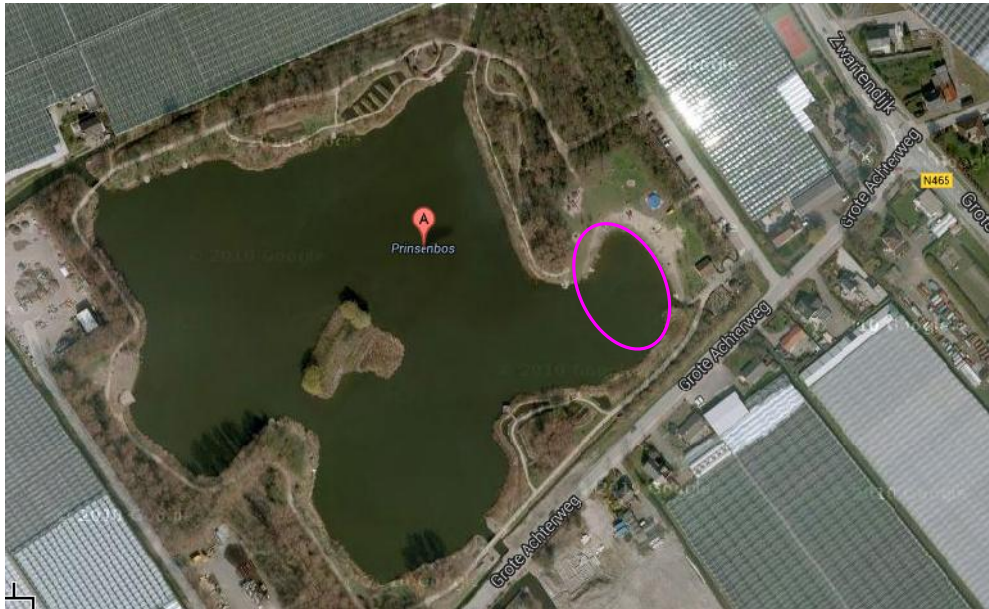


Figure 4.10: Satellite picture of Prinsenbos. The circle shows the eastern location for the scum sample collection (the satellite image was obtained from Google earth).

Kralingse Plas

Kralingse Plas, located close to Rotterdam, is also a shallow lake with an average depth of 2.5 m. It covers an area of 1.13 km². During the summer of 2012 the lake suffered from a massive bloom of *Gloetrichia*. On the 17th of September that year we collected a scum sample from the shore of the lake (Figure 4.11).

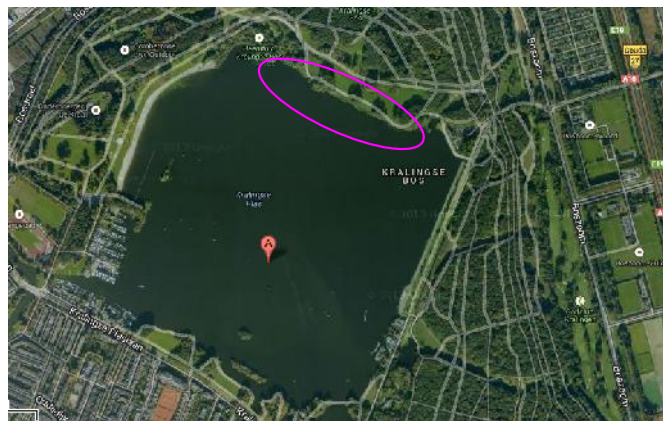


Figure 4.11: Map of Kralingse Plas. The circle shows the location for the scum sample collection (the satellite image was obtained from Google earth).

4.4.2 Collection of samples

During the summer of 2011 and 2012 three samples of floating cyanobacteria scum were collected close to mid-day. The samples were transported to the laboratory and within two or three hours they were placed inside the Riebesell chamber. In every case the water with the scum sample was left for half an hour. During this time the conditions were almost similar between field and laboratory (temperature, dissolved oxygen levels). After this half hour period the majority of the colonies floated to the surface of the chamber. Table 4.2 summarizes the temperature and oxygen levels of the samples, in the field and at the laboratory.

Table 4.2: Temperature, dissolved oxygen and oxygen supersaturation measured in the field and the laboratory.

Lake	Date	Field			Laboratory		
		Temperature [°C]	Oxygen [mg/l]	Supersaturation [%]	Temperature [°C]	Oxygen [mg/l]	Supersaturation [%]
Delftse Hout	05-09-11	20,3	14,36	156,9	20,5	13,89	152,4
Prinsenbos	07-08-12	20,8	19,36	213,6	20,8	10,76	117,4
Kralingse							
Plas	17-09-12	26,9	12,46	155,1	27,2	14,38	179,9

4.4.3 Experimental procedure

The samples of *Planktothrix* and *Gloeotrichia* were subject to two procedures. The first procedure aimed to determine the rising speeds and colony sizes. The second procedure (Riebesell chamber) aimed to achieve a reversal in buoyancy status after compression. The *Microcystis* scum sample was subjected to the Riebesell experiment only.

Still chamber

For this experiment we used a chamber with similar dimensions as the Riebesell chamber. This chamber was filled with water collected from the same lake from where the scum sample was taken. The colonies in the scum were carefully placed with the aid of a peristaltic pump in a plastic tube (diameter 1.5 cm). The colonies were collected inside the tube. Later, the tube was placed at the bottom of the still chamber and the colonies entered the still chamber. A camera was placed next to the

chamber for video recording and further analysis of natural rising speeds and colony sizes with the aid of PTV (Particle Tracking Velocimetry) software.

Riebesell chamber

After the scum sample was placed in the Riebesell chamber and left for half an hour, the chamber was closed on both ends. No air was left between the lid and the top of the scum. The entire experiment was carried out under natural light conditions. The light inside the laboratory was higher than the minimum light required for accumulation of carbohydrates (in the case of *Microcystis*). A digital camera was placed next to the chamber to record images for further determination of colony sizes and vertical sinking speeds. Small movies were recorded at each pressure interval.

In this study we used particle tracking velocimetry (PTV) to determine the rising and sinking velocities of all particles. In PTV two consecutive images are compared and the displacement of the particles is computed. The determination of the average particle displacement is realized by spatial cross-correlation of the particle images. Usually a laser is used for illumination but in this study a regular lamp was used. The window of observation of our experiments was 1200x1200 pixels. The accuracy of the method depends on particle image size, noise data (seeding density, camera noise), shear rate (velocity gradients) and the characteristic particle displacement. Errors may arise from the experimental set-up, experimental conditions and processing method (Adrian and Westerweel, 2010).

The experiment started when the pressure inside the chamber was gradually increased with steps of one bar. At each pressure step a movie was recorded to analyze possible changes. After each pressure incrementing step, the sample was left for 30 min at this new pressure. If the pressure is suddenly increased, to the full pressure increment of 3-4 Bar, the gas vesicles would collapse.

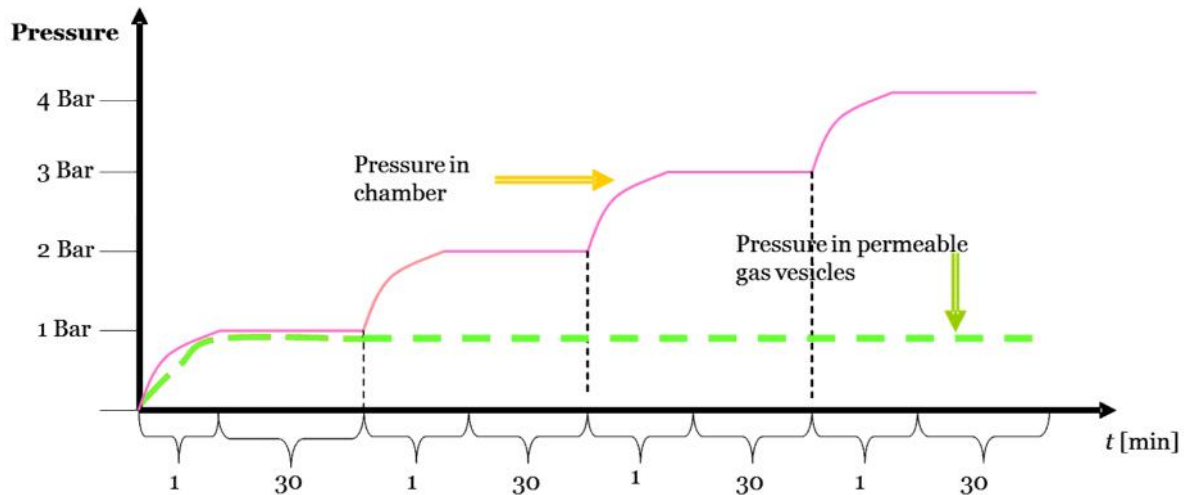


Figure 4.12: Pressure increments in the Riebesell experiment. The pressure in the chamber is increased in steps of 1 Bar and then left for 30 minutes each time. The dashed line shows the pressure inside the gas vesicles.

4.5. Results

The scum formed by *Microcystis* changed its buoyant status after reaching a pressure of 4 Bar inside the chamber (the colonies started to sink at that pressure). The scums formed by *Planktothrix* and *Gloeotrichia* changed their buoyancy status at 3 Bar. If the gas vesicles are not collapsed the reverse buoyancy status is due to the dissolution of gas bubbles. Table 4.3 summarizes the pressure requirements for changing buoyancy status and for gas vesicles collapse. P_c refers to the critical pressure to collapse isolated gas vesicles, P_t is the turgor pressure (pressure exerted by the cell material around the gas vesicles) and P_o is the pressure required to collapse gas vesicles immersed in cell material (natural form). The applied pressure for buoyancy status reversal (second column) must be lower than the critical pressure P_o in order to ensure that gas vesicles are not collapsed.

Table 4.3: Required pressures for the reversal from floating to sinking for each cyanobacterial genus. P_o is the critical pressure to collapse gas vesicles in intact cells, P_c is the critical pressure for collapsing isolated gas vesicles and P_t is the turgor pressure, the pressure that the cell exert on the gas vesicles.

Cyanobacteria	Applied Pressure for buoyancy status reversal [Mpa]	P_o [Mpa] Critical Pressure turgor cell	P_c [Mpa] Critical Pressure	P_t [Mpa] Turgor Pressure
<i>Microcystis</i>	0,4	0.6 -0.9	0.9-1.1	0,2
<i>Planktothrix</i>	0,3	0,6	0,99	0,3
<i>Gloeotrichia</i>	0,3	0,5	0,75	0,2

The Particle Tracking Velocimetry (PTV) software was used to determine the rising and sinking velocities of the colonies. Figure 4.13 shows the Probability Density Functions (PDF) of the rising and sinking velocities determined in the Still Chamber and the Riebesell Chamber. Note that the vertical coordinate is positive downwards.

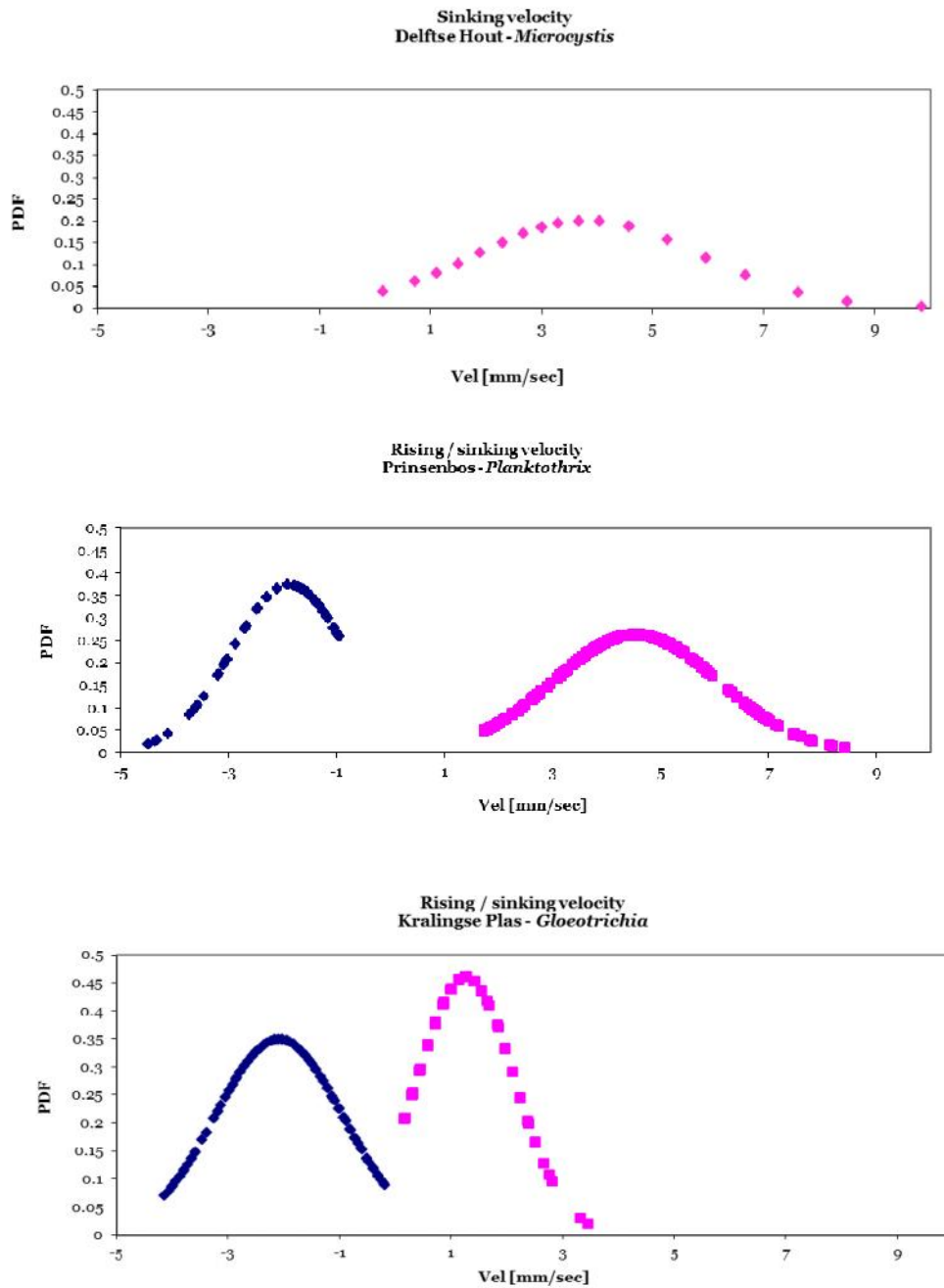


Figure 4.13: Sample compression leading to buoyancy reversal due to dissolution of gas bubbles. Vertical velocities Probability Density Function (PDF). a) PDF of sinking velocities of *Microcystis*, b) PDF of rising and sinking after 3 Bar of pressure of *Planktothrix* and c) PDF of rising and sinking after 3 Bar of pressure of *Gloeotrichia*. Note that the vertical coordinate is positive downwards.

For the colony size determination we have assumed spherical colonies of *Microcystis* and *Gloeotrichia* whereas for *Planktothrix* we have assumed an ellipsoidal shape (Walsby, 1994). Table 4.4 summarizes the results of the measurements using the PIV software. The last three columns are approximated as follows. The colony mass-density ρ_{col} is estimated from the Stokes vertical velocity using the measured colony velocity and size ($w_s = (\rho_w - \rho_{col})d^2g/18\nu$). The cell mass-density ρ_{cell} is estimated by using equation 2 and assuming n_{bub} zero. Finally, n_{bub} is estimated by using the cell-mass density ρ_{cell} and the colony mass-density ρ_{col} in the ascending mode (all terms in equation 2).

Table 4.4: Summary of the parameters estimated with the PTV software for the three samples and for the two experiments in the Still Chamber and the Riebesell chamber. The mean velocity and colony size are estimated using PIV, Std refers to the standard deviation of the calculation. ρ_{col} , ρ_{cell} and n_{bub} are estimated using equation 2.

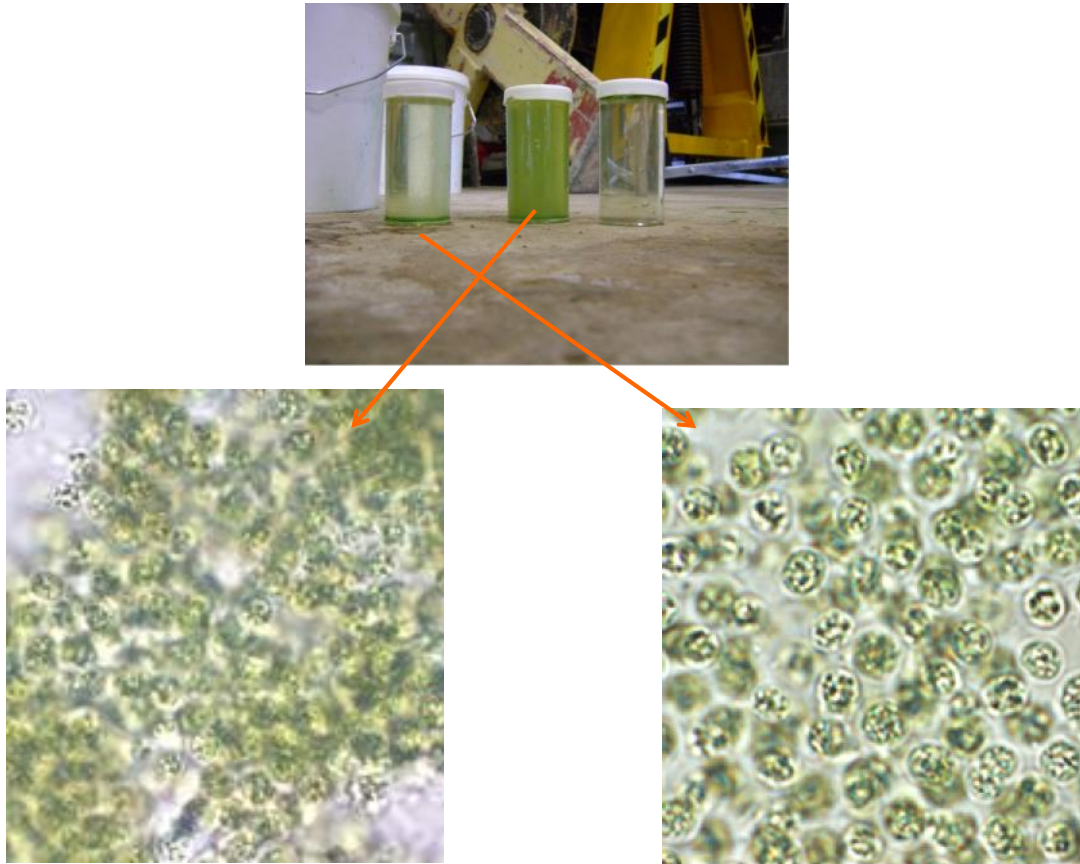
		Velocity		Colony		ρ_{col}	ρ_{cell}	n_{bub}
		mean	Std	Size	[mm]	kg m ⁻³	kg m ⁻³	%
				mean	Std			
Delftse Hout	Ascending	N.A.	N.A.	N.A.	N.A.			
<i>Microcystis</i>	Descending	3,8	1,3	3,2	0,9	998,9	1075,0	
Prinsbos	Ascending	2,2	1,0	1,0	0,4	993,2	1071,8	0,52
<i>Planktothrix</i>	Descending	4,6	1,5	5,8	0,9	998,3		
Kralingse								
Plas	Ascending	2,1	1,1	2,0	0,4	996,7	1081,5	0,34
<i>Gloeotrichia</i>	Descending	1,3	0,9	1,2	0,1	1000,1		

Gas vesicles contract 0.9 % per 10 Bar of pressure exerted on them (Walsby, 1994). The contraction of gas vesicles under 4 Bar pressure do not explain the change in buoyancy status of the cyanobacteria colonies. In the case of *Planktothrix* (Prinsbos) a reduction of 0,27% in gas vesicle volume would increase the colony mass-density from 993,2 kg m⁻³ to 993,4 kg m⁻³. In the case of *Gloeotrichia* (Kralingse Plas) the same reduction on gas vesicle volume would increase the colony mass-density from 996,7 kg m⁻³ to 996,9 kg m⁻³. In both cases the colonies would still be in rising mode. Additionally, after finalizing each experiment the pressure was slowly reduced to normal conditions and the colonies remained at the bottom of the

chamber. If the gas vesicles would have been simply compressed, releasing the pressure would bring the colonies to the floating mode again.

Furthermore, samples of *Microcystis* colonies before and after the compression experiment were microscopically inspected by AQUON laboratories (Figure 4.14). The gas vesicles of the samples after the compression test remained intact (pers. Comm. AQUON).

The possibility of gas vesicles collapses during the pressure experiments cannot be ruled out entirely. It has been observed that *Microcystis* at 50 meters depth (Granget reservoir) still maintain their gas vesicles intact (Latouer *et al.*, 2007). To exclude this factor it will be necessary to perform detail measurements on the percentage of gas vesicles before and after the compression experiments.



Microcystis before pressure experiment

Microcystis after pressure experiment

Figure 4.14: Microscopic observation of gas vesicles in colonies of *Microcystis* before and after the compression experiments. The shining parts inside the cells are the reflection of gas vesicles (the photographs were taken by AQUON).

4.6 Discussion and Conclusions

The results of our experiments and analysis suggest that cyanobacteria colonies reach an irreversible buoyancy status due to oxygen gas bubble formation within the mucilage as in autoflotation. Also we have reviewed several reasons for scum formation proposed in literature. The oxygen bubbles hypothesis is a very likely explanation for scum formation. With exception of the shortage of CO₂ hypothesis (Paerl and Ustach, 1982) that could promote colonies to reach and stay at the air-water interface. The question remains open whether the formation of a scum is an ecological advantage as suggested by Zohary and Robarts (1990) or a fortuitous end of cyanobacteria bloom.

The three conditions for scum formation are still valid and complemented by our hypothesis. Firstly, an existing population of cyanobacteria which create supersaturation levels of oxygen. Secondly, positively buoyant colonies that can reach the upper areas in the lake. Thirdly, stability of the water column (epilimnion) which limits the vertical migration of cyanobacteria and restricts the diffusion of oxygen through the air-water interface. The new variable that would control the formation of a scum would be the supersaturation of oxygen in the environment surrounding the colonies. With this addition the forecasting of scum formation can be realized.

Bubbles have been observed and measured in hyperscums (Zohary and Roberts, 1990). These bubbles formed by methane, carbon dioxide, nitrogen and oxygen would contribute to maintain the scum at the surface. As described in the introduction hyperscums sometimes follow a scum.

The implications of gas bubbles growth could bring new measures to prevent the formation of surface scums or different interpretation of the phenomena. For instance the application of aeration systems could be useful in mixing the water column and preventing oxygen supersaturation levels. Additionally, water quality models could profit from including oxygen levels as control parameter.

Acknowledgments

The authors are thankful to Akke Hofma for giving us the idea to look after gas bubbles as responsible for scum formation. We would also like to thank John Cornelisse, Marcel Busink and Marcel Grotenburg from Deltares for helping us during field work and constructing the Riebesell chamber. We are thankful to Ulf Riebesell for discussion and borrowing us the Riebesell chamber. We are thankful to AQUON for cooperating with this research. This research has been funded by Deltares and the Technical University of Eindhoven.

4.7 References

- Adrian, R.J., Westerweel, J. (2010). Particle Image Velocimetry. Cambridge University Press.
- Aparicio Medrano, E., Uittenbogaard, R.E., Dionisio Pires, L.M. van de Wiel, B.J.H. and Clercx, H.J.H. (2013). Coupling hydrodynamics and buoyancy regulation in *Microcystis aeruginosa* for its vertical distribution in lakes. *Ecological Modelling*, 248, 41-56.
- Arbelaez, J., Koopman, B. and Lincoln, E.P. (1983). Effects of dissolved oxygen and mixing on algal autoflotation. *Journal of water pollution control federation*, 55, 1075-1079.
- Arieli, R., Marmur, A. (2011). Decompression sickness bubbles: are gas micronuclei formed on a flat hydrophobic surface?. *Respiratory Physiological Neurobiology*, 177, 19–23.
- Borkent, B.M., Dammer, S.M., Schonherr, H., Vancso, G.J. and Lohse, D. (2007). Superstability of Surface Nanobubbles. *Physical Review Letters*, 98, 204502.
- Bosak, T., Bush, J.W.M., Flynn, M. R., Liang, B., Ono, S., Petroff, A. P. and Sim, M. S. (2010). Formation and stability of oxygen-rich bubbles that shape photosynthetic mats. *Geobiology*, 8, 45–55.
- Brenner, M.I. P. and Lohse, D. (2008). Dynamic equilibrium mechanism for surface nanobubble stabilization. *Physical Review Letters*, 101, 1-4.
- Codd, G.A., Morrison, L.F., Metcalf, J.S. (2005). Cyanobacterial toxins: risk management for health protection. *Toxicology Applied Pharmacology*, 203, 264–27.
- Cole, J.J., Caraco, N.F., Kling, G.W. and Kratz T.K. (1994). Carbon Dioxide supersaturation in the water supersaturation of lakes. *Science*, 265, 1568-1570.
- Craig, V.S.J. (2011). Very small bubbles at surfaces – the nanobubble puzzle. *Soft Matter*, 7, 40-48.
- Dammer, S.M., Lohse, D. (2006). Gas enrichment at liquid-wall interfaces. *Physical Review Letters* 96, 206101.
- De Philippis, R., Vincenzini, M. (1998). Exocellular polysaccharides from cyanobacteria and their possible applications. *FEMS Microbiology Reviews* 22, 151-175.
- Epstein, P.S., Plesset, M.S. (1950). On the stability of gas bubbles in liquid-gas solutions. *Journal of Chemical Physics*, 18, 1505-1509.
- Goldman, S. (2009). Generalizations of the Young–Laplace equation for the pressure of a mechanically stable gas bubble in a soft elastic material. *The Journal of Chemical Physics*, 131, 184502.
- Ibelings, B.W., Mur, L.R. and Walsby, A.E. (1991). Diurnal changes in buoyancy and vertical distribution of *Microcystis* in two shallow lakes. *Journal of Plankton Research*, 13, 419–436.

- Ibelings, B.W. and Mur, L.R. (1992). Microprofiles of photosynthesis and oxygen concentration in *Microcystis* sp. scums. *FEMS Microbiology Ecology*, 86, 195-203.
- Ibelings, B.W., Maberly S.C. (1998). Photoinhibition and the availability of inorganic carbon restrict photosynthesis by surface blooms of cyanobacteria. *Limnology and Oceanography*, 43, 408-419.
- Ibelings, B.W., Vonk, M., Los, H.F.J., van der Molen, D.T., Mood, W.M. (2003). Fuzzy Modeling of Cyanobacterial Surface Waterblooms: Validation with NOAA-AVHRR Satellite Images. *Ecological Applications*, 13, 1456-1472.
- Jodolowski, A. (2002). Effect of pre-oxidation on flocculated algal cells autoflotation. *Environment protection engineering*, 28, 57-68.
- Kralchevsky, P.A. (1996). Conditions for Stable Attachment of Fluid Particles to Solid Surfaces. *Langmuir*, 12, 5951-5955.
- Kromkamp, J. and Walsby, A.E. (1990). A computer model of buoyancy and vertical migration in cyanobacteria. *Journal of Plankton Research*, 12, 161-183.
- Latour, D., Salençon, M.-J., Reyss, J.-L. & Giraudet, H. (2007). Sedimentary imprint of *Microcystis aeruginosa* (Cyanobacteria) blooms in Grangent Reservoir (Loire, France). *Journal of Phycology*, 43, 417-425.
- Long, S.P., Humphries, S. and Falkowski, P.G. (1994). Photoinhibition of photosynthesis in Nature. *Annual Review of Plant Physiology and Plant Molecular Biology*, 45, 633-662.
- Marks, R. and Pytel, M. (2011). Bubbles, Dissolved Oxygen saturation and coastal abrasion in the southern Baltic Sea. *Journal of Coastal Research*. ICS2011 Proceedings.
- Maberly, S.C. (1996). Diel, episodic and seasonal changes in pH and concentrations on inorganic carbon in a productive lake. *Freshwater Biology*, 35, 579 - 598.
- Paerl, H.W. and Ustach, J.F. (1982). Blue-green algal scums: An explanation for their occurrence during freshwater blooms. *Limnology and Oceanography*, 27, 212-217.
- Paerl, H.W., Tucker, S.C., (1995). Ecology of blue green algae in aquaculture ponds. *Journal of World Aquaculture society*, 26.
- Papadopoulou, V., Eckersley, R.J., Balestra, C., Karapantsios, T.D., Tang, M.X. (2013). A critical review of physiological bubble formation in hyperbaric decompression. *Advances in Colloid and Interface Science*, 1.
- Petsev, N.D., Shell, M.S., Leal, L.G. (2013). Dynamic equilibrium explanation for nanobubbles' unusual temperature and saturation dependence. *Physical Review E*, 88, 010402.
- Ploug, H. (2008). Cyanobacterial surface blooms formed by *Aphanizomenon* spp. and *Nodularia spumigena* in the Baltic Sea: Small-scale fluxes, pH, and oxygen microenvironments. *Limnology and Oceanography*, 53, 914-921.

- Ramsey, L.W. (1962). Bubble growth from dissolved oxygen near the sea surface. *Limnology and Oceanography*, 7.
- Revsbech, N.P., Jørgensen, B.B., Blackburn, T.H., Cohen, Y. (1983). Microelectrode studies of the photosynthesis and O₂, H₂S, and pH profiles of a microbial mat. *Limnology and Oceanography*, 28, 1062-1074.
- Reynolds, C. S., Walsby, A. E. (1975). Water blooms. *Biological reviews of the Cambridge Philosophical Society*, 50, 437-481.
- Reynolds, C.S., Jaworski, G.M.H., Cmiech, H.A., Leedale, G.F. (1981). On the annual cycle of the blue-green alga *Microcystis aeruginosa* Kuntz. emend. Elenkin. *Philosophical Transactions of the Royal Society London, Series B*, 293, 419-477.
- Reynolds, C.S., Oliver, R.L. and Walsby, A.E. (1987). Cyanobacterial dominance: The role of buoyancy regulation in dynamic lake environments. *New Zealand Journal of Marine and Freshwater Research*, 21, 379-390.
- Riebesell, U. (1992). The formation of large marine snow and its sustained residence in surface waters. *Limnology and Oceanography*, 37, 63-76.
- Robarts, R.D., Waiser, M.J., Arts, M.T. and Evans, M.S. (2005). Seasonal and diel changes of dissolved oxygen in a hypertrophic prairie lake. *Lakes and Reservoirs: Research and Management*, 10, 167-177.
- Seddon, J.R.T and Lohse, D. (2011). Nanobubbles and micropancakes: gaseous domains on immersed substrates. *Journal of Physics of Condensed Matter*, 23, 133001.
- Seddon, J.R.T., Lohse, D., Ducker, W.A., Craig, V.S.J. (2012). A deliberation on nanobubbles at surfaces and in bulk. *Journal of Chemical Physics and Physical Chemistry*, 13, 2179-2187.
- Shapiro, J. (1997). The role of carbon dioxide in the initiation and maintenance of blue-greens dominance in lakes. *Freshwater Biology*, 37, 307-323.
- Soranno, P.A. (1997). Factors affecting the timing of surface scums and epilimnetic blooms of blue-green algae in a eutrophic lake. *Canadian Journal of Fisheries and Aquatic Sciences*, 54, 1965-1975.
- Stachowitsch, M., Fanwko N., and Richter, M. (1990). Mucus aggregates in the Adriatic Sea: An overview of types and occurrences. *Marine Ecology*, 11, 327-350.
- Visser, P. M., J. Passarge, and L. R. Mur. (1997). Modelling the vertical migration of the cyanobacterium *Microcystis*. *Hydrobiologia*, 349, 99-109.
- Vuuren, L.R.J., Meiring, P.G.J., Henznen, M.R. and Kolbe, F.F. (1965). The floatation of algae in water reclamation. *Air and water pollution*, 9, 823-832.
- Walsby, A. E. (1980). The water relations of gas vacuoles prokaryote. *Proceedings of the Royal Society of London*, 208, 73-102.

- Walsby, A.E., Hayes, P.K., Boje, R. and Stal, L.J. (1997). The selective advantage of buoyancy provided by gas vesicles for planktonic cyanobacteria in the Baltic Sea. *New Phytologist*, 136, 407-417.
- Walsby, A. E. (1994). Gas vesicles. *Microbiological Reviews*, 58, 94-144.
- Wanninkhof, R.H., Bliven, L.F.(1991). Relationship between Gas Exchange, Wind Speed, and Radar Backscatter in a Large Wind Wave Tank. *Journal of Geophysics*, 96, 2785-2796.
- Yount, D.E. (1979). Skins of varying permeability: a stabilization mechanism for gas cavitation nuclei. *Journal of Acoustical Society of America*, 65,11429–1439.
- Yount, D.E. (1982). On the evolution, generation, and regeneration of gas cavitation nuclei. *Journal of Acoustical Society of America*, 71, 1473–1481.
- Zohary, T., and Robarts, R.D. (1990). Hyperscums and the population dynamics of *Microcystis aeruginosa*. *Journal of Plankton Research*, 12, 423–432.

Chapter 5

Conclusions

Scum formation

Scum formation refers to the concentration of cyanobacteria at the surface of a lake which persists for longer than a day (Ibelings *et al.*, 1991). The main problem is that most of the scum forming cyanobacterial species are toxic and can damage humans and wildlife. The most common physical-chemical reasons for scum formation are vertical migration of cyanobacteria, photoinhibition, shortage of CO₂ and self-shading (see Chapter 4). This thesis tries to improve the understanding of the processes involved in scum formation. The approach here combines theory, advance computations, applied computations and field and laboratory experiments.

In the present study the focus on the processes of vertical migration as a potential mechanism for scum is explored in the first part. Chapter 2 and 3 are devoted to the study of vertical migration of cyanobacteria colonies as a result of a complex interplay between hydrodynamics and active biological mass-density regulation. Each chapter has a different approach. Chapter 2 combines a hydrodynamic model approach (1DV), using the k- ϵ turbulence model, with a simple biological model in order to simulate the vertical migration of *Microcystis*. Chapter 3 combines an advance hydrodynamic model DNS (direct numerical simulations) which solve the Navier-Stokes equation explicitly with computations of individual particle trajectories to quantify the vertical migration of *Microcystis* based on a similar biological model as Chapter 2. Both approaches show that formation of persistent scum cannot be directly attributed to vertical migration effects due to biological density regulations and turbulence.

Therefore, in Chapter 4 an alternative mechanism potentially contributing to scum formation is proposed: growing gas bubbles attached to the *Microcystis* colonies. The reason for this bubble growth may be oxygen supersaturation, due to photosynthetic activity, in the water column just below the surface.

Vertical migration of cyanobacteria coupled to hydrodynamics

Vertical migration of cyanobacteria has been an intriguing phenomenon during several decades. Several hypotheses were formulated to explain the observations of early morning cyanobacteria collected at the surface of lakes and their disappearance later during the day (Reynolds and Walsby, 1975; Paerl and Ustach, 1982). Initially it was thought that gas vesicles played a major role in vertical migration by a regulation between collapse and renewal of gas vesicles (Walsby, 1980). Later, a dependency on the density regulation due to carbon assimilation was shown by laboratory experiments (Kromkamp and Walsby, 1990; Visser *et al.*, 1997). The carbon assimilation and respiration is light and time dependent. The first reports (Kromkamp and Walsby, 1990) showed for *Oscillatoria* (currently known as *Plankthotrix*) such a dependency. In the case of *Microcystis aeruginosa*, Visser *et al.* (1997), defined two functions to describe the increase and decrease of the mass-density of cells.

Chapter 2 of this thesis was devoted to include the diurnal changes of vertical migration and the hydrodynamic variability of lakes into one coupled model. Most models study the vertical distribution of cyanobacteria by assuming a fixed value for vertical velocity of colonies (Huisman and Hulot, 2005). This approach leaves out the fact that the vertical velocities of colonies change throughout the day as a result of changing its mass-density and turbulent velocity fluctuations. The objective of Chapter 2 was achieved by using a Fokker Planck equation that describes the changes in vertical position due to changes in colony mass-density and the advection and diffusion of the flow (flow hydrodynamics). The basic idea behind the Fokker Planck equation is the consideration of an ensemble average of colonies paths.

The model results were compared with field measurements of vertical distributions of colonies in Lakes Vinkeveen and IJsselmeer. The results compare satisfactorily with the measurements, in the model most colonies concentrate near the surface early in the morning and lower in the water at the end of the day-light. This provides confidence in applying the proposed model for further analysis.

Three main conclusions were drawn in this chapter. Firstly, colony size influences the migration depth. Large colonies ($\geq 800 \mu\text{m}$) can temporarily reach the surface of a lake and sink further than small colonies ($\approx 400 \mu\text{m}$) because they are heavier.

Secondly, it has been shown that the level of turbulence driven by wind influences the final vertical distribution. Low wind speeds allow the colonies to follow a quasi-deterministic path in response to the mass-density dynamics due to carbon assimilation/respiration. High wind speeds tend to disperse the colonies uniformly across the epilimnion. Thirdly, the formation of a persistent scum cannot be explained by vertical migration alone. It was shown that even under very mild wind conditions the colonies sink after their mass-density becomes higher than water.

The second approach of this thesis (Chapter 3) was to explicitly show the effect of small-scale turbulence on vertical migration. This was achieved by solving the Navier-Stokes equations via Direct Numerical Simulations. In this way it is not needed to rely on any specific turbulence closure model. The colonies (particles) in DNS are treated individually. Each colony (particle) changes its density according to its depth-dependent light environment. The complication faced at this stage is the issue of different time scales. Flow time scales are in the order of seconds whereas colony mass-density changes are in the order of hours. Therefore, no straight forward simulations can be performed. This challenge was tackled by developing a scaling procedure that bridges the gap between these time scales. The scaling was proved to be successful in a way that it easily allows simulation of a three day-night cycles within one DNS simulation.

This approach produced results that were quantitatively similar to the results obtained with the parameterized model approach of Chapter 2 (Fokker-Planck): 1) the depth of migration is largely influenced by colony size; 2) the intensity of turbulence in the water influences the vertical distribution of the colonies. At high turbulence intensities no clear vertical migration could be observed and colonies appeared to be uniformly dispersed in the epilimnion. 3) The formation of a scum cannot be explained by small-scale turbulence and vertical migration.

The model was also used to study the influence of day light length and light extinction on the vertical distribution of *Microcystis*. It was shown that if the water has a high extinction coefficient the colonies show shorter vertical migration paths (less photosynthesis, thus decreasing cell mass-density). The dimensionless analysis allows the determination of a dimensionless number, the Buoyancy Stokes number.

This number compares the strength of turbulence versus the strength of buoyancy status of the colonies in order to characterize the typical spreading of colonies around the mean.

An important conclusion of this fundamental approach based on DNS combined with individual particle tracking is that the computationally much cheaper Fokker-Planck approach shows high potential to be used as an effective tool for modeling vertical distribution of colonies in large-scale and seasonal simulations of *e.g.* lakes and reservoirs.

It is also important to mention that the methods investigated in Chapters 2 and 3 cover a broader methodology and application than the methods published in scientific literature. The model presented in Wallace and Hamilton (2000) combines turbulence modeling and particle tracking in shallow lakes. The model presented by Krompkamp and Walsby (1990) uses particle tracking applied to shallow lakes. The methodology presented in Chapters 2 and 3 combines, particle tracking, ensemble averaging, turbulence modeling and direct numerical simulations for their application in shallow and in deep lakes (Table 5.1).

Table 5.1: Cyanobacteria vertical distribution modeling methods

	Turbulence model	DNS	Particle Tracking	Fokker Planck	Shallow	Deep
Wallace and Hamilton	X		X		X	
Krompkamp and Walsby			X		X	
This thesis	X	X	X	X	X	X

Scum formation due to photosynthetic oxygen production

In Chapter 4 the most common reasons found in literature to explain scum formation were reviewed. Besides the possibility of vertical migration yielding a scum by weight loss due to shortage of CO₂ none of the other arguments seem to hold in all occasions. Although active buoyancy regulation by carbon assimilation in the absence of strong turbulence mixing may lead to temporarily preferred concentrations close to the surface, it cannot explain the appearance of persistent scum (Chapters 2 and 3). Rather those ingredients can be seen as pre-requisites for scum formation.

Therefore, in this thesis a different hypothesis for the formation of a scum has been put forward. The hypothesis is that scum formation occurs due to oxygen gas bubbles in or on the mucilage of the cyanobacteria colonies. There are prerequisites for growth of gas bubbles. The existence of nucleation sites is essential and appears to be an intriguing subject of recent and present research. These nucleation sites would allow for heterogeneous bubble growth *i.e.* on solid walls such as the mucilage surrounding the colonies. Bubble growth is expected to occur if the oxygen supersaturation in the water leads to partial pressures higher than the pressure inside bubbles. The supersaturation of oxygen originates from the photosynthetic activity of cyanobacteria. Large or consecutive blooms would provide the water with enough cyanobacteria producing oxygen that eventually could lead to supersaturation. Mild wind conditions contribute to a reduction of gas escaping from the air-water interface. The growth of oxygen gas bubbles inside or attached to the mucilage, (bubbles with a typical maximum size of 5 μm), or at the cell wall of cyanobacteria will eventually lead to irreversible buoyancy and thus contribute to the imminent formation of scums.

To support the hypothesis presented here, compression experiments were performed. The experiments consisted on placing a scum sample in a chamber, referred to the Riebesell chamber, and increasing the pressure to dissolve or collapse gas bubbles. Three samples of scum from different lakes were tested, one formed mainly by *Microcystis*, the second formed by *Planktothrix* and the third formed by *Gloeotrichia*. The sample of *Microcystis* changed its buoyancy status from floating to sinking when the pressure in the chamber was increased to 4 Bar (equivalent to 40 m water depth). The other two samples (*Planktothrix* and *Gloeotrichia*) changed their buoyancy status when the pressure in the chamber was increased to 3 Bar.

The results of these experiments contribute to explain the formation of a (persistent) scum. The most important parameter to determine the formation of a scum seems to be oxygen saturation levels in water.

Summarizing, it can be concluded that the three conditions required for scum formation are: existence of a large population of cyanobacteria, positively buoyant colonies that reach the surface of a lake and stability of the water column (stratification). These conditions are essential but must be complemented with the oxygen supersaturation degree in the water needed for bubble growth.

These mostly physical processes of scum formation should be complemented with biological processes. This includes the selection of cyanobacteria or algae that could create a scum because only those species with the ability to approach the water surface (due to buoyancy regulation) in the shallow top layer suitable for possible bubble formation are candidates for forming a scum.

Our findings are directly relevant for modeling purposes as, for example, carried out by Deltares with EWACS, which is a methodology developed for forecasting scum formation (Burger *et al.*, 2008). The methodology is based on coupling several model modules *e.g.* hydrodynamic characteristics (Delft 3D), nutrients availability (DELWAQ), algae composition (BLOOM) and a fuzzy logic methodology to statistically determine the likelihood of a scum. The outcome of this research contributes to this methodology, specifically in the inclusion of vertical migration of cyanobacteria and the criteria of oxygen supersaturation as a condition for scum formation.

Recommendations

1. The procedure investigated in Chapter 2 using the Fokker-Planck equation appears applicable for models which deal with the dynamics of cyanobacteria and forecasting models.
2. The findings of Chapter 4 on conditions for heterogeneous growth of oxygen bubbles can be implemented in computer codes of forecasting models for scum formation by computing oxygen supersaturation.
3. Known methods of reducing or suppressing scums by mixers such as bubble plumes and propellers should be reviewed. For instance bubble plumes and other mixers reduce the supersaturation condition near the water surface and vertically circulate the colonies, having oxygen bubbles, to water depths where the bubbles collapse. In addition, these mixers create intense small-scale shearing that reduces the colony sizes and thus the amplitude of vertical migration.
4. Other new methods should be based on avoiding supersaturation conditions. In contrast also anoxic conditions should be prevented to avoid fish kill and possible release of phosphorus from the sediment.

5. Water quality monitoring efforts should include monitoring the near-surface oxygen levels at hourly intervals as a predictor of scum formation. When the supersaturation conditions reach levels of 140% it is likely that bubbles will grow.

5.2 References

- Burger, D.F., Hulsbergen, R.P., Los, F.J. and Groot, S. (2008). EWACS, Early Warning Against sCumS. Deltares report prepared for STOWA.
- Huisman, J. and Hulot, F.D. (2005). Population dynamics of harmful cyanobacteria, p. 143–176. In J. Huisman, H.C.P. Matthijs, and P.M. Visser (ed.), *Harmful Cyanobacteria*. Springer, Dordrecht, The Netherlands.
- Ibelings, B.W., Mur, L.R. and Walsby, A.E. (1991). Diurnal changes in buoyancy and vertical distribution of *Microcystis* in two shallow lakes. *Journal of Plankton Research*, *13*, 419–436.
- Kromkamp, J. and Walsby, A. E. (1990). A computer model of buoyancy and vertical migration in cyanobacteria. *Journal of Plankton Research*, *12*, 161– 183.
- Paerl, H.W. and Ustach, J.F. (1982). Blue-green algal scums: An explanation for their occurrence during freshwater blooms. *Limnology and Oceanography*, *27*, 212-217.
- Reynolds, C. S., Walsby, A. E. (1975). Water blooms. *Biological reviews of the Cambridge Philosophical Society*, *50*, 437-481.
- Visser, P. M., J. Passarge, and L. R. Mur. (1997). Modelling the vertical migration of the cyanobacterium *Microcystis*. *Hydrobiologia*, *349*, 99-109.
- Wallace, B. B. and D. P. Hamilton, (2000). Simulation of water-bloom formation in the cyanobacterium *Microcystis aeruginosa*. – *Journal of Plankton Research*, *22*: 1127–1138.
- Walsby, A. E. (1980). The water relations of gas vacuoles prokaryote. *Proceedings of the Royal Society of London*, *208*, 73-102.

Annex A

Measurements in Lake Vlietland

A.1 Introduction

The present annex presents a summary of field measurements performed in Lake Vlietland during the year 2009. Two different institutions were responsible for the observations: Water Board Rijnland and Deltares. Observed parameters include nutrients, water temperature, dissolved oxygen, pH, light extinction and algae composition.

As a first step in this study the variation of nutrients was analyzed in connection with blooms and scum events. Although some studies mention a decrease in nutrients concentrations during blooms or during scums, here no clear changes in the nutrients concentrations were found. The lake appears to remain highly eutrophic during the entire year. Next, the water temperature was monitored in order to validate the hydrodynamic simulations made with the 1DV model (see Chapter 2). Additionally, the light extinction coefficient was determined as a function of time. This quantity provides information used in the models as an input to compute mass-density changes which, due to carbohydrates assimilation/respiration, depend on light availability. An observation of relatively high pH values points at depletion of carbon dioxide in the water. In absence of direct measurements of carbon dioxide, the measurements of pH are used as a proxy.

The Annex is organized as follows. The first part describes the general characteristics of the lake. Next, the seasonal changes during the experiment are discussed with respect to meteorology and water temperature. Here it will be shown that operational management measures like artificial mixing can have a strong impact on the vertical temperature structure of lakes. Finally, relevant parameters like water temperature, light extinction and nutrients concentrations are discussed.

A.2 Lake Vlietland

Lake Vlietland is located in the west of the Netherlands. The lake is used for recreational purposes. It consists of two basins: the northern basin which is 28 m deep (surface area: 0.8 km²) and the south basin which is 36 m deep (surface area: 0.6 km²). Both basins are connected by two shallow canals (see Fig. A.1 for a map).

The lake is holomictic with a seasonal stratification cycle from late April until late October when the upper layer (epilimnion) is warmer than lower layer (hypolimnion). The lake is connected to an extensive agricultural area providing an abundance of nutrients. Therefore, the lake is highly eutrophic and cyanobacterial blooms frequently occur and often lead to scum formation along the shores. About 80% of the cyanobacteria population during summer is composed of *Microcystis* species, studied in the present thesis. No nutrient limitations occur during blooms of *Microcystis*. During the summer of 2008 an aeration system was installed in the north basin in order to improve mixing and possibly reduce the formation of scums. In 2009, the aeration system started to operate in April and lasted until October.

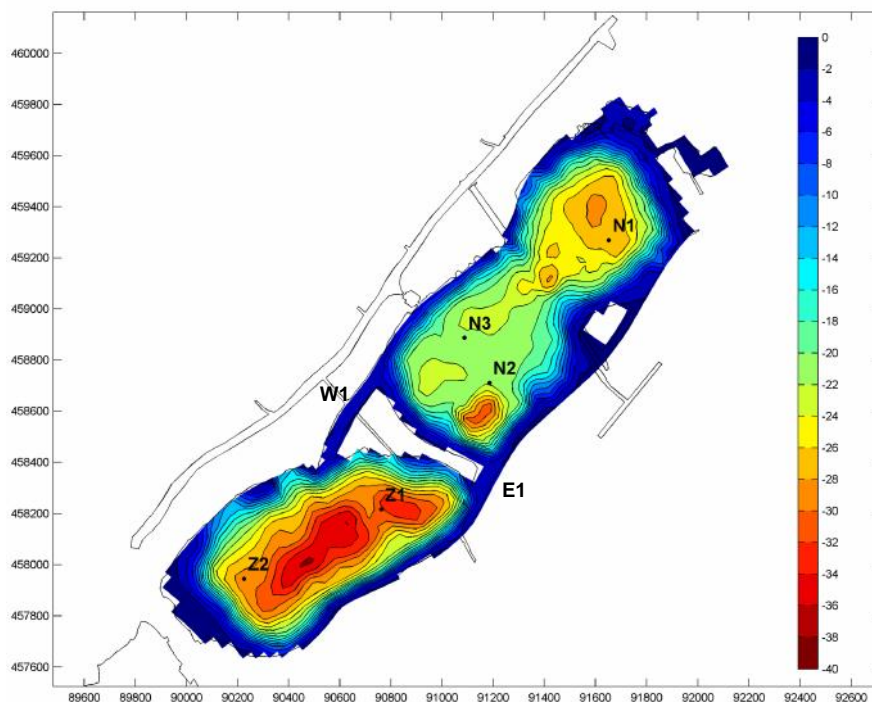


Figure A.1: Bathymetry of Lake Vlietland. The bar on the right shows the depth of the lake, from deepest (red) to shallowest (blue). The measurement stations N1, N2, N3, E1, W1, Z1 and Z2 are shown in the figure.

In 2009 the Water Board Rijnland and Deltares set up a measurement campaign to monitor Lake Vlietland. Four stations were measured on a weekly basis (Figure A.1). Two stations in the north basin (N1 and N2) and two stations in the south (Z1 and

Z2). Occasionally, station N₃ was used as a measuring location. In addition to measurements on routinely basis, an intensive observational 24 hr campaign was carried out during 27 – 28 August 2009. During this period, measurements of water temperature and dissolved oxygen profiles were taken every 6 hours for 6 locations, namely: N₁, N₂, Z₁, Z₂, E₁, W₁. The two extra locations E₁ and W₁ are located in the shallow canals which connect the basins.

The list of parameters measured by the Water Board Rijnland is shown in Table A.1. Figure A.2 shows the corresponding locations. Table A.2 lists the dates of the routine measurements taken by Deltares (water temperature, dissolved oxygen and light extinction). The name of the locations are different for Rijnland (Rox) and Deltares (N_x,Z_x).

Table A.1: Monitoring Program 2009 (for the locations see Figure A.2).

Vlietland Measurements 2009			
1. Rijnland routinely program			
Starting time:	May 1st		
Bi-weekly	Measurements Nutrients (TP, TN, NH ₄ , NO ₃ , SRP, TDC, POC, DOC) Cell counts	Location R0897-R0299-R0298 R0897-R0299-R0298	Depth 0-8 meters, 12, 18, 26m 0-8 meters
	Chl-a sample sample + pigments	R0897-R0299-R0298	0.5, 0-8m
weekly	Fluoro probe (chl-a, phytoplankton groups)	R0897-R0299-R0298-R0891	0.5, 4, 8, 12, 18m
	DO	R0897-R0299-R0298-R0891	0.5, 2, 4, 6, 8, 12, 14, 18, 22, 26m
	Temp	R0897-R0299-R0298-R0891	0.5, 2, 4, 6, 8, 12, 14, 18, 22, 26m
	Conductivity	R0897-R0299-R0298-R0890	0.5, 2, 4, 6, 8, 12, 14, 18, 22, 26m
	pH if on probe	R0897-R0299-R0298-R0891	0.5, 2, 4, 6, 8, 12, 14, 18, 22, 26m
	Kd	R0897-R0299-R0298-R0891	0.5, 1, 2, 4, 6
	Fluoro probe	10 sites	surface
Daily	Presence /absence of scums	R0893	
2. In situ measurement (Deltares)			
	Temperature	R0897-R0299-R0298	2 m depth intervals
	DO	R0897-R0298	3 depths one at, one above, one below thermocline
	Chl-a	R0897	surface
	Meteo Station	R0890	
3. Intensive measurements (Deltares)			
	(Focus on scum formation)	To be confirmed	
	Temp	Several locations along the horizontal and vertical	
	DO	3 days in three occasions	
	Chl-a		
	Cell counts		
	Scamp profiler		
	CTD (?)		

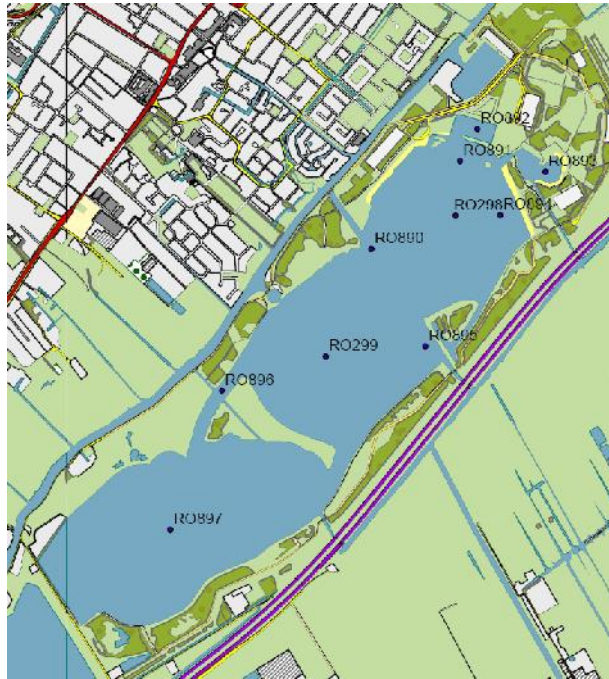


Figure A.2: Position of Rijnland's observation stations on Lake Vlietland. There are two stations in the north basin RO299 and RO298. In the south basin there is only one station RO897.

Table A.2: Routine measurements obtained by Deltares (for the locations see Figure A.1).

Manual measurements 2009 Deltares	
	Stations measured
April 7th	N1-N2-Z1-Z2
April 16th	N1-Z1-Z2
May 5th	N1-N2-Z1-Z2 - W1 - N3
May 20th	N1-N2-Z1-Z2 - E1 - W1
June 8th	N1-N2-Z1-Z2 - E1 - W1
June 22nd	N1-N2-Z1-Z2 - E1 - W1
July 3rd	N1-Z1
July 14th	Z1
July 27th	N1-N2-Z1
Aug 3rd	N1-N2-Z1-Z2
Aug 14th	N1-N2-Z1-Z2 - E1 - W1

A.3. Meteorology

Valkenburg meteorological station is located approximately 7 km away from Lake Vlietland. This station is used to derive meteorological input for the model used in the study discussed in Chapter 2. Additionally, Deltares placed a meteorological station in the lake during 2009, unfortunately the station was damaged after a few

days of operation. Figure A.3 provides an overview of the meteorological characteristics during the season (wind speed, wind direction, solar radiation and air temperature). It also shows the small window of available observations obtained at Vlietland meteorological station. From this comparison it appears that the measurements of the station located in Lake Vlietland are quite similar to the measurements from Valkenburg station.

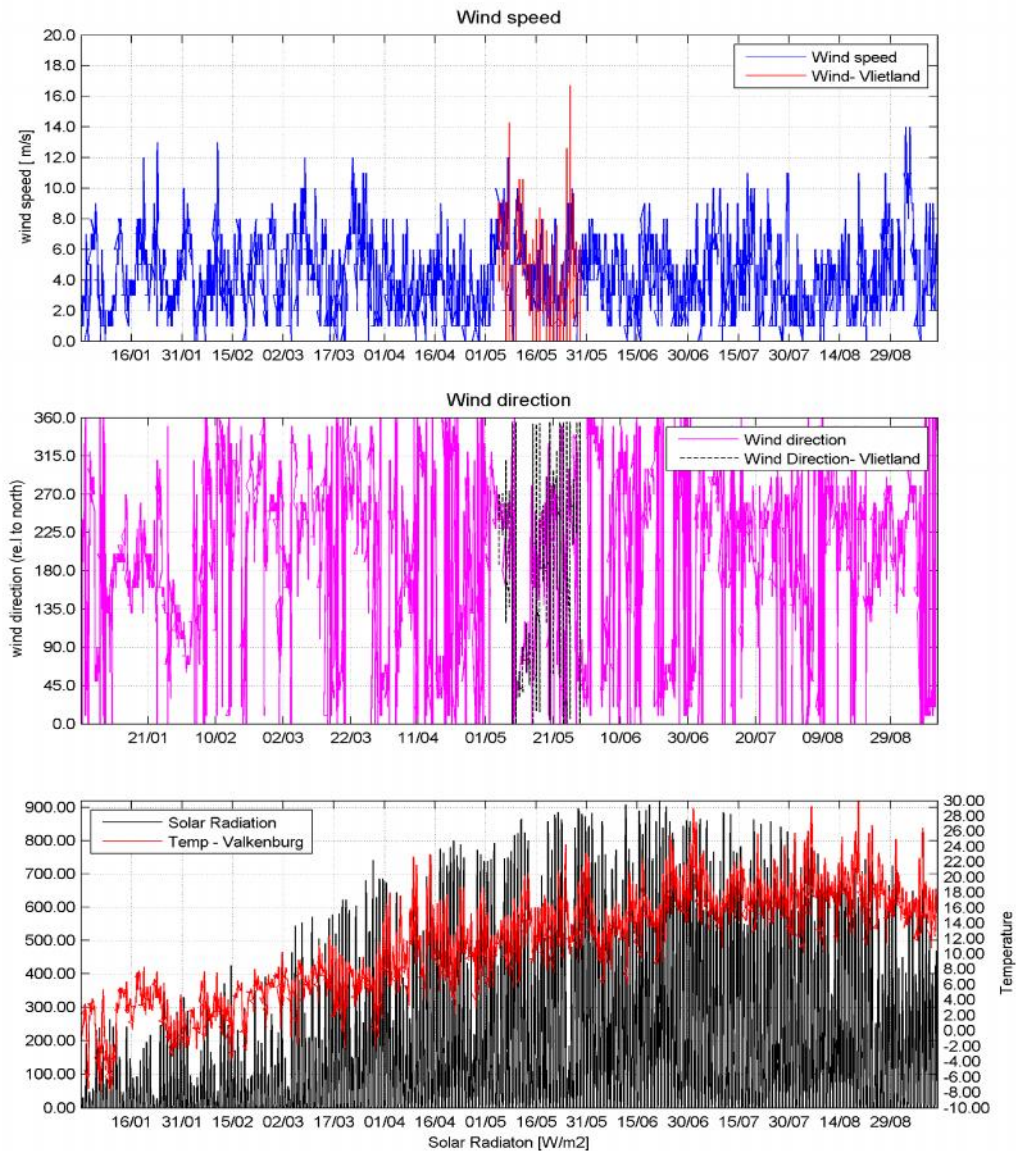
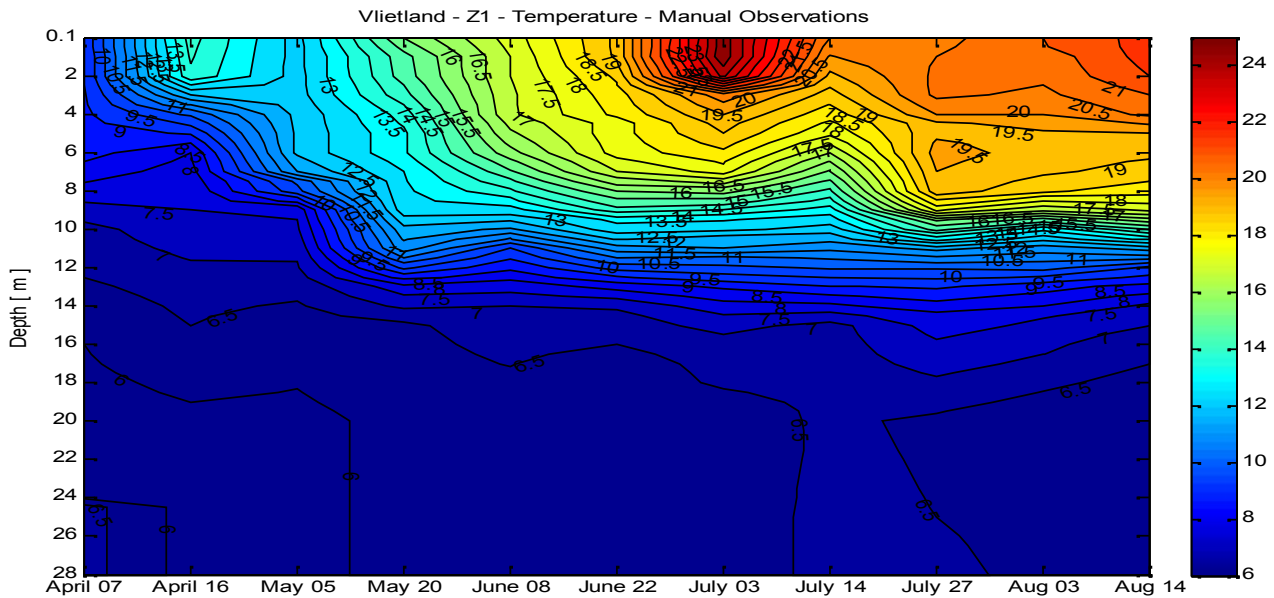


Figure A.3: Meteorology from Valkenburg meteorological station in 2009 and limited data from Deltares measurements at Lake Vlietland.

A.4 Measurements of Water Temperature and Dissolved Oxygen: effects of artificial mixing

A.4.1 Water Temperature

Figure A.4 shows the temperature measurements in the South Lake. It appears that operation of the aeration system in the north basin does not significantly affect the development of the thermocline in the south basin. The thermocline is located at 8 meters below the surface. A strong stratification develops from June and lasts during all summer.



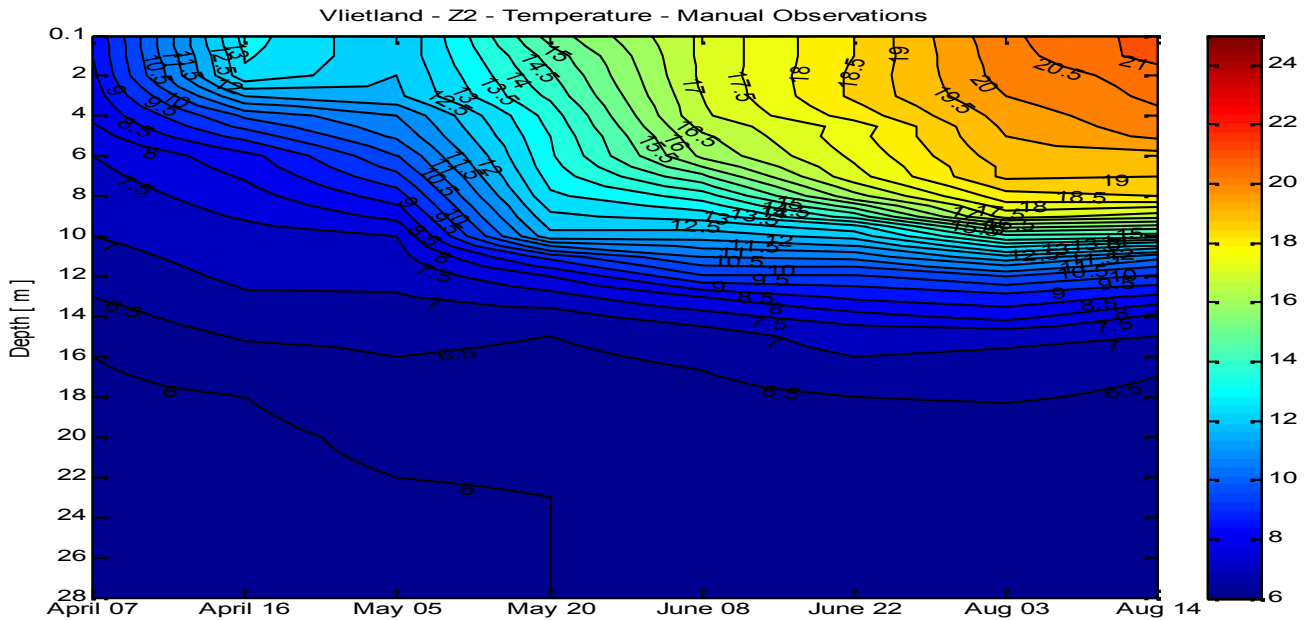


Figure A.4: Manual observations of temperature in locations Z1- Z2 (south basin).

Figure A.5 shows the manual water temperature measurements in the north locations: N1, N2. The aeration started in April 2009 before a strong stratification occurred. The temperature profiles were uniform along the vertical after 3 days of operation of the aeration system (see Figure A.6). The higher water temperatures were reached at the beginning of July, were in spite of the aeration system there was a small stratification at 2 meters depth in the north lake.

It is important to notice that in location N2 for depths below 22 meters the water temperatures are much lower than in location N1. The main reason is the topography of the lake. Before the deep part of N2 there is a hill at 22 meters (Figure A.1). This occurrence creates a thermocline at 22 meters in the north lake, which is also accompanied by low oxygen levels, due to detritus respiration.

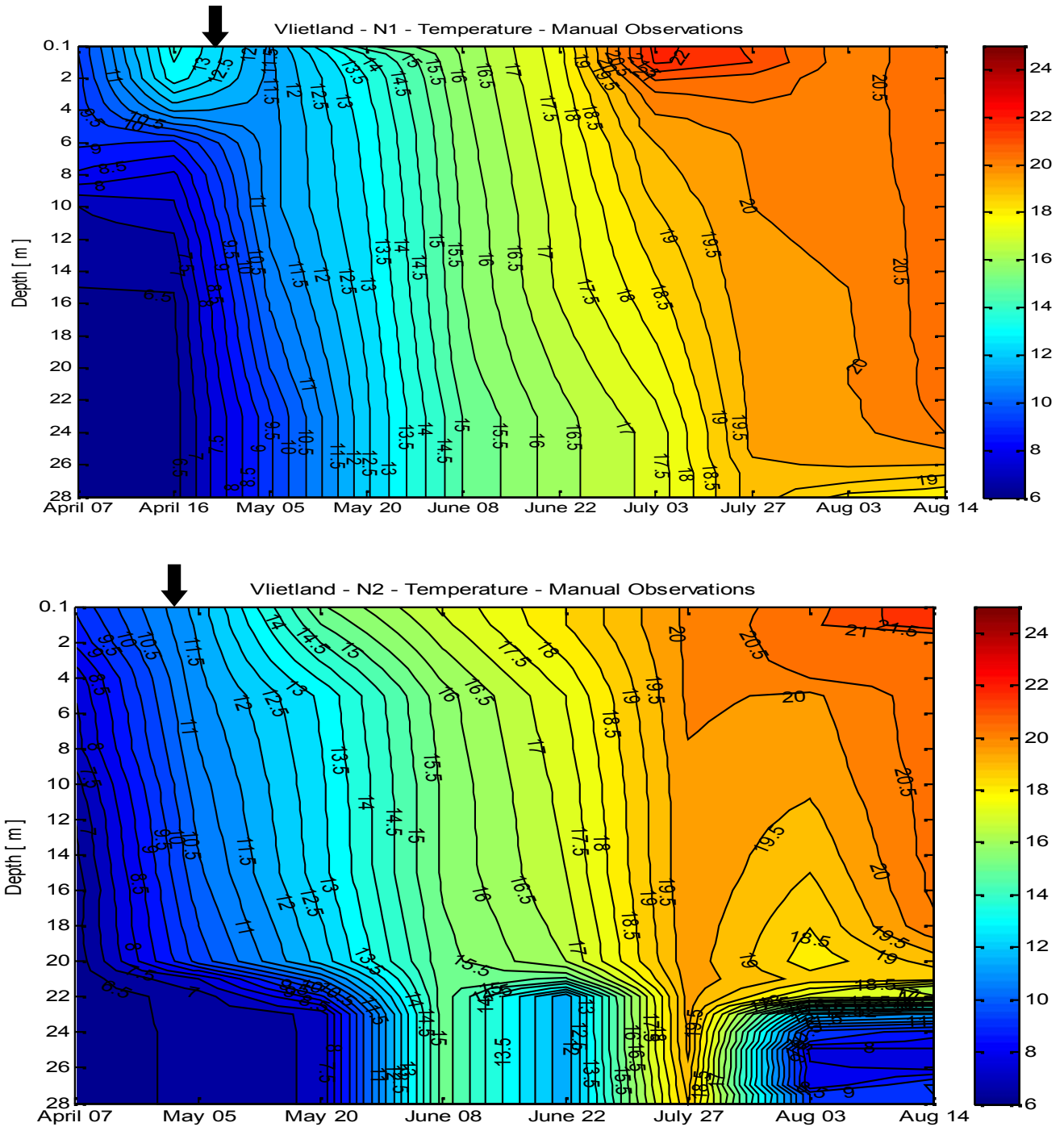


Figure A.5: Manual observations of temperature in locations N1- N2 (north basin). The arrow shows the start of the aeration system.

Figure A.6 shows the measurements with water temperature sensors. The measurements were made with five minutes interval. The daily variations of water temperature are visible in these graphs. Observe that the temperature measurements in the north basin are uniform like in figure A.5.

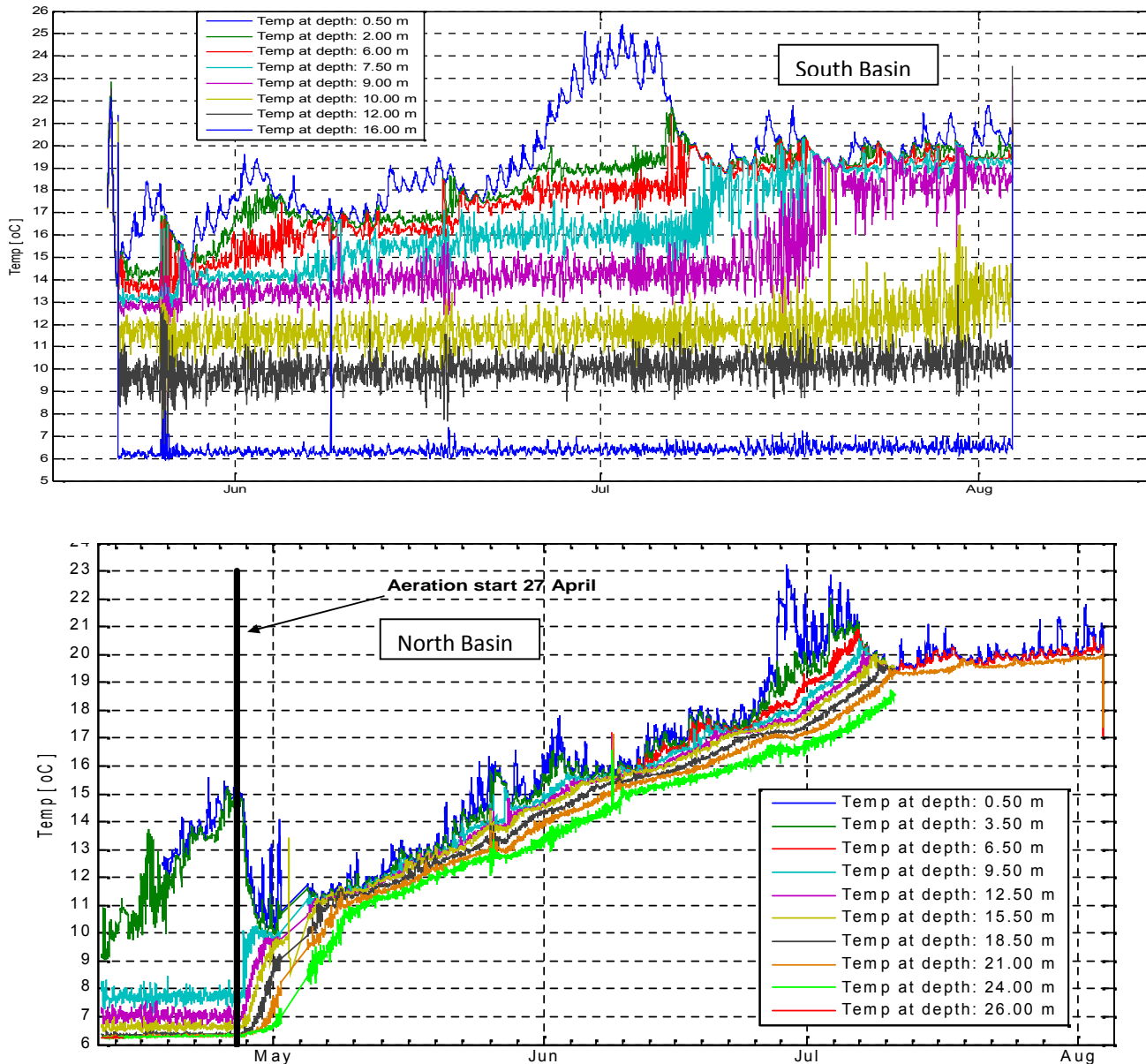
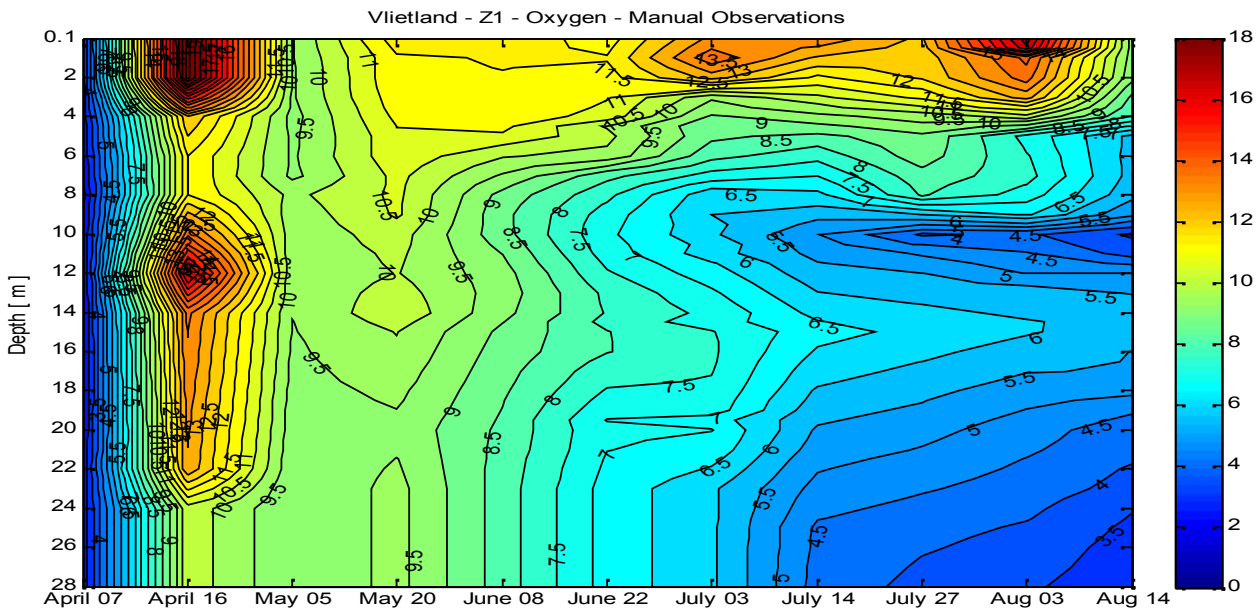


Figure A.6: Temperature measurements at locations Z1 (south) and N1 (north) with temperature sensors.

A.4.2 Measurements of Dissolved Oxygen

Figure A.7 shows the measurements of oxygen in the south lake. The oxygen minimum can be observed in the north lake at 22 meters depth, and in the south lake at 10 meters, precisely where the thermocline is located. The minimum level of oxygen occurs due to several reasons: due to shortage of light algae consume more oxygen than what they produce, therefore there is more respiration. Additionally, detritus is located in that position due to the thermocline location and it consumes oxygen.



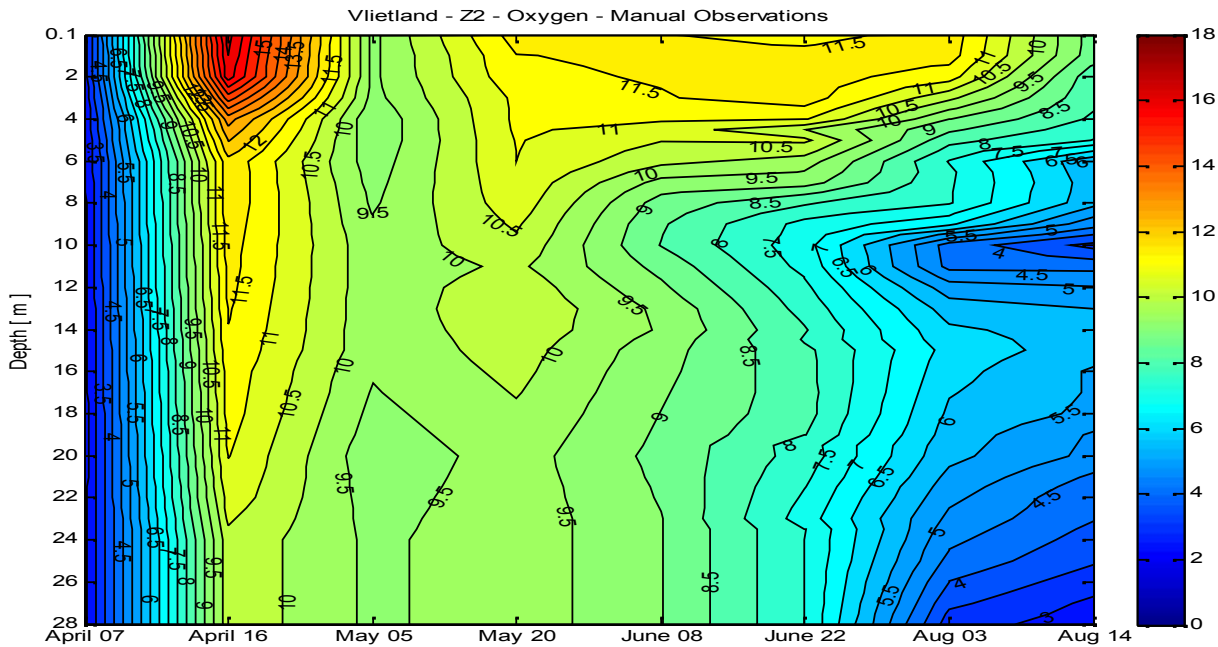


Figure A.7: Dissolved oxygen measurements in mg/l at locations Z1 and Z2.

Figure A.8 shows the oxygen measurements in the north basin. If the distribution of oxygen would be mainly determined by turbulent mixing it would be expected uniform profiles as consequence of the mixing generated by the aeration system. However, oxygen levels depend on various spatially dependant variables such as: production of oxygen by algae, consumption of oxygen by algae, mineralization and others. This is shown for instance in the measurements for location N2 on August 3rd. At this time there is high concentration of oxygen in the upper layer (with thickness of approximately 1 meter) which is due to photosynthesis resulting in the production of large quantities of oxygen.

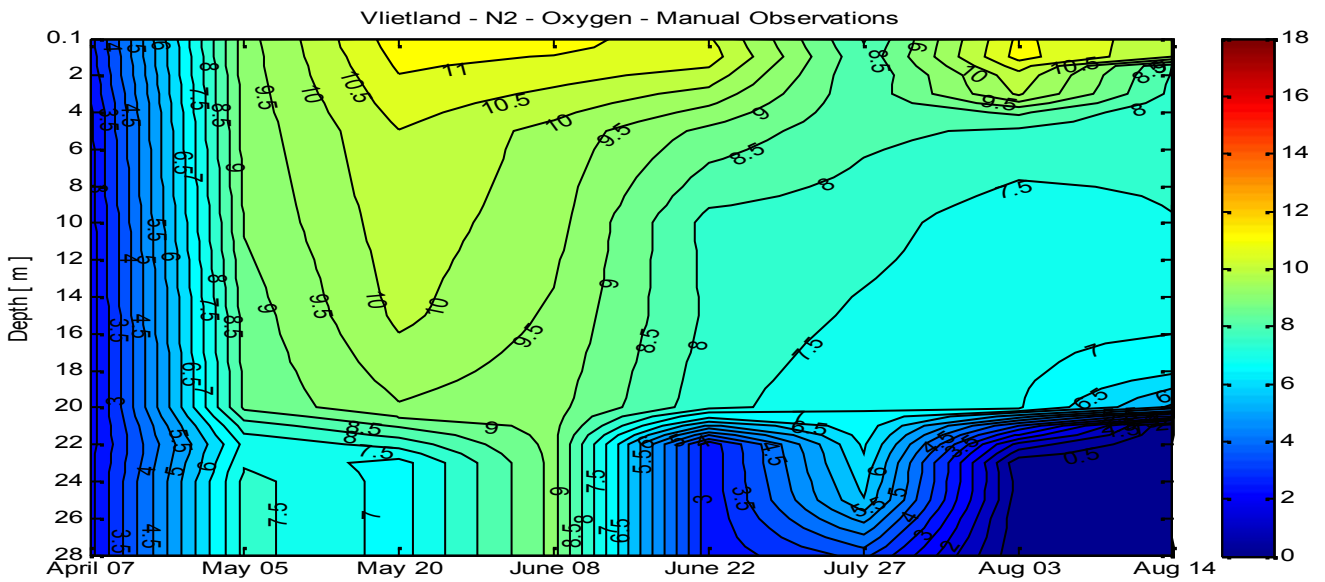
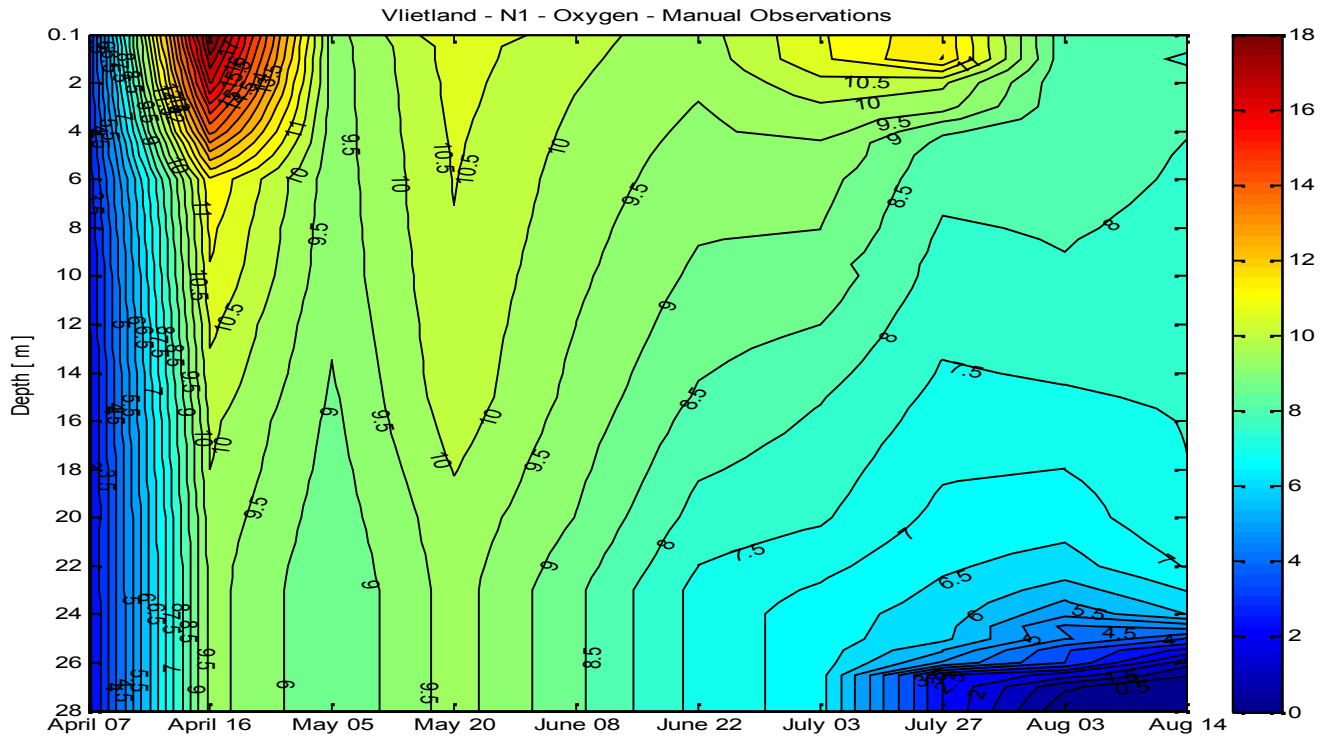


Figure A.8: Dissolved oxygen measurements in mg/l at locations N1 and N2.

A.4.3 Oxygen Saturation

The oxygen saturation gives a better insight into the absolute oxygen content of the water column. High levels of dissolved oxygen at high water temperatures results in a higher degree of super saturation than at lower temperatures. Figure A.9 shows the solubility of oxygen at different temperatures. In general, warmer water can contain less oxygen. The supersaturation of oxygen in the water column can be considered as a proxy for the photosynthetic activity.

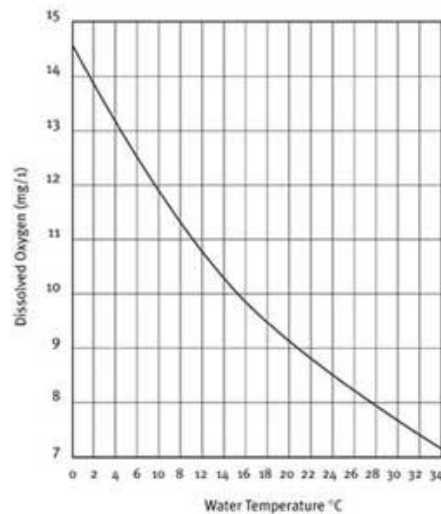


Figure A.9: Solubility of oxygen as function of water temperature.

Figure A.10 shows the oxygen saturation levels in the south basin. The oxygen saturation levels reach 160%, showing large photosynthetic activity.

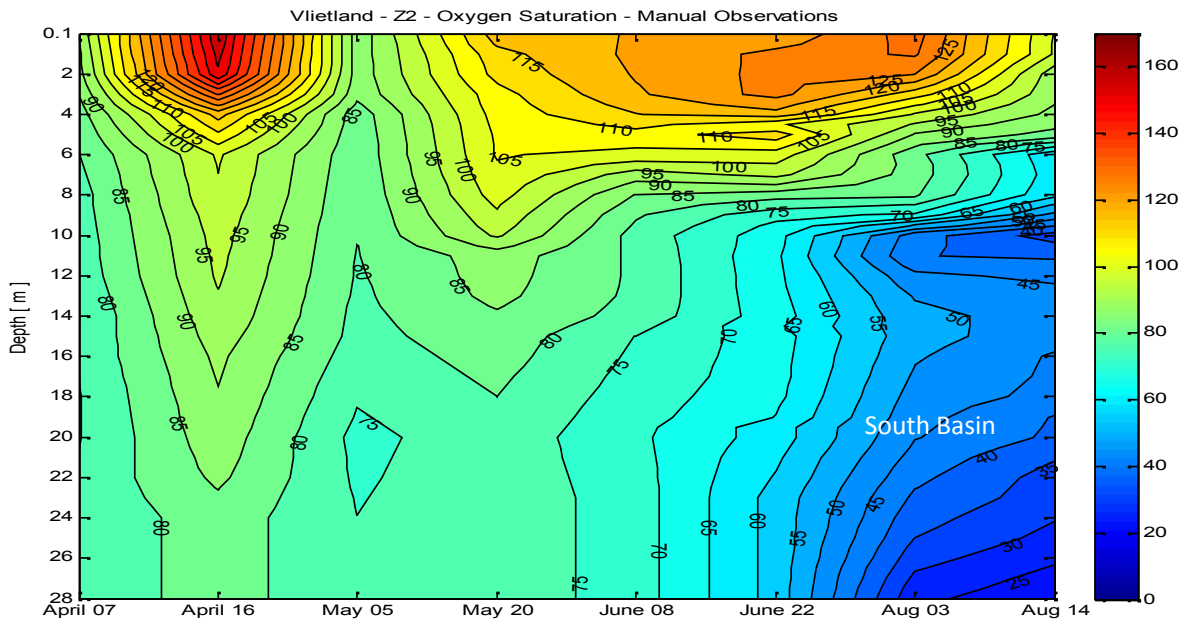
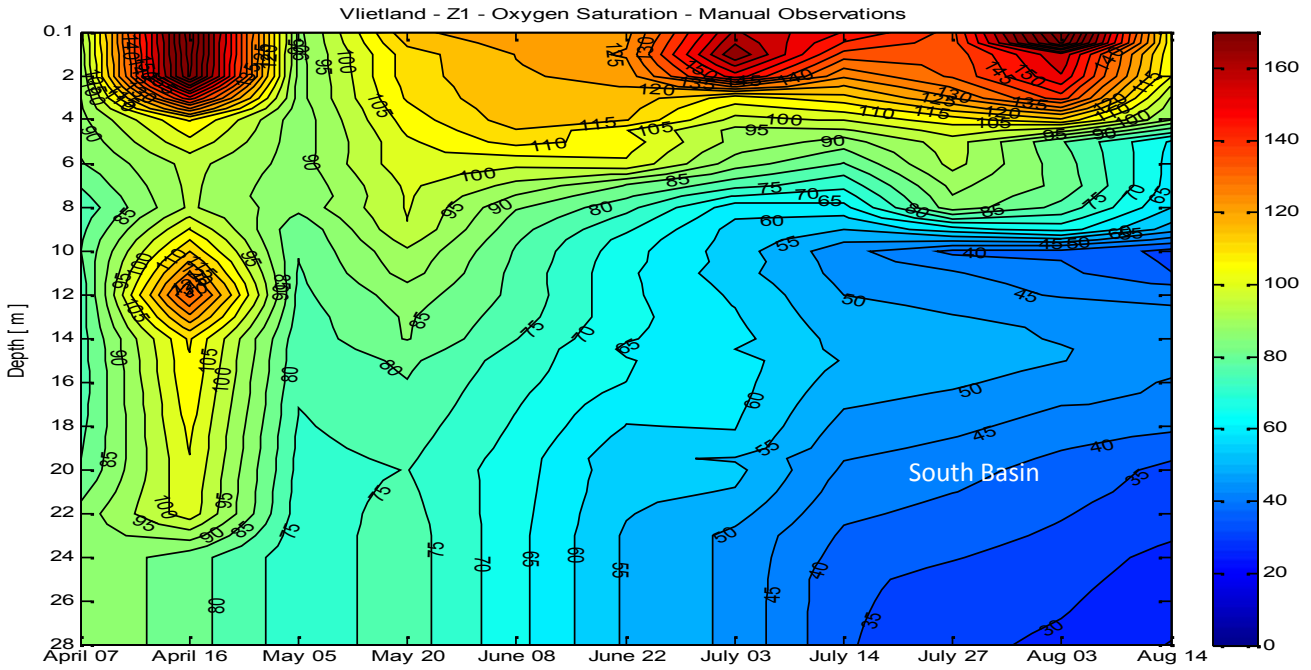


Figure A.10: Oxygen Saturation levels in locations Z1 and Z2.

Figure A.11 shows the oxygen saturation in the North Lake. Location N1 shows supersaturation reaching 130% during July. Location N2 shows similar supersaturation values at the beginning of August. The effect of artificial mixing is

visible in the north basin; however there are higher concentrations near the surface due to photosynthesis of algae.

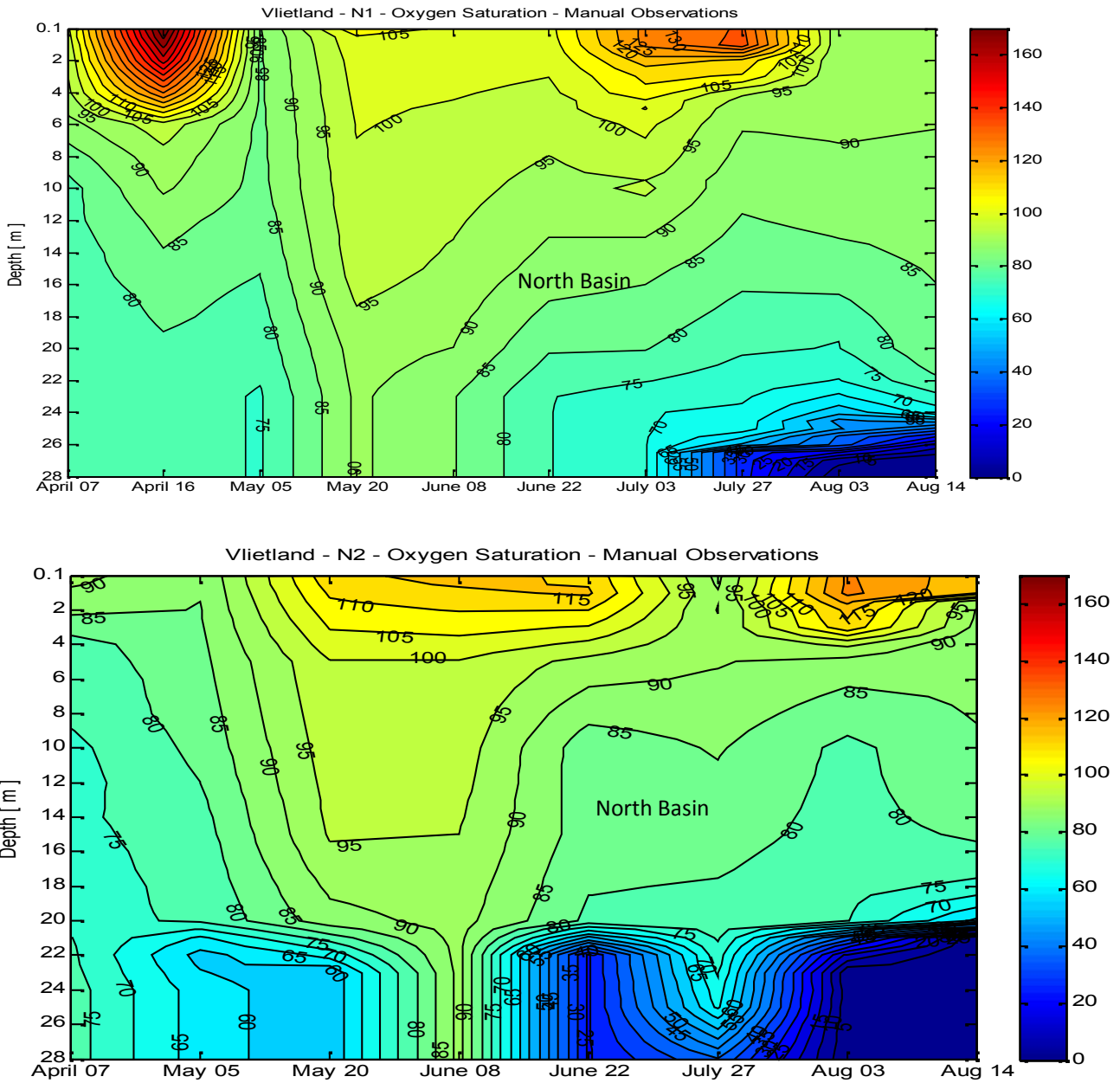


Figure A.11: Oxygen Saturation levels in locations N1 and N2.

A.5. Light extinction coefficient

Figure A.12 shows the extinction coefficient as a function of time for two stations in the north basin and one in the south. Large Chlorophyll values do not correspond with high extinction coefficients (Figure A.13).

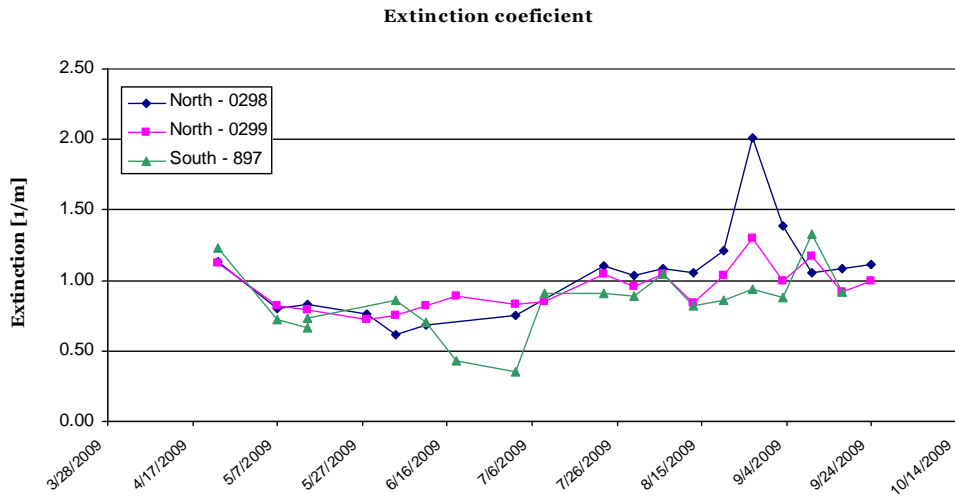


Figure A.12: Extinction coefficient in locations North – 298 and 299, South 0897.

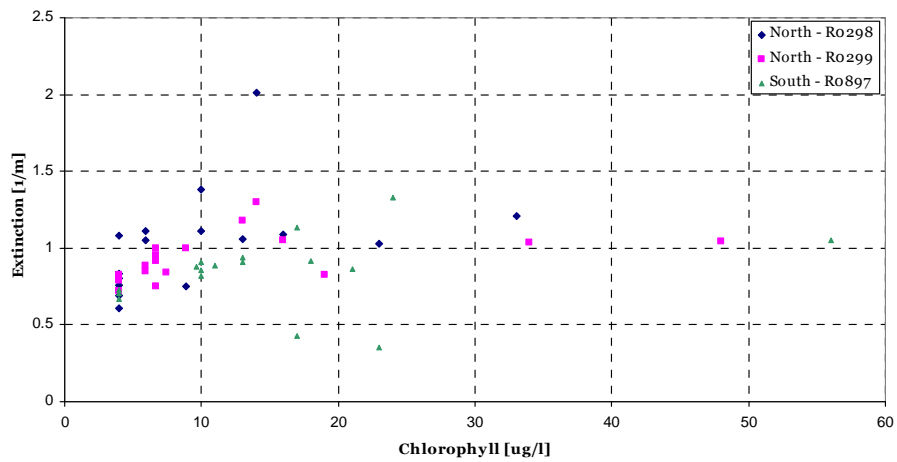


Figure A.13: Correlation between Chlorophyll measurements and light extinction.

A.6. pH Measurements

Figure A.14 shows the pH measurements for the north and south basins. Overall the south lake has a higher pH than the north basin. The range of variation is normal for lakes in the region.

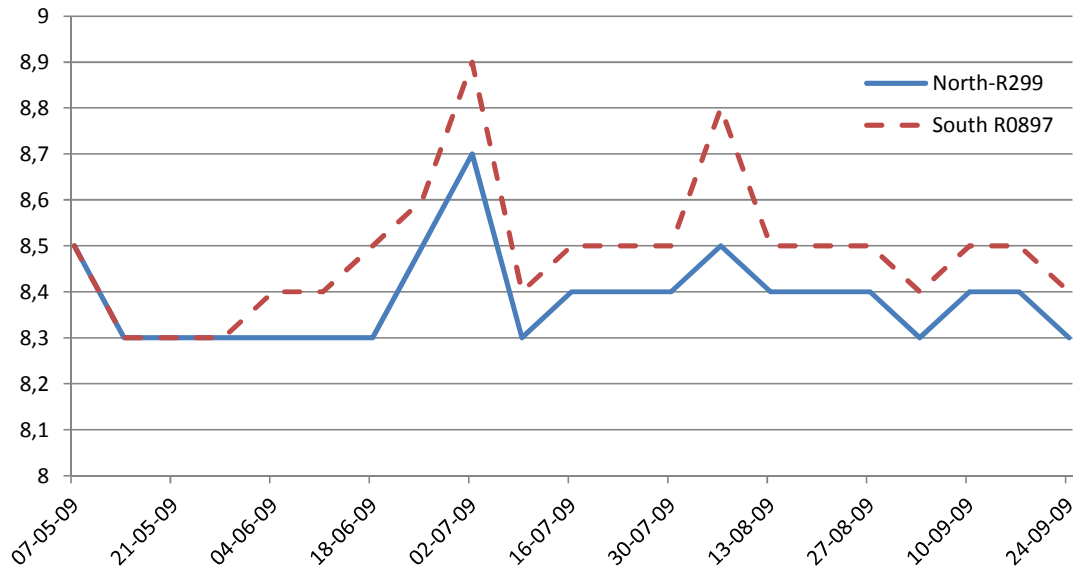


Figure A.14: pH measurements for the North and South basins.

A.7 Measurements of Nutrients

Nitrogen

Total Nitrogen in the south basin varied between 1.8 and 2.2 mg/l (Figure A.15). Values lower than 1 mg/l will represent a limitation for the growth of *Microcystis*. The blooms started in July 2009, in this period there is a mild reduction in nitrogen in the epilimnion. In October as the thermocline is disappearing the nitrogen is better mixed along the epilimnion.

Total nitrogen in the north basin varied between 1.8 and 2.8 mg/l (Figure A.16). Nitrogen is well mixed along the water column.

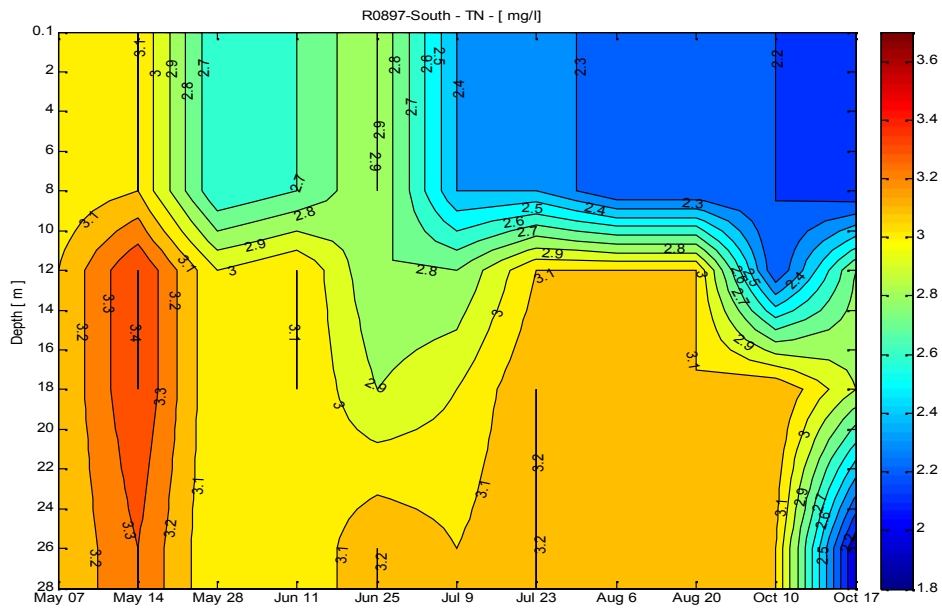


Figure A.15: Total Nitrogen in station R0897- South basin.

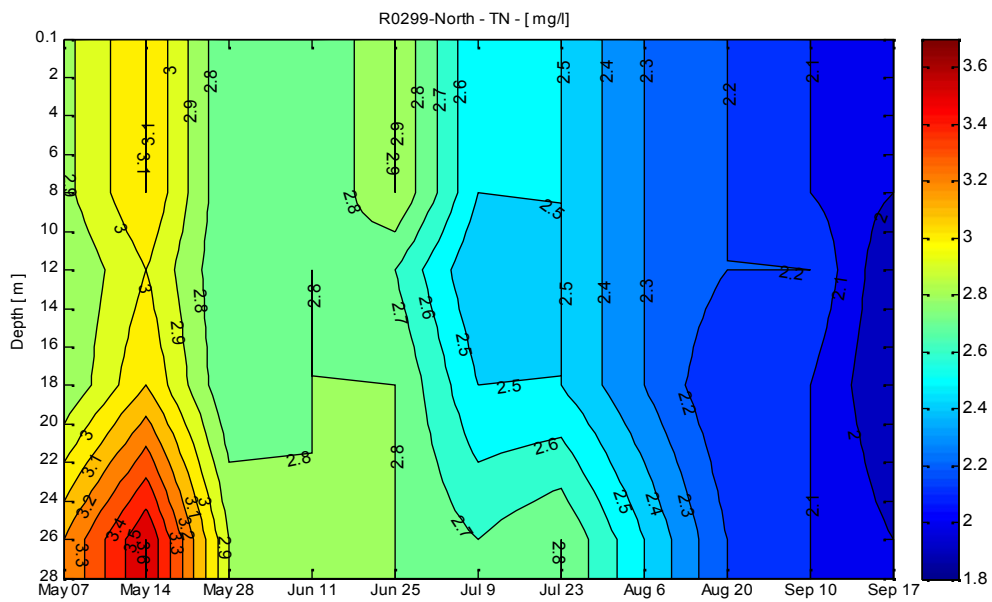


Figure A.16: Total Nitrogen in station R0299- North basin.

Phosphorus

Total phosphorus in the south basin varied between 0.2 to 0.4 mg/l (Figure A.17). There is no large variation during the year and along the vertical. The amount of total phosphorus in the north basin is similar to the south basin (Figure A.18). The distribution is quite uniform along the depth. In both basins the total phosphorus is sufficient for the growth of cyanobacteria.

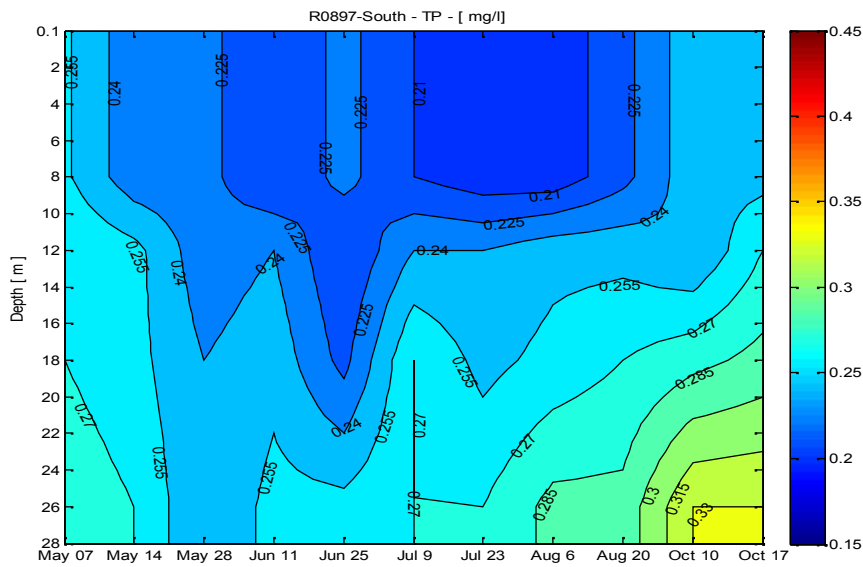


Figure A.17: Total Phosphorus in station R0897- South basin.

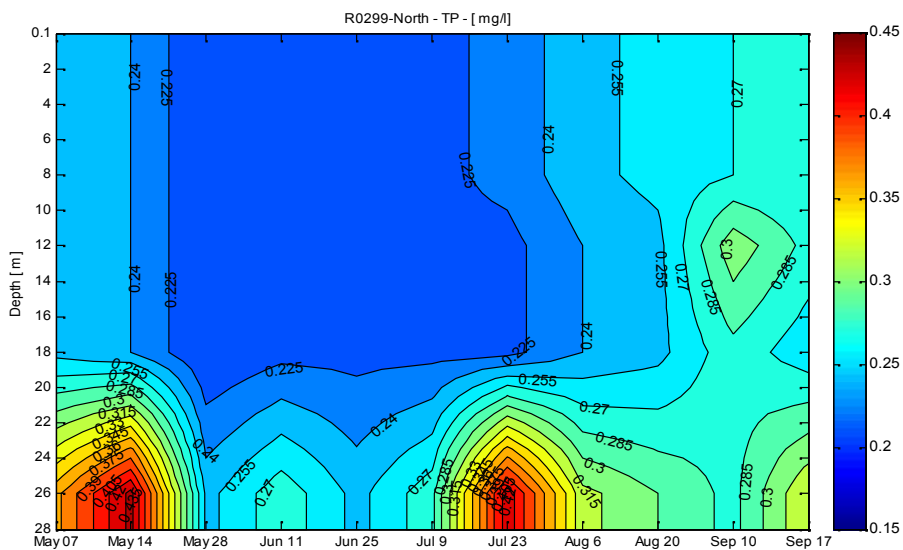


Figure A.18: Total Phosphorus in station R0299- North basin.

Dissolved Organic Carbon

Figure A.19 shows the measurements of dissolved organic carbon (DOC) in the south basin. It varies between 14 – 20 mg/l. The concentration is higher in the epilimnion during the period of stratification. At the beginning of October as the thermocline disappears the organic carbon is mixed along the vertical. Figure A.20 shows the measurements of DOC in the north basin. It varies between 14 – 16 mg/l. There is less DOC in the north than in south basin.

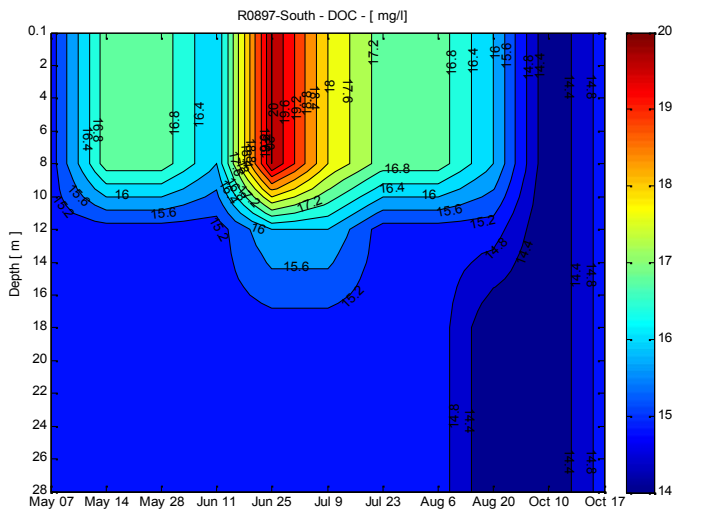


Figure A.19: Dissolved Organic Carbon in station R0897- South basin.

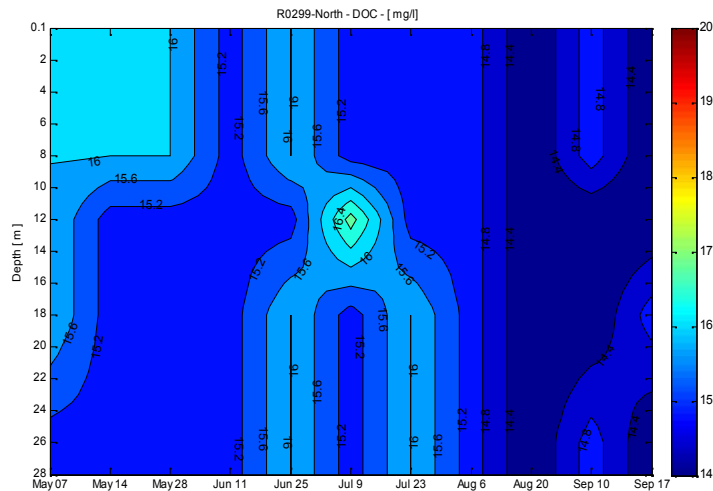


Figure A.20: Dissolved Organic Carbon in station R0299- North basin.

A.8 Algae Measurements

An interesting aspect of the algae measurements is their larger concentrations in the north aerated basin compared to the south basin. Figure A.21 shows the chlorophyll measurements at 0.5 meters deep and the integrated measurements of 8 meters deep in the south basin. Figure A.22 shows the measurements of 4 algae species: Blue green, Diatoms, Green and Cryptophyta. The absolute measured values are very low compared to visual observations of algae in the lake. The total algae measured fluorometrically is approximately 50% less (Figure A.22) of the spectrometrically measured chlorophyll (Figure A.21). The results show that algae concentrations are higher in the epilimnion (until 10 meters deep). Starting at the end of July the majority of the algae is mainly composed by blue greens.

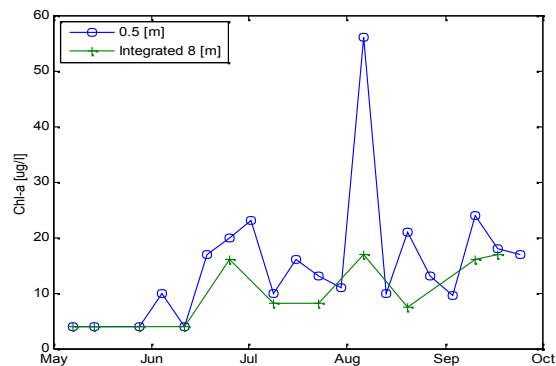


Figure A.21: Chl-a measurements at 0.5 m and integrated of 8 meters, location R0897 in the South lake.

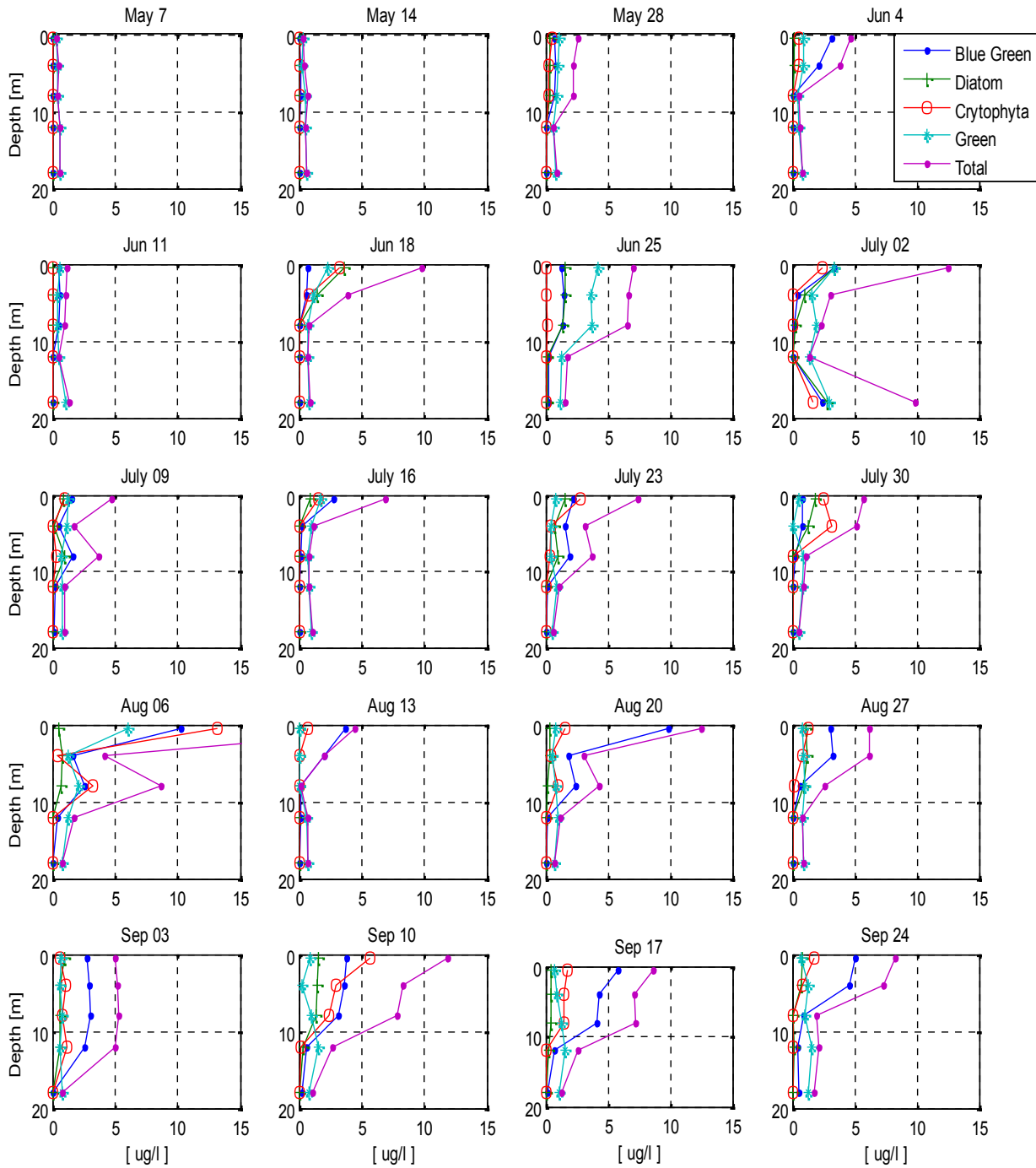


Figure A.22: Individual profiles of type of algae, location R0897 in the South lake.

Figure A.23 shows the chlorophyll measurements at 0.5 meters deep and the integrated measurements of 8 meters deep in the north basin. Figure A.24 shows the measurements of 4 algae species: Blue green, Diatoms, Green and Cryptophyta. The surface chlorophyll measurements show more algae in the south basin. However, the individual profiles (Figure A.24) show more algae in the north than in the south, especially during August. During the summer most of the algae is mainly composed of blue-greens.

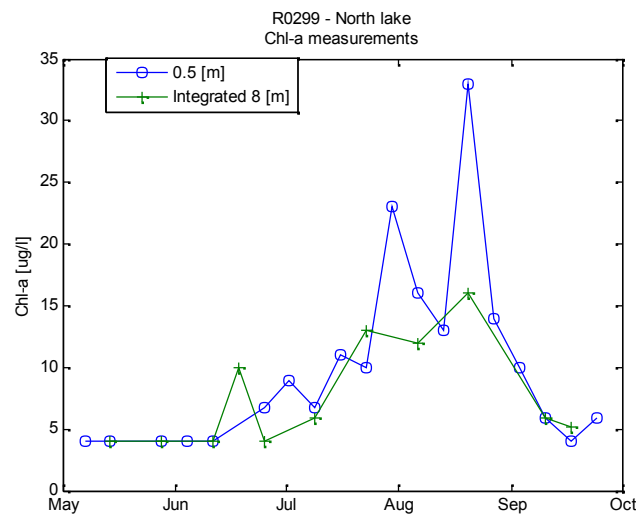


Figure A.23: Chl-a measurements at 0.5 m and integrated of 8 meters, location R0299 in the North lake.

The effect of the aeration system is very effective in the north basin in the sense that temperature is well mixed along the depth. However, scums could not be prevented during hot windless day in the summer.

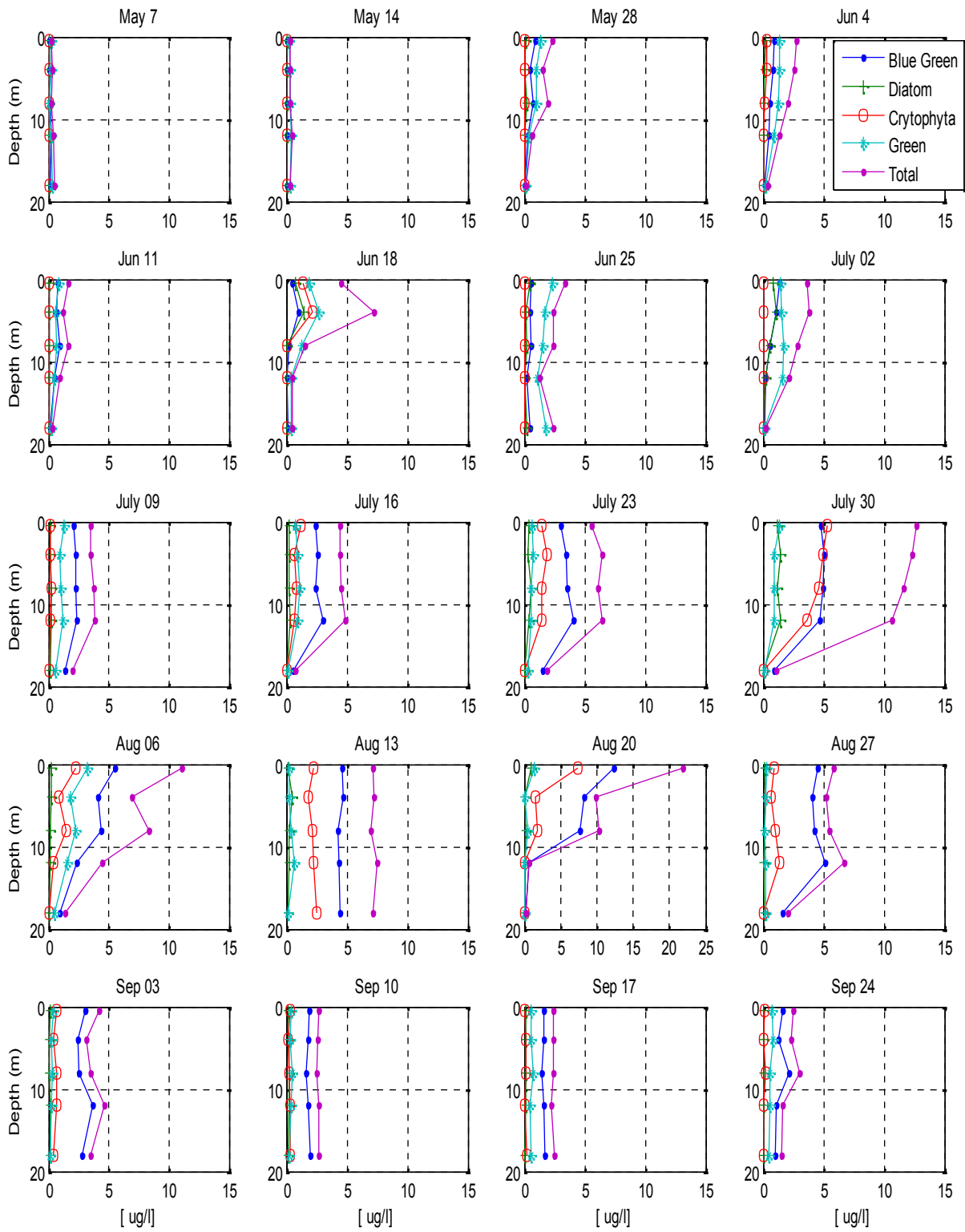


Figure A.24: Individual profiles of type of Algae, location R0299 in the North lake.

Physical Aspects Explaining Cyanobacteria Scum Formation in Natural Systems

Summary

Bloom forming and toxin producing cyanobacteria create considerable nuisance, because they might produce scum. A scum is defined as very high concentrations of algae covering the water surface of a lake, which can affect wildlife and recreation. This is currently a problem of global dimensions. The aspect of a scum is like a green/paint cover floating on water. In this thesis, the mechanisms responsible for cyanobacteria scum formation are investigated. The thesis explores, using an integrated approach, the role of lake hydrodynamics, in particular (stratified) turbulence, the physiological response of cyanobacteria to light and the buoyancy created by the growth of oxygen bubbles in cyanobacteria vertical migration and scum formation. The main focus is on the ubiquitous cyanobacteria *Microcystis aeruginosa*. Usually, the *Microcystis* cells are embedded in their mucus thereby forming colonies. The colony mass-density of *Microcystis aeruginosa* can be actively regulated by a physiological response to light, as such to adjust their buoyancy. However, this property alone does not explain their formation into a scum.

My first investigated approach consists of modelling hydrodynamics and cyanobacteria physiological responses, explicitly including the buoyancy regulation under the influence of light intensity in the *Microcystis* cells. The combined effects of turbulence mixing and buoyancy regulation on the vertical migration of cyanobacteria under natural conditions are applied through the Langevin-Fokker-Planck (LFP) approach. This approach simulates the total colony number concentration along the water column. Concurrently, turbulence mixing is simulated by the $k-\varepsilon$ turbulence model including thermal buoyancy effects. The Fokker-Planck combined with a model for turbulent mixing allows for describing sinking and rising velocities of colonies of different sizes and compositions when subjected to turbulent mixing. The results show that turbulence intensity and colony size play a major role in the distribution of *Microcystis* through the water column.

The second approach I investigated, couples Direct Numerical Simulations of turbulent flow with particle tracking of *Microcystis* colonies. The *Microcystis* colonies are treated as biologically active organisms because the cell mass–density is continuously changing. However, the intrinsic gap between biological and flow time scales makes such an endeavor a non-trivial exercise. In order to conceal time scales of flow and biology a normalization-scaling procedure is proposed by which biological responses of *Microcystis* cell are accelerated thereby reducing the bandwidth in time scales to computationally feasible conditions. The results of diurnal changes in the vertical migration modeled with the proposed approach show good resemblance with the first modelling approach (LFP). Furthermore, the major forces responsible for the vertical migration of *Microcystis* are basically the Stokes drag and the buoyancy force.

Compared to observations in nature, the results of both modelling methodologies are deemed suitable to represent the vertical daily migration of *Microcystis aeruginosa*. Notable, the LFP methodology is applicable for studying seasonal variations. Nevertheless, in view of what creates scums of cyanobacteria, a combination of the hydrodynamics and physiological responses of cyanobacteria are not sufficient for explaining scum formation.

The third approach of my thesis consists of laboratory experiments that help in the understanding of the physical mechanism responsible for cyanobacteria scum formation. The hypothesis presented in this thesis is that irreversible buoyancy of cyanobacteria occurs due to the growth of gas bubbles in the colonies, most likely oxygen due to supersaturation by strong photosynthesis of high concentration of cyanobacteria cells (called a bloom). These oxygen bubbles can be located within or attached to the mucus. The experiments consisted on placing a water sample containing a field sample of a cyanobacteria scum (from a typical Dutch lake) inside a pressure chamber. Subsequently, the pressure is slowly increased. Upon reaching 4 bars, the floating cyanobacteria colonies change their buoyancy status from rising to sinking. The observed change from floating to sinking by the increased water pressure suggests that gas bubbles are present within the scum sample. My experiments therefore support the main hypothesis.

Although there are several simplifications applied in the modelling and laboratory experiments performed, the results show the essential components that are needed for a reasonable modelling representation of the vertical migration of *Microcystis aeruginosa*. Furthermore, this thesis provides supporting evidence that the presence of oxygen gas bubbles in a colony will lead to the formation of a scum.

Acknowledgements

Compared to writing a PhD dissertation this section *should* be easy. That is what I thought, however it is not completely true. It should be formal, but emotions play a major role. I certainly think that comparing this journey with a roller coaster ride is justified. There is some excitement, curiosity, fear and of course joy and pride.

First, I would like to thank my professor and supervisors Herman Clercx, Rob Uittenbogaard, Bas van de Wiel and Miguel Dionisio Pires. For they have supported and encouraged me continuously during my PhD. I am in great debt with all of you.

I would like to thank the members of my thesis committee: Anton van Steenhoven, Wim Uijttewaal and Wolf Mooij for taking time to asses my thesis.

By the time I was finishing my master thesis I knew that I wanted to continue doing research. Since then and during my PhD Rob Uittenbogaard has played a very important role. I have learned to explore fields outside my comfort zone. Rob, I want to thank you for your continuous motivation and for sharing your vast knowledge with me.

During my research, I performed field, laboratory and computational experiments and each time I was lucky enough to find the right people who helped me. For that I am very grateful. I started my research by visiting Lake Vlietland on a weekly basis, together with Rob Uittenbogaard, Miguel Dionosio Pires and Victor Langeberg. Gerhard te Loo from the watersport marina at Lake Vlietland was very helpful during our measuring campaigns. Arie de Waardt helped me with installing a meteorological station in the middle of the lake and temperature sensors at another three locations. I would also like to thank waterboard Rijnland for performing and sharing water quality measurements in Lake Vlietland, especially to Johan Osterbaan, Bart Schaub and Diane Slot.

For my laboratory experiments I received great assistance from Marcel Busink, Marcel Grotenburg and John Cornelisse from Deltares. I would like to thank Marleen van Aartrijk for providing me with the DNS code and Michel van Hinsberg for helping me with the implementation of the particle density changes functions.

My research was performed in Delft at Deltares and in Eindhoven at the University. In both places I found myself surrounded by very friendly and helpful colleagues. I would like to thank Marjan Rondeburg for her help and friendship. I really enjoyed our walks and conversations after lunch. I would also like to thank Alexey Rodriguez and Sandra Gaytan for being such dear friends and for always given me words of encouragement.

During these interesting and challenging years I received the love and support of my beloved husband Rick. Thank you for everything “amorcito”.

Special thanks to my beloved parents Jose and Maria Rosario, sisters Nadinne and Kharol and the rest of my family and close friends for their patience and unconditional love.

Evelyn Aparicio Medrano

Delft, 2014

Curriculum Vitae

Evelyn Aparicio Medrano was born on 6 December 1979 in Cochabamba, Bolivia.

After finishing her Bachelor in Science in Civil Engineering in 2002 at Mayor de San Simon University in Cochabamba, Bolivia, she worked during three years in the field of water and sanitation for small urban areas. Then, she studied Water Resources Management at the Technical University of Delft in Delft, The Netherlands. In 2008 she graduated (with distinction) within the Water Resources Management on Urban Surface Water as Energy Source. From 2009 she started a PhD project at the Technical University of Eindhoven at Eindhoven, The Netherlands of which the results are presented in this dissertation.